TESTING MODELS OF LOW-$\delta^{18}O$ SILICIC MAGMATISM IN THE MID-MIOCENE SANTA ROSA-CALICO VOLCANIC FIELD, NV

by

KATE E. AMRHEIN

B.S., Grand Valley State University, 2009

A THESIS

submitted in partial fulfillment of the requirements for the degree

MASTER OF SCIENCE

Department of Geology
College of Arts and Sciences

KANSAS STATE UNIVERSITY
Manhattan, Kansas

2013

Approved by:

Major Professor
Matthew E. Brueseke

Abstract

Low-$\delta^{18}O$ silicic magmas are found in many volcanic provinces throughout the world, including the Snake River Plain-Yellowstone volcanic province (SRPY). The origin of SRPY low-$\delta^{18}O$ silicic magmas is controversial, and centers on two disputed models: [1] a caldera collapse model that proposes reworking of the hydrothermally altered intra-caldera fill into the underlying silicic magma body, where each successive eruption lowers the $\delta^{18}O$ of the magma eventually producing a low-$\delta^{18}O$ magma and [2] melting previously hydrothermally altered mid-upper crust to form low-$\delta^{18}O$ magmas. The mid-Miocene Santa Rosa-Calico volcanic field (SC) lies in northern Nevada. Brueseke and Hart (2008) described the geology and petrology of the SC, but did not deal with the ^{18}O compositions of any locally sourced silicic magma. In the existing geological framework of the SC, this project aims to evaluate the two disputed models for low-$\delta^{18}O$ silicic magma generation by analyzing the $\delta^{18}O$ values of SC silicic eruptive products. Fifteen representative samples of locally erupted silicic units (e.g. ash-flow tuffs and lavas) were chosen for ^{18}O analyses based on Sr-Nd-Pb isotope compositions, whole rock geochemistry, and field/temporal relationships. Each sample was crushed, sieved, and quartz and feldspar crystals were handpicked, described, and analyzed for their ^{18}O compositions. Our results show that low-$\delta^{18}O$ values exist in the SC and are limited to the youngest erupted silicic unit, the 15.8 to 15.4 Ma Cold Springs tuff, which was also the only unit erupted from a caldera. Cold Springs tuff $\delta^{18}O$ feldspar values range from 2.36 to 4.05‰; the unit is not quartz-bearing. Older silicic lavas that are not petrogenetically related to the Cold Springs tuff are characterized by normal $\delta^{18}O$ feldspar values that range from 7.19 to 10.04‰. Magma mixing models indicate that the source of the Cold Springs is a mixture of hydrothermally altered Granite Peak-Sawtooth granitoid and local mid-Miocene basalt, with an approximate range of $\delta^{18}O$ values of 2-4‰, by fluids (with $\delta^{18}O$ values ranging from -12‰ to + 7‰) from the nearby hydrothermal system at Buckskin Mountain. This result follows the model by Boroughs et al. (2005) of prior alteration and melting, forming low-$\delta^{18}O$ silicic magmas.

Table of Contents

List of Figures

List of Tables

Acknowledgements

I first would like to thank Dr. Matthew Brueseke for allowing me the opportunity to work on this project as well as the many discussions, support, and encouragement provided the last two years. Without it, I would have not been able to achieve this life goal of mine. I would like to thank the Geological Society of America for funding my project and providing a travel grant to present at a sectional meeting. Also, I would like to thank Dr. Peter Larson at Washington State University for his help with this project along with Drs. Saugata Datta, Matthew Kirk, and Sambhudas Chaudhuri, for serving on my committee. I would like to thank Dr. George Clark for providing support and funding for graduate students to attend conferences and Lori Page-Willyard for not only making the department run smoothly but for the many great conversations we have shared. I would also like to thank my professors at Grand Valley State University for preparing me for graduate school. I would also like to thank my current office mates and graduate students, past and present, for all the great and hilarious conversations and for making the last two years fun. I would like to say a big thank you to Casey Bulen and Andrea Leggett for being the best two friends anyone could ever ask for! You two made my last two years the most amazing time of my life and I don't think I could have made it through without you guys! Last but not least I want to thank my family and my parents for their endless support and belief in me. I love all of you so much!

Chapter 1 - Introduction

Compositionally bimodal basalt-rhyolite volcanism in the northern Great Basin and Pacific Northwest (U.S.A.) initiated during the Mid-Miocene and was widespread throughout Oregon, Washington, Idaho, and Nevada (Brueseke and Hart, 2008). This period of volcanism is associated with the initiation of the Yellowstone hotspot (Pierce and Morgan, 1992). The Steens-Columbia River flood basalt group started erupting around 16.7 Ma and along with the mafic eruptions, there was extensive silicic volcanism (Camp et al., 2003; Brueseke et al., 2007; Brueseke and Hart, 2008; Coble and Mahood, 2012). Many of the silicic volcanic fields associated with the Yellowstone hotspot have been studied extensively (Heise volcanic field, Watts et al., 2011; Central Snake River Plain, Boroughs et al., 2005, Boroughs et al., 2011, Ellis et al., 2010, Ellis and Wolff, 2012, Cathey and Nash, 2009, Nash et al., 2006; Santa Rosa-Calico volcanic field, Brueseke and Hart, 2008; Yellowstone, Bindeman and Valley, 2000; Bindeman and Valley, 2001) (Figure 1.1). It has been suggested that the silicic magmas in the Snake River Plain (SRP) were produced by partial melting and hybridization of water-poor calc-alkalic upper crust by basalt intrusions (Leeman et al., 2008; Watts et al., 2010). These rhyolites are similar to A-type granites, which are granites that range from alkali to calc-alkalic and metaluminous to peralkaline in composition and originate typically in intra-plate settings via partial melting of the crust (Leeman et al., 2008; Frost and Frost, 2011).

Within the SRP, four volcanic fields, Bruneau-Jarbidge, Twin Falls, Picabo, and Heise (Figure 1.1) have erupted approximately 10,000 km^3 of rhyolite. While studying the petrogenesis of these fields and those surrounding the region, a significant observation was made that there is an abundance of low-$\delta^{18}O$ rhyolites present (e.g. silicic magmas that have a $\delta^{18}O$ value of <6‰$_{VSMOW}$, Taylor, 1968). To produce these low-$\delta^{18}O$ magmas, there needs to be a significant component of low-$\delta^{18}O$ meteoric water interacting with the shallow crust (<10 km) (Watts et al., 2011). Since oxygen is the most abundant element in these silicic rocks, it is important to study why these rhyolites are depleted in ^{18}O to fully understand the petrogenesis of silicic magmatism in the SRP and Yellowstone region, as well as providing insight into shallow rhyolite production across the world especially in equatorial regions and lower latitude regions

where meteoric water is not as strongly depleted in ^{18}O and do not create subsequent low-$\delta^{18}O$ values that indicate shallow crustal sources (Watts et al., 2010; Watts et al., 2011).

There is much debate as to the origin of these rhyolites. Studies focused on the petrogenesis of Yellowstone and the central SRP have found very different processes occurring to produce these low-$\delta^{18}O$ rhyolites. In order to have a clear picture as to how the SRP-Yellowstone hotspot track formed and a better understanding of shallow rhyolite production, the origin of the low-$\delta^{18}O$ signature must be known. From this debate two endmember models are disputed as to how these units became depleted in ^{18}O. One model centers on the melting of pre-existing hydrothermally altered crust (Boroughs et al., 2005, King et al., 2008, and Zierenberg et al., 2013) and the second involves magma production via repeated eruption-caldera collapse, hydrothermal alteration, and then melting of intra-caldera fill that is then incorporated into an evolving magma body eventually producing low-$\delta^{18}O$ magmas (Bindeman and Valley, 2000; Watts et al., 2011). The model of Boroughs et al. (2005) was developed from studying lavas and ash flow tuffs of the Central Snake River Plain (CSRP) which include the Bruneau-Jarbidge (BJ) and Owyhee Plateau (OP) volcanic fields (Figure 1.1). The Bruneau-Jarbidge volcanic field is characterized by voluminous rhyolite ash-flow tuffs and lavas, which is typical of CSRP volcanism. The majority of the rhyolite was erupted between 12.6 and 10.8 Ma forming the Cougar Point tuff. The rhyolite lavas of the Owyhee Plateau were erupted between 15 to 13 Ma and are characterized by multiple lavas and are chemically and petrographically similar to the Bruneau-Jarbidge rhyolites (Boroughs et al., 2005; Bonnischen et al., 2008). Through the various data Boroughs et al. (2005) acquired, it was found that the low-$\delta^{18}O$ values in CSRP rhyolites do not vary depending on age and stratigraphic position; no normal-$\delta^{18}O$ rhyolites ($\delta^{18}O$ values that are greater than 6‰) were found to exist in the CSRP. A study performed by Criss and Taylor (1983) showed that Tertiary and Cretaceous plutons of the Idaho Batholith that are located spatially at the same longitude as the CSRP were hydrothermally altered during the Eocene (49-37 Ma; Figure 1.2). Various areas of Eocene hydrothermal systems developed around the Cretaceous granitic plutons where deep water circulation (5 to 7 km) by meteoric water with a $\delta^{18}O$ value of -16‰ lowered the $\delta^{18}O$ of the surrounding granitoids to ~2‰ to -8‰. From this, it was proposed by Boroughs et al. (2005) that the areas of the Cretaceous Idaho Batholith that underwent Eocene alteration were then melted and formed the source for CSRP rhyolites. Major and trace element geochemical modelling and radiogenic isotope data were

used by Boroughs et al. (2005; 2012) to demonstrate that the CSRP rhyolite magmas could have formed via upper-crustal melting of the Idaho Batholith.

In contrast to this model, Bindeman and Valley (2001) and later Watts et al. (2011), propose that the origin of low-$\delta^{18}O$ rhyolites in Yellowstone (and Heise) formed due to repeated caldera collapse and remelting of hydrothermally altered intra-caldera fill (Figure 1.3). The original study by Bindeman and Valley (2001) at Yellowstone focused on the $\delta^{18}O$ values of quartz and zircon grains because of their resistance to hydrothermal alteration. Bindeman and Valley (2001) found that after every major caldera cycle, there was a lowering of the zircon and quartz $\delta^{18}O$ values, starting with a normal- $\delta^{18}O$ magma. Only after the 604 ka Lava Creek tuff cycle (e.g. the third major Yellowstone eruptive) was there a large drop of $\delta^{18}O$ values (as high as ~5‰ in some samples). These $\delta^{18}O$ values of quartz and zircon were compared with $\delta^{18}O$ values of quartz and zircon in lavas erupted outside of the third cycle caldera and those from the Lava Creek tuff were found to be much lower in $\delta^{18}O$ than the later lavas. This indicated that the intra-caldera fill was being remelted, which lowered the $\delta^{18}O$ of the magma that was erupted again during the next caldera eruption. There was lowering in the previous two cycles but neither is as great as what is seen in the Lava Creek tuff. In the Huckleberry Ridge tuff the $\delta^{18}O_{quartz}$ values go from 8 to7‰ to 4 to 3‰ and in the Mesa Falls tuff the $\delta^{18}O_{quartz}$ values go from ~6‰ to 5‰ (Bindeman and Valley, 2001). This newly erupted material was then influenced by hydrothermal alteration and remelted again forming an even lower $\delta^{18}O$ magma. Recent work by Watts et al. (2011) confirmed this model by analyzing the $\delta^{18}O$ values of quartz and zircons from The Kilgore tuff (~4.5 Ma) of the Heise volcanic field (~6.6 to 4.4 Ma; Figure 1.1) and comparing these results to Yellowstone. When compared to Yellowstone, Watts et al. (2011) observed similar trends at Heise, with an original normal- $\delta^{18}O$ magma that was erupted and a progressive lowering of $\delta^{18}O$ after each successive eruption of around 3 to 4‰.

Boroughs et al. (2012) analyzed 56 different samples of rhyolites from a region spanning the Owyhee Plateau to the CSRP and found that only rhyolites in the WSRP have normal $\delta^{18}O$ values of above 6‰. There weren't any clear spatial or temporal correlations found with major/minor trace elements or radiogenic isotopes but Boroughs et al. (2012) found that the oxygen values are higher at the eastern and western margins of the CSRP and lowest near the Bruneau-Jarbidge volcanic field in the CSRP center. These low-$\delta^{18}O$ rhyolites are uniformly low and have an average value of 2.4‰ (Boroughs et al., 2012). This is unlike the Heise and

Yellowstone systems where the majority of erupted silicic units are normal and only the post collapse units are strongly depleted in $\delta^{18}O$ (Bindeman and Valley, 2001 and Watt et al, 2011).

To get a better understanding of the petrogenesis of the these magmas, it is important to test these models in other silicic volcanic fields to see if one model is more applicable in other settings or if both can be valid models for low-$\delta^{18}O$ silicic magma production. Since low-$\delta^{18}O$ rhyolites are found within large violent caldera systems it is essential to understand the processes and hazards involved in these large systems so that in the event of large scale eruption (i.e. Yellowstone) the public can better be informed and protected. The mid-Miocene Santa Rosa-Calico volcanic field (SC), northern Nevada (Figure 1.1) offers a good location to test these two competing models and the purpose of this study is to obtain $\delta^{18}O$ values for the SC silicic units that have an established (e.g. physical, temporal, spatial, geochemical/isotopic) context as well as to better understand the petrogenesis of the youngest silicic unit in the SC, the 15.5-15.8 Ma Cold Springs tuff. Since the SC is located directly adjacent to the Bruneau-Jarbidge and Owyhee Plateau areas studied by Boroughs et al. (2012) and the geologic context of the SC is well constrained by Brueseke (2006), Brueseke and Hart (2008), and studies by Vikre (1985, 1987, and 2007) focused on local mid-Miocene epithermal Au-Ag mineralization, it is an ideal location to test the competing models of low-$\delta^{18}O$ silicic magmatism. Additional emphasis will be directed toward the Cold Springs tuff, which not only is the youngest silicic unit present in SC, but is also made up of multiple cooling units that were erupted from a small caldera and has distinctly different Sr-Nd-Pb isotope values from the other older SC silicic units.

Regional Geology

During the Paleozoic, much tectonic activity affected western North America that is now preserved in the northern Great Basin (King et al., 2004). Two major collisions affected northern Nevada; the Antler Orogeny occurred during the late Devonian to Early Mississippian and was a collision between an island arc and the continent. During this event, Paleozoic rocks were thrust east along the Roberts Mountain Thrust (Hanson et al., 2000 and King et al., 2004). The second major orogeny, the Sonoma Orogeny, occurred between the Permian and Triassic and are associated with another major thrust fault (the Golconda Thrust), which thrust the Golcanda allochthon over the previously deformed sedimentary strata associated with Antler deformation (King et al., 2004). The Paleozoic Arc, which is made up of metamorphosed volcaniclastics,

mafic lavas, minor felsic lavas, shales, siltstones, sandstones, and limestones, is the basement for the Early Mesozoic arc assemblages in northwest Nevada and northern California and the Golcanda allochthon is the basement for the early Mesozoic shelf terrain (Wyld, 1992; Wyld, 2000). The Luning-Fencemaker fold and thrust belt in Nevada was a third shortening event that occurred in the Jurassic before 142 Ma and possibly as early as ~190 Ma which saw basal terrains (composed of deep marine clastics) thrust eastward onto the continental margin along the Fencemaker thrust fault (Wyld et al., 2003). Throughout the Early Triassic, uplift and subsidence events deposited carbonates, there was coarse siliciclastic deposition, and some volcanism in the basal terrain and the continental shelf region (Wyld, 2000). In the Late Triassic, flooding of the shelf caused the deposition of muds and quartz-rich sand derived from the Precambrian craton and these deposits are greater than 1.8 km thick (Wyld, 2000).

A fourth shortening event began during the early Cretaceous and continued to the early Tertiary and was the Sevier Orogeny (King et al., 2004). Sevier deformation caused almost 50% crustal thickening and thrusting to the east along the Sevier fold and thrust belt, which extends from northeastern NV into central UT, and to the north into Canada (King et al., 2004). Extension of the Great Basin began in the Oligocene after the Sevier Orogeny and continued into the Miocene along low angle faults (King et al., 2004; Henry et al., 2011). During, the mid-Miocene, around 17 to16 Ma, widespread extension related to the modern Basin and Range extension began possibly due to the Pacific-North American plate boundary changing to a transform boundary, which was influenced by the falling remnant Farallon slab that allowed the mantle to warm the Mesozoic orogenic plateau to the east (Colgan and Henry, 2009). This produced northeast trending (~282° extension direction) faults across the area (Colgan, 2013). At around 16.7 Ma, concurrently with the onset of bimodal basalt-rhyolite volcanism, a rift began to form in northern Nevada, the northern Nevada Rift. This 250 km long rift originated at the onset of the Yellowstone hotspot, between 17 to 15 Ma, and is primarily composed of several mafic dikes orientated in a north-northwest direction (Colgan and Henry, 2009; Colgan, 2013; Brueseke et al., in press). It was inferred in the past that the 245-250° orientation of the rift represented the Basin and Range extension direction in the mid-Miocene and switched to the modern day direction of 290-300° (Colgan, 2013). Colgan (2013) reevaluated the rift orientation with existing and new data and showed that modern day extension (290-300°) was the same as during the mid-Miocene and that the northern Nevada Rift was superimposed on the regional

stress field due to the Yellowstone hotspot (Colgan, 2013). Furthermore, all of the Miocene extension allowed mafic magmas to move into to the upper crust and also helped create multiple epithermal precious metal deposits via circulation of hydrothermal fluids, metals, and metalloids (Brueseke and Hart, 2008; Saunders et al., 2008).

Since many terrains have been accreted to the North American continent, the composition of accreted terrain crust will differ from the older North American Craton. Knowing the location of the boundary between those two provides better insight into the petrogenesis of the different magmatic systems found in the Great Basin. Various studies have tried to pinpoint the exact location of the edge of the Precambrian North American Craton. Kistler and Peterson (1973 and 1978) Armstrong et al. (1977), and Leeman et al. (1992), show that the western boundary of the North American craton is demarcated at $^{87}Sr/^{86}Sr$ 0.706 isopleth as recorded in Mesozoic and younger igneous rocks. As you move west, you enter a transition zone that lies between the Precambrian craton and accreted terrains from the Mesozoic collisions, (between the $^{87}Sr/^{86}Sr$ 0.706 and $^{87}Sr/^{86}Sr$ 0.704 isopleths; Figure 1.1). King et al. (2004) used zircons from Mesozoic granitoid plutons throughout northern Utah and Nevada, since zircons are resistant to any alteration, to see where the craton boundary lies based on $\delta^{18}O$ values. What they determined is that there is a major crustal boundary that coincides with the previously documented $^{87}Sr/^{86}Sr$ 0.706 isopleth. High $\delta^{18}O$ values were found to the east of the 0.706 isopleth and lower $\delta^{18}O$ values were found to the west. Lower $\delta^{18}O$ values in the plutons indicate less evolved crustal material involved in melt production or a lower proportion of evolved crustal material present in the studied granitoids (King et al., 2004).

Igneous activity in northern Nevada began in the Mesozoic with the formation of the Sierra Nevada arc and over time, arc volcanism progressed eastward to Colorado and ultimately ceased at the time of the Laramide Orogeny (~80 to 40 Ma). There is some debate as to how magmatism could have occurred so far inland from the trench, though it is commonly attributed to the progressive shallowing of the Farallon Plate (Lipman et al., 1971 and Coney and Reynolds, 1977). Most of the granitoid plutons in Nevada are Cretaceous in age and were formed from this pulse of magmatism, that moved inland. Granitoid rocks in the study area (Figure 1.4), are an example of the Cretaceous arc magmatism in northern Nevada. There are two distinct groups that make up these plutons, the Santa Rosa-Andorno Group (103-102 Ma) and the Granite Peak-Sawtooth Group (~95 Ma) (Stuck, 1993; Brown et al., 2011) (Figure 1.4). These

intrude Late Triassic to Early Jurassic metapelitic rocks. Around these intrusions are zones of contact metamorphism that deform previously regionally metamorphosed metapelites (Compton, 1960; Taylor, 1968). The Santa Rosa-Andorno Group is made up of mostly biotite granodiorite with minor amounts of quartz monzodiorite and granite and quartz monzonite (Stuck, 1993). This group is also cross cut by Cretaceous aplite dikes and likely mid-Miocene olivine diabase dikes (Stuck, 1993). The Granite Peak-Sawtooth Group is composed of granodiorite to granite in the Sawtooth Stock and porphyritic biotite granodiorite to fine grained biotite granite in the Granite Peak Stock. Aplite dikes are also commonly found in this group (Stuck, 1993).

The Idaho Batholith, located in the Rocky Mountains of central Idaho and Montana, is another large mass of intrusive bodies that formed during the Jurassic to Eocene, with the majority of the ages being Cretaceous (Criss and Taylor, 1983; Gaschnig et al., 2010; Gaschnig et al., 2011) (Figure 1.5). The Atlanta lobe to the south and the Bittersweet lobe to the north are broad classifications of the different sections of the batholith. Both lobes are dominated by peraluminous granites. The Atlanta lobe is composed mostly of peraluminous 83-67 Ma biotite granodiorites (Gaschnig et al., 2011). The Bittersweet lobe contains mostly peraluminous 66-53 Ma biotite granodiorites that are very similar to the ones found in the Atlanta lobe (Gaschnig et al., 2011). There is also a small belt of fringing metaluminous plutons (75-69 Ma) that have a range of compositions from quartz diorite to granodiorite (Gaschnig et al., 2011). Both of these plutons are intruded by Eocene plutons (51-44 Ma) associated with the Challis Volcanics. These intrusions can be divided into a pink granite suite that resembles A-type granites and a quartz monzodiorite suite (Gaschnig et al., 2011). Hydrothermal systems developed around these intrusions, and altered the upper crustal rocks adjacent to the intrusions causing the zones of low-$\delta^{18}O$ values as described earlier (Criss and Taylor, 1983).

Starting from the Late Cretaceous to Eocene, with the greatest activity occurring during the latter, the northwestern margin of North America experienced a plus of magmatism that was initiated by slab rollback of the Farallon Plate with the North American Plate to its current position. Most of the magmatism was intermediate in composition and included the Challis and Absaroka volcanics (Norman and Leeman, 1989). This subduction related intermediate composition activity continued into the Oligocene and up until the mid-Miocene erupting the

Salmon Creek volcanics in northern Idaho and various other local vents in the region (Norman and Leeman, 1989; Norman and Mertzman, 1991; Brueseke and Hart, 2009).

Extensive volcanism began again during the mid-Miocene in the Pacific Northwest and northern Great Basin. The most voluminous volcanism was characterized by the eruption of the Columbia River Basalt Group from ~17-14 Ma. These flood basalts were erupted from N-NW trending feeder dikes and shield volcanoes (Church, 1985, Camp et al., 2003, Camp and Ross, 2003, Brueseke et al., 2007, and Brueseke and Hart, 2008). Figure 1.1 shows the major geologic phenomena of the Mid-Miocene that shaped the region. At the same time and ending around 12 Ma, silicic magmatism occurred across the same region (Brueseke and Hart, 2008). These silicic volcanics were erupted from numerous eruptive loci such as the McDermitt volcanic field, the Lake Owyhee volcanic field, the Juniper Mountain volcanic field, the Santa Rosa-Calico volcanic field, and the Jarbidge volcanic field along with numerous small volume rhyolite centers (Jordan et al., 2004, Brueseke and Hart, 2008, Callicoat, 2010, Hasten, 2012; Coble and Mahood, 2012). The Owyhee Plateau and Juniper Mountain volcanic field lie just south of the Western Snake River Plain (WSRP). Adjacent to the Owyhee Plateau in the Owyhee Mountains are ~16.6 Ma basalt flows that are overlain by ~16 Ma rhyolite lavas (Hasten, 2012). Silicic volcanism in the region was sourced in the Juniper Mountain volcanic field from about 14.7-13 Ma (Ekren et al., 1984; Manley and McIntosh, 2002). Underneath these Miocene volcanics lie Cretaceous granitoid which are part of the Idaho Batholith (Kolb et al., 2011). The rhyolite lavas erupted from the Juniper Mountain volcanic center are not associated with caldera-forming activity and are composed of voluminous lava flows (Ekren at al., 1984; Manley and McIntosh, 2002).

At ~14-12 Ma silicic volcanism activity began to decline in abundance and with respect to the Owyhee Plateau, became focused along two age progressive tracks; one younging to the northwest creating the Oregon High Lava Plains and the other to the northeast creating the Snake River Plain-Yellowstone track (Jordan et al., 2004; Brueseke and Hart, 2008). High Lava Plains volcanism is compositionally bimodal with silicic volcanism being more voluminous than basaltic magmatism, and is characterized by rhyolite lavas and domes that get younger to the northwest and basalt eruptions that do not show any age progression (Jordan et al., 2004 and Ford et al., 2013). The WSRP formed during a period of NE-SW extension between 12-7 Ma and its southern margin overlaps with the Bruneau-Jarbidge volcanic field in the CSRP. The

Bruneau-Jarbidge volcanic field (~14-8 Ma) is characterized by voluminous rhyolite lavas that erupted after the caldera-forming volcanism of the Cougar Point tuff (Bonnichsen et al., 2008; Almeev et al., 2012). The Cougar point tuff erupted from 12.7 to 10.5 Ma and is a composite unit composed of nine ash-flow tuff sheets (Nash et al., 2006; Bonnichsen, et al., 2008; Cathey and Nash, 2009). As one moves towards the northeast toward Yellowstone, each SRPY silicic volcanic field gets progressively younger. This includes the 10.5-8.5 Ma Twin Falls volcanic field, the 10.2-9.2 Ma Picabo volcanic field, the 6.6-4 Ma Heise volcanic field, and the dormant Yellowstone volcanic field that initiated at around 2.05 Ma (Nash et al., 2006; Watts et al., 2010). The mechanism for generating the YSRP silicic magmas is likely crustal melting by upwelling mafic magma (Pierce and Morgan, 1992 and Boroughs et al., 2012). There is debate as to whether or not the basalts are related to a deep mantle plume (Camp and Ross, 2004) or whether they formed solely from upper mantle (e.g. asthenosphere and/or lithosphere) convection and extension (Christiansen et al., 2002; Leeman et al., 2009). Moving eastward from the craton boundary the crust becomes fairly heterogeneous and the composition of the Cenozoic rhyolites move toward lower temperatures, more evolved compositions, are more isotopically variable, and have lower eruption frequencies (Pierce and Morgan, 1992, Nash et al., 2006, and Boroughs et al., 2012). In addition to Cretaceous and Eocene modification of the crust (e.g. Idaho Batholith and Challis magmatism), further modification occurred from the injection of basalts into the lower to mid-crust throughout the Cenozoic (Bonnichsen et al., 2008, McCurry and Rodgers, 2009, Boroughs et al., 2012).

Rhyolites in the Snake River Plain are A-type (anorogenic) in composition and it is commonly thought that they are the product of partial melting of the continental crust. Christiansen and McCurry (2008) used trace elements to develop a possible partial melting model to determine how the Snake River Plain rhyolites were formed. Instead of partial melting of upper crustal rocks or lower crustal granulite, their best fit model involved partial melting of a gabbroic equivalent (4 to 8%) of the basalts found in the Snake River Plain. These rhyolite partial melts, which are less dense, rise into the middle and upper crust. In some cases cooling in the upper crust could create large shallow magma chambers that form similar caldera systems like Yellowstone (Christiansen and McCurry, 2008). McCurry and Rodgers (2009) determined that the maximum crustal input into the rhyolite petrogenesis could only be 40% by using the Neodymium Crustal Index (NCI) of DePaolo (1992). From this, McCurry and Rodgers (2009)

created a mass-balance model that determined a layer of gabbro 14 km thick was added to the continental crust along the Yellowstone hotspot and Snake River Plain. From this addition of gabbro, a batholith 5-10 km thick developed under the Snake River Plain (McCurry and Rodgers, 2009). The volume of this batholith is comparable to other batholiths found in western North America. Oxygen isotopes also play a large role in determining the amount of mantle or crustal input. Since initially erupted rhyolites in the eastern Snake River Plain were found to have $\delta^{18}O$ values between 5.5‰ to 7‰, which are best indicators of the original melt, and Snake River Plain basalts have an average $\delta^{18}O$ value between 4.8 to 5.2‰ whereas Archean crustal xenoliths have an average $\delta^{18}O$ value of 6.7 to 9.2‰, the simple mass-balance model limits the basalt input to <75% (McCurry and Rodgers, 2009). When this number is combined with the NCI number, the data is consistent with having only a maximum of 40% crustal contribution (McCurry and Rodgers, 2009). However, a study performed by Nash et al., (2006) analyzing NCI values on rhyolites along the Yellowstone hotspot track came up with 60-80% crustal contribution by basing the crustal component on the Proterozoic crust and not Archean crust. Since McCurry and Rodgers (2009) propose that the Central Snake River Plain and Eastern Snake River Plain are underlain by Archean crust as opposed to Proterozoic crust based on recent zircon work in the region, it is possible then that the differences seen between the two NCI values of McCurry and Rodgers (2009) and Nash et al. (2006) are attributed to the different types of crustal composition.

Local Geology

The Santa Rosa-Calico volcanic field (SC) lies in northern Nevada, just west of the northern Nevada Rift and southwest of the Snake River Plain (Fig. 1.1). It is bounded by the Owyhee Plateau to the north and east, a basin-bounding normal fault at the north end of Paradise Valley to the south, and the Quinn River valley to the east (Brueseke and Hart, 2008; Figure 1.7). Under the mid-Miocene volcanics, lie intensely deformed Triassic metasedimentary rocks that have been intruded by two groups of Cretaceous granitoids, the Santa Rosa-Andorno group (~103 Ma) and the Granite Peak-Sawtooth group (~94 Ma) (Brown et al., 2011). There are also distinct compositional and textural differences between the two groups based on petrographic, geochemical, and isotopic data. The older Santa Rosa-Andorno group is composed of biotite granodiorite with minor amounts of quartz monzodiorite and granite and quartz monzonite and are metaluminous to weakly peraluminous. This group has a range of SiO_2 from 64-71 wt. %, is

enriched in Ba and Rb, and is lower in $^{87}Sr/^{86}Sr_i$ (0.704) and higher in $^{144}Nd/^{143}Nd_i$ (0.51270) (Stuck, 1993). The Granite Peak-Sawtooth group is composed of granodiorite to granite in the Sawtooth Stock and porphyritic biotite granodiorite to fine grained biotite granite in the Granite Peak Stock and are all peraluminous. The range of SiO_2 in this group is from 72-76 wt. %, concentrations of Cr, Ni, Sc are very low (<2 ppm), and $^{87}Sr/^{86}Sr_i$ (0.7055-0.7062) is higher and $^{144}Nd/^{143}Nd_i$ (0.51240-0.51250) is lower than the Santa Rosa-Andorno group (Stuck, 1993). There are also fined-grained aplite dikes found in both groups. The aplite dikes in the Santa Rosa-Andorno Group are weakly peraluminous whereas the aplite dikes in the Granite Peak-Sawtooth Group have more of an alumina saturation which is consistent with the presence of garnet (Stuck, 1993). Aplite $^{87}Sr/^{86}Sr$ values is lower than the most evolved host rocks but the Nd values are comparable. Stuck (1993) concluded that the aplites represent late stage remnants of the original melt. Based on the observations of both groups it was concluded that the Santa Rosa-Andorno Group is geochemically similar to the Sierra Nevada batholith in that they are both I-type granites and the Granite Peak-Sawtooth Group is similar geochemically to the Idaho Batholith in that they both have S to A-type characteristics (Stuck, 1993; Brown et al., 2011).

Volcanism in the SC began at 16.7 Ma and along with silicic magmatism which dominated the volumes locally, there were also mafic and intermediate products erupted (Brueseke and Hart, 2008). Mafic through silicic activity in the western SC took place between 16.4-14 Ma and occurred coevally with volcanism at the McDermitt and Lake Owyhee volcanic fields. Fallout and flow facies of ash-flow tuffs are found along the western flanks of the Santa Rosa Range and are possibly associated with caldera eruptions from McDermitt (Brueseke and Hart, 2008). There is also a thick package of basalt that likely erupted from Steens Mountain (Figure 1.7) along the western flanks of the SC; these are different lavas than the locally erupted mafic package (Brueseke and Hart, 2008 and Brueseke, 2011). In the central part of the SC there is a topographic depression (e.g. Goosey Lake depression) that is cross-cut by N-NW trending faults. The Goosey Lake depression formed via syn-magmatic extension in the Miocene (Brueseke, 2006; Brueseke and Hart, 2008) and within this larger topographic low, is a small caldera (2.5 by 3.5 km) that is the only caldera present in the volcanic field. The only unit to have erupted from this caldera is the ~15.5 to 15.8 Ma Cold Springs tuff, the youngest SC silicic unit (Brueseke and Hart, 2008). Following the nomenclature of Brueseke and Hart (2008), SC silicic units can be found primarily in the western and eastern SC with five units in the west

[Hinkey Summit-Coal Pit Peak dacites-rhyolites (Thc), Eightmile Mountain lava flows (Tem), porphyritic rhyolite (Tpr), western margin lava flows (Twsc), and flow-banded rhyolite lava (Tbr)], three in the east [(Calico Mountain area silicic units (Tcm), Odell Mountain area silicic units (Tom), and Coyote Mountain-Zymns Butte area silicic units (Tct)], and the Cold Springs tuff (Tcst) from the central portion of the volcanic field. The five silicic units in the west erupted over a 1 myr time interval and come from separately evolving magmatic systems from each other, as well as from those from the east (Brueseke and Hart, 2008). The three units from the east erupted from 16.5 to 16.4 Ma and have been petrogenetically tied to one magmatic system (Brueseke and Hart, 2008). The majority of all of the silicic units erupted from domes and fissures and as previously mentioned, the only unit to have erupted from a caldera is the Cold Springs tuff (Figure 1.7) (Brueseke and Hart, 2008).

Initial volcanism in the SC began with mafic lava flows in the southwestern part of the volcanic field. The first erupted silicic unit, was Hinkey Summit-Coal Pit Peak dacites to rhyolites (Thc), which occurred at 16.4 Ma (Brueseke and Hart, 2008). These dacites and rhyolites form thick (15-120 m) lavas that stratigraphically lie over the older mafic package. This unit is easily distinguished by the abundant feldspar phenocrysts in a light gray to purple matrix (Brueseke and Hart, 2008). The exact location of the eruptive vent or loci is not known but based on thick exposures the source is inferred to be in the Hinkey Coal-Pit area along the southern margin of the volcanic field (Brueseke and Hart, 2008). Around the same time that the Hinkey Summit-Coal Pit Peak unit was erupting, Coyote Mountain-Zymns Butte area (Tct) lavas and welded ash-flow tuffs were erupting in the southeast from two eruptive centers and one dome. North of Coyote Mountain, at essentially the same time, Odell Mountain area (Tom) and Calico Mountain area (Tcm) silicic lavas were erupting from local domes (Brueseke and Hart, 2008). At ~16.2 Ma, western margin lavas (Twsc) were erupted. These are characterized by plagioclase, potassium feldspar, clinopyroxene, orthopyroxene, sparse biotite, and quartz (Brueseke and Hart, 2008). At 16.2 Ma, silicic volcanism became concentrated in the southwest portion of the SC and ceased in the east. Porphyritic rhyolite lavas (Tpr) erupted from two well defined domes and abundant Tpr shallow intrusive bodies are found adjacent to both domes, including numerous N-NW trending dikes (Brueseke and Hart, 2008). This is the only unit in the SC that contains abundant hydrous minerals (e.g. hornblende and biotite). These rocks also contain plagioclase and potassium feldspars, quartz, and Fe-Ti oxides (Brueseke and Hart,

2008). At ~15.8 Ma, Eightmile Mountain lava flows (Tem) were erupted from fissures in the northwestern part of the SC. They slightly resemble the Hinkey Summit-Coal Pit Peak unit lavas in hand sample (e.g. feldspar phenocrysts in a purple-gray matrix) (Brueseke and Hart, 2008). As mentioned earlier, the youngest unit in the SC is the Cold Springs tuff (Tcst). This unit is characterized by basal fall deposits that are overlain by ~2 m of ground surge, which grades upwards into the lower section of the main ash-flow tuff deposit (Brueseke and Hart, 2008). An oval geomorphic feature is present in the western Goosey Lake depression that is visible in aerial images and delineated by faults (Figure 1.6). Cold Springs tuff flows are thickest around this oval feature and the only lithic fragments present identified thus far in the Tcst, are located in deposits that crop out here (Brueseke and Hart, 2008). Rare, imbricated pumice fragments are seen in one location north of this oval feature; all of this information was interpreted by Brueseke (2006) and Brueseke and Hart (2008) to suggest that this feature is the caldera-source for the Cold Springs tuff. Cold Springs tuff distal fall deposits have been found as far north as the Silver City mining district near Silver City, Idaho in the Owyhee Mountains (Hasten, 2012).

Geochemistry of SC Units

The following summary of geochemistry of SC silicic units comes from Brueseke and Hart (2008), while SC granitoid data is from Stuck (1993) and Brown et al. (2011); all are summarized below. An alkali silica diagram (Figure 1.8) from Le Bas et al. (1986) shows that most of the silicic units, defined by their physical, petrologic, and geochemical characteristics, are classified as rhyolites with a few lower silica samples showing up as more intermediate in composition and plotting in the trachydacite to dacite fields. Also the diagram shows the subalkaline array of the units.

The silicic units are also metaluminous to peraluminous and not peralkaline like some other silicic eruptive products sourced from the McDermitt and Lake Owyhee volcanic fields (Brueseke and Hart, 2008). This can be seen in Figure (Figure 1.9) which is Shand's alumina saturation index (ASI) (Shand, 1943). The majority of the samples have an ASI of about 1 but can be found in a range from 0.8-1.2 with the ASI increasing as SiO_2 increases.

According to the classification of Pearce et al. (1984) (Figure 1.10), most of the silicic units of the SC fall within the within plate granite (WPG) field. A few samples from two of the units, Eightmile Mountain lava flows (Tem) and porphyritic rhyolite lavas (Tpr), plot in the

volcanic arc granite (VAG) field showing the diversity within the units, the western margin lavas (Twsc) unit plots completely within the VAG field. These differences again highlight the geochemical differences of SC units reflecting their different peterogenetic histories. The Cretaceous granitoids of the SC are also plotted in the diagram and both groups plot in the VAG field which is consistent with the subduction-related magmatism occurring when these granitoid groups were being formed (Farmer and DePaolo, 1983). Figure 1.11 is a diagram of granitoid classification from Whalen et al. (1987) and shows that most of the silicic SC units are A-type rhyolites. A-type granitoids typically occur in within-plate settings and are thought to form anorgenically via melting of existing crust. I-type granitoids typically form in volcanic arcs (e.g. an "igneous source"; Frost et al., 2011).

Major Element Geochemistry

SC silicic units display a SiO_2 range of 67-76 wt. % (Hinkey Summit-Coal Pit Peak); 69-78 wt. % (porphyritic rhyolite); 65-74 wt. % (Eightmile Mountain); >76 wt. % (flow-banded rhyolite); 63-74 wt. % (western margin lava flows); >73 wt. % (Odell Mountain area silicic units); 63-76 wt. % (Calico Mountain area silicic units); 64-75 wt. % (Coyote Mountain-Zymns Butte area silicic units); and 67-77 wt. % (Cold Springs tuff). Figure 1.12 shows Harker diagrams for each of the units. MgO, FeO*, CaO, Al_2O_3, TiO_2, and P_2O_5 all show an inverse relationship as SiO_2 wt. % increases, the major element wt. % decreases. For K_2O, as wt. % increases, so does the wt. % SiO_2. Na_2O is invariant with respect to SiO_2.

Trace Element Geochemistry

Figure 1.13 shows selected trace element concentrations against wt. % SiO_2. There are major differences that help to differentiate between the units (in conjunction with field and geochronologic data). The Western margin lava flows (Twsc) are enriched in Ni and Ba more so than the other units. With Sc and Sr, there is an inverse relationship as SiO_2 increases, the concentration of Sc decreases. Rb concentrations increase as SiO_2 increases. All units show a wide range of Zr concentrations, with the Cold Springs tuff easily standing out being the only unit with Zr concentrations greater than 650 ppm. Most of the silicic units are uniform in La and Nb concentrations expect for the Cold Springs tuff which shows a higher enrichment in both elements, at a given SiO_2 concentration.

Figure 1.14 depicts diagrams of the trace elements normalized to upper continental crust from Taylor and McLennan (1985). Again differences in concentrations of the units are apparent. It is quite clear that the Cold Springs tuff units has enrichments in La, Sm, Y, Yb, and Lu, relative to the other silicic units. Also the Cold Springs is not as depleted in Sr or Ti as compared to the other units. Overall, the younger Cold Springs tuff shows significant trace element differences from the older silicic units of the SC, consistent with derivation from a different magmatic system (Brueseke and Hart, 2008).

Radiogenic Isotope Geochemistry

SC silicic samples and Santa Rosa-Andorno/Granite Peak-Sawtooth granitoids with radiogenic isotope data are depicted in Figures 1.15 to 1.17 (data from Stuck, 1993; Brueseke and Hart, 2008; Brown et al., 2011). Figure 1.15 A and B are plots of initial $^{87}Sr/^{86}Sr$ and $^{143}Nd/^{144}Nd$ as a function of wt. % SiO_2. The Santa-Rosa-Andorno group isotopic values for $^{87}Sr/^{86}Sr$ and $^{143}Nd/^{144}Nd$ were calculated at 16.5 Ma (Stuck, 1993; Brueseke and Hart, 2008). With regards to $^{87}Sr/^{86}Sr_i$, most of the SC units overlap with each other, except for the porphyritic rhyolite which shows a range of $^{87}Sr/^{86}Sr_i$ values from 0.7048 to 0.7076. The Granite Peak-Sawtooth granitoids also show higher $^{87}Sr/^{86}Sr_{16.5\ Ma}$ values along with an increase in alumina saturation. This points to a Precambrian crustal component in their petrogenesis, because granitoids throughout the western part of North America that have a $^{87}Sr/^{86}Sr$ value of $\geq$0.706 and are higher in alumina saturation, are assumed to be sourced from Precambrian crust or crust that contains a significant component of Precambrian detritus (Struck, 1993; King et al., 2004). Mafic SC units do not overlap with SC intermediate and silicic units. SC intermediate units overlap with one western margin lava flow sample (Twsc) (Figure 1.5A). In regard to $^{143}Nd/^{144}Nd_i$ (Figure 1.15B), there are distinct differences between the SC silicics and granitoids as evident in two different groups. One group contains most of the SC silicic units, along with the Santa Rosa-Andorno granitoids; the other is made up of the Cold Springs tuff (Tcst) and Granite Peak-Sawtooth granitoid. The same relationships are clear in a plot of $^{87}Sr/^{86}Sr_i$ vs. $^{143}Nd/^{144}Nd_i$ (Figure 1.16). The Cold Springs tuff and Granite Peak-Sawtooth group granitoid rocks have lower $^{143}Nd/^{144}Nd_i$ values than the rest of the SC silicics and Santa Rosa-Andorno group granitoids. Intermediate SC units overlap with all SC silicic units except for the Cold Springs tuff (Tcst).

In Pb isotope space, (Figure 1.17A) the Cold Springs tuff (18.710-18.716) is lower in $^{206}Pb/^{204}Pb$, compared to the other units and granitoids (19.021-19.213). The Cold Springs (15.614-15.640) do however fall within the range of $^{207}Pb/^{204}Pb$ values (Figure 1.17B) for the rest of the units (15.608-15.657). The CST also has higher $^{208}Pb/^{204}Pb$ (38.968-39.104) values than the other silicic units and granitoids (38.703-38.914). In regards to the SC mafic and intermediate units, the SC mafic units overlap with Eightmile Mountain (Tem), Coyote Mountain-Zymns Butte (Tcm), and Odell Mountain (Tom) units in Figure 1.17A, where as in Figure 1.17B, SC intermediate units overlap with SC silicics except for the Cold Springs tuff (Tcst) which in both plots, do not overlap with the mafic or intermediate units.. Overall, the Cold Springs tuff shows marked geochemical and radiogenic isotope differences from the other SC silicic units, but similarities to Granite Peak-Sawtooth group granitoids, implying a potential peterogenetic link (Brueseke, 2006; Brueseke and Hart, 2008).

Local Hydrothermal Activity and Epithermal Mineralization

On the northern part of the Santa Rosa Mountain Range on the slope of Buckskin Mountain (and extending to the north) just west of the Goosey Lake depression, lies the National District which has been historically mined for gold, silver, and mercury (Figure 1.6). Within the district, north-south faults contain primarily quartz-hosted epithermal vein deposits (Vikre, 1985). These veins cut a thick package of Mid-Miocene volcanics from the SC. There are three main veins that contain the precious metal deposits in the district. The Bell vein is located on the eastern slope of Buckskin Mountain and strikes north-south. It is completely enclosed by rhyolite lavas and four hydrothermal stages can be observed within the vein mineralogy. Stage 1 does not comprise any precious metal-bearing minerals, but quartz along with kaolinite+muscovite fill vugs (Vikre, 1985). Stage 2 is composed of banded quartz, clays, sulfides (pyrite, marcasite), selenides, sulfosalts and electrum. More than 95% of the phases in this stage are quartz and clays. Gold and silver bearing minerals, such as electrum, pyrargyrite, miargyrite, silver selenides, and tetrahedrite, are also found (Vikre, 1985). Stage 3 is composed of sulfur-bearing phases. These sulfides can be found in thin, wavy bands that are parallel to Stage 2 bands. The main minerals formed in this stage are marcasite, pyrite, aresenopyrite, and stibnite, kaolinite, chalcedonic silica with rare cinnabar, and pyrite. Stage 4 is composed of vug and fracture-filling quartz and sulfides. Minerals present in this stage are quartz, chalcedonic

silica, stibnite, and rare cinnabar and pyrite (Vikre, 1985). The other two major veins present are the National and Birthday veins.

The National vein strikes north-south and is enclosed by porphyritic rhyolite (Tpr), andesite-dacites of Staunton Ridge (Tad_2), and quartz latite. The precious metals are only found in quartz. The veins are composed of quartz, pyrite, marcasite, arsenopyrite, electrum, tetrahedrite, berthierite, stibnite, sphalerite, chalcopyrite, silver sulfosalts, and galena. The Birthday vein again strikes north-south and is enclosed by porphyritic rhyolite (Tpr), andesite-dacites of Staunton Ridge (Tad_2), and quartz latite. The minerals found in the vein consists of coarse-grained quartz, pyrite, marcasite, tetrahedrite, antimony-arsenic sulfide, silver sulfosalts, sphalerite, chalcopyrite, galena, and arsenopyrite. Electrum is rarely seen in this vein (Vikre, 1985). In the veins near the National district, two types of breccias are found that have been altered by hydrothermal activity. Tectonic breccias are near veins and are formed due to brittle deformation along faults. These tectonic breccias contain fragments of chalcedony to alunite, kaolinite, or illite-montmorillonite which depends on the amount to hydrothermal zoning (Vikre, 1985). Bilithic breccias predate hydrothermal activity since the veins cross-cut the breccias (Vikre, 1985). These breccias are also not related to faults and the matrix is composed of hydrothermal phases which include the following minerals: chalcedonic silica, alunite, kaolinite, and illite-montmorillonite depending on the hydrothermal zoning (Vikre, 1985).

The timing of vein formation and metal deposition began at about 16.1 Ma, with sinter deposits and silicification and mercury mineralization of the underlying rhyolite, epiclastic deposits, and volcanoclastic deposits, and formed veins at depth (Vikre, 1985; Vikre, 2007). This mineralization is the first of three hydrothermal events. The second event is when the sinter, rhyolites and the clastic rocks were altered by acid-sulfate fluid and the matrices and rock fragments of the clastics were altered to alunite and clay minerals. Quartz and barite were also deposited. This event occurred between 15.8 and 15.6 Ma (Vikre, 2007). The final event occurred when opal-A replaced the matrices, rock fragments and alunite. The timing of the final event was $\leq$ 15.6 Ma. The hydrothermal system was active for about 500,000 years and the end of this hydrothermal system coincides with Cold Springs tuff volcanism (Vikre, 1987; Brueseke and Hart, 2008; Vikre, 2007; Brueseke, 2011).

Vikre (1987) determined the oxygen isotope compositions of vein minerals to get a better understanding of the hydrothermal system. Miocene groundwater was calculated to have a $\delta^{18}O$

value of -10.7‰. The hydrothermal fluids have various $\delta^{18}O$ values ranging from -12‰ to +6‰ (Figure 1.19) (Vikre, 1987). Three whole rock samples from the Eightmile Mountain unit (Tem) were analyzed for $\delta^{18}O$ adjacent to the Bell vein (Vikre, 1985; Vikre, 1987). All three of the rhyolites were found to be depleted in oxygen with values of 4.7, 4.1, and 2.1‰. The 2.1‰ value is from a drill core section located 2,350 ft. below the paleosurface. The other samples were taken from 500 ft. and 1,000 ft. below the paleosurface (Vikre, 1987).

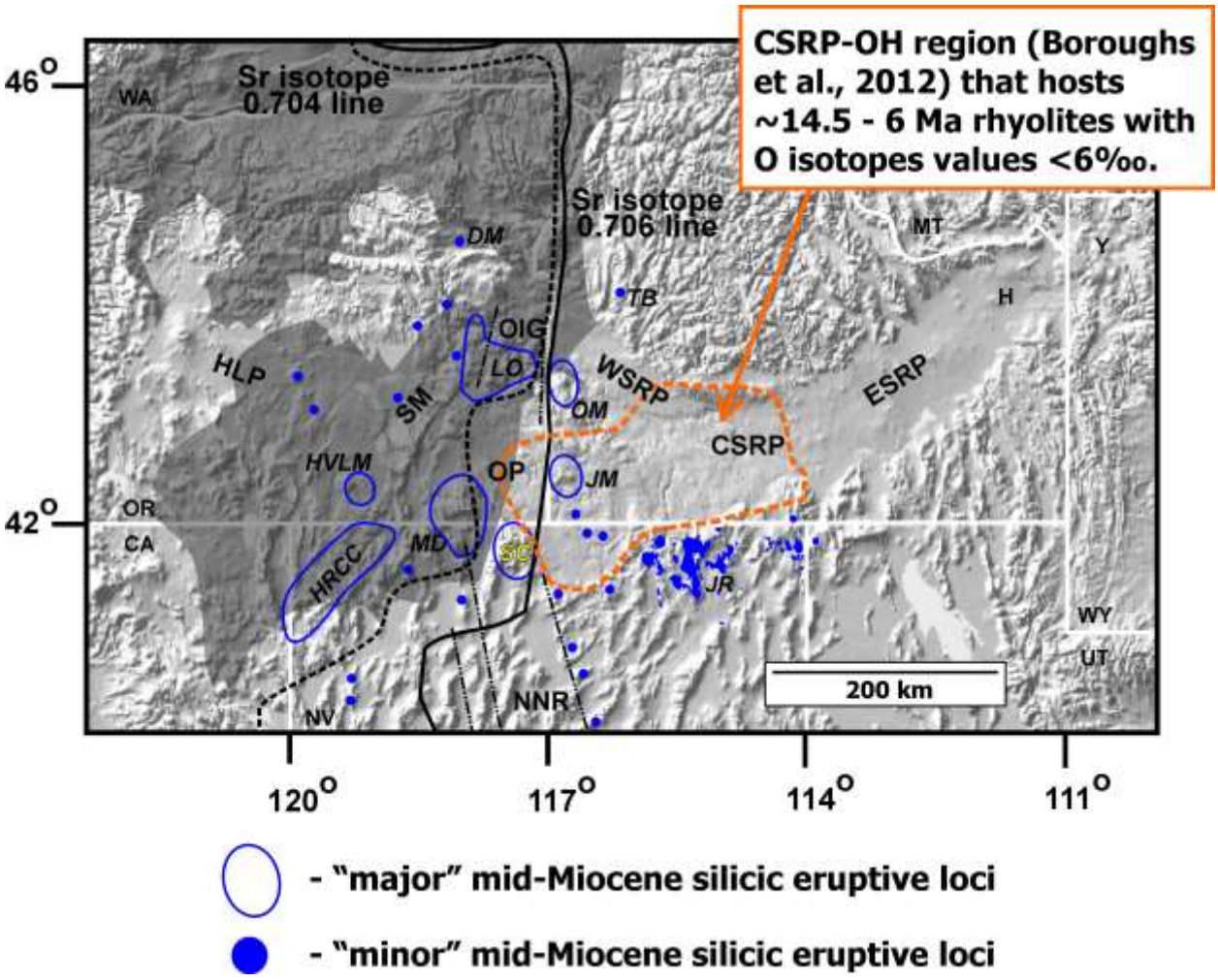
CSRP-OH region (Boroughs et al., 2012) that hosts ~14.5 - 6 Ma rhyolites with O isotopes values <6‰.
46°
42°
120°
117°
114°
111°
WA
OR
CA
NV
MT
Y
H
WY
UT
Sr isotope 0.704 line
Sr isotope 0.706 line
DM
TB
OIG
LO
HLP
SM
WSRP
OM
ESRP
CSRP
HVLM
OP
JM
MD
SC
HRCC
JR
NNR
200 km
- "major" mid-Miocene silicic eruptive loci
- "minor" mid-Miocene silicic eruptive loci

Figure 1.1: Regional Map

Map of the northwestern United States depicting selected Cenozoic tectonomagmatic features (after Brueseke and Hart, 2008). Gray shading depicts the region where mid-Miocene Columbia River (WA-OR-ID) and Steens (OR-NV-ID-CA) flood basalt lavas crop out. Magnetic anomalies corresponding to zones of lithospheric extension/mafic magma emplacement and mapped extensional features (e.g. the northern Nevada rift [NNR], the Oregon-Idaho graben [OIG], and others) are depicted as dashed black lines. The SC is labeled in yellow. The location of large mid-Miocene volcanic fields are depicted: MD, McDermitt; LO, Lake Owhyee; HRCC, High Rock Caldera Complex; SC, Santa Rosa-Calico volcanic field; JR, Jarbidge Rhyolite domes and flows; JM, Juniper Mountain volcanic center; OM, Owyhee mountains and Silver City district centers; DM, Dooley Mountain; TB, Timber Butte; HVLM, Hawks Valley-Lone Mountain complex. Blue dots are other coeval silicic eruptive loci. Y, Yellowstone volcanic field; H, Heise volcanic field. HLP, Oregon high lava plains; OP, Owyhee Plateau; WSRP, western Snake River plain; CSRP, central Snake River plain; ESRP, eastern Snake River plain. The initial $^{87}Sr/^{86}Sr$ 0.706 and 0.704 isopleths are depicted as dotted and dashed black lines. These are commonly interpreted to define the western edge of the Precambrian North American craton (the 0.706 isopleth), and a zone of transitional lithosphere (after Armstrong et al., 1977; Kistler and Peterman, 1978; Leeman et al., 1992; Crafford and Grauch, 2002).

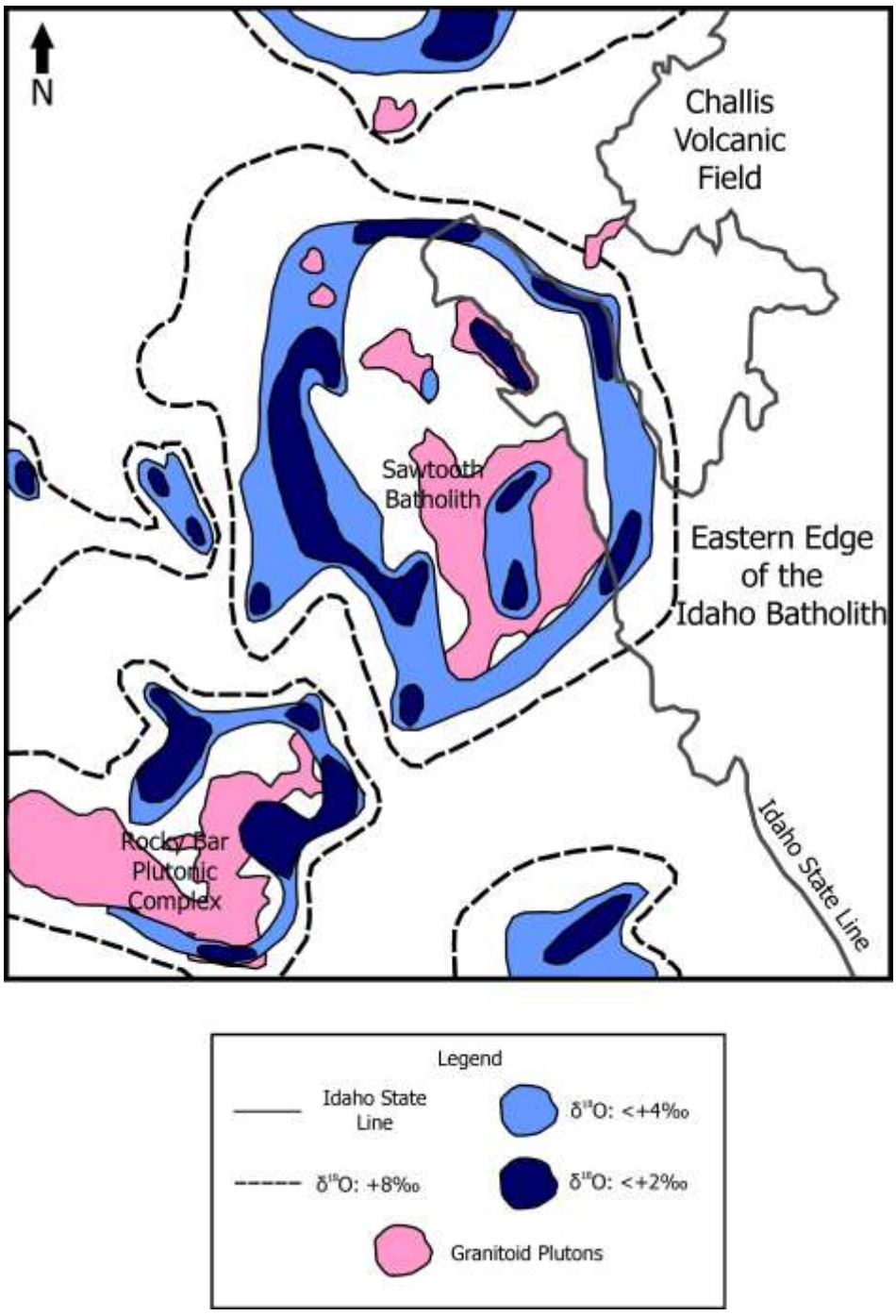

Figure 1.2: Eocene Alteration of Idaho Batholith

This is a map after Criss and Taylor (1983) depicting areas of strongly ^{18}O depleted portions of the Idaho Batholith and is the basis for the prior alteration model of Boroughs et al. (2005)

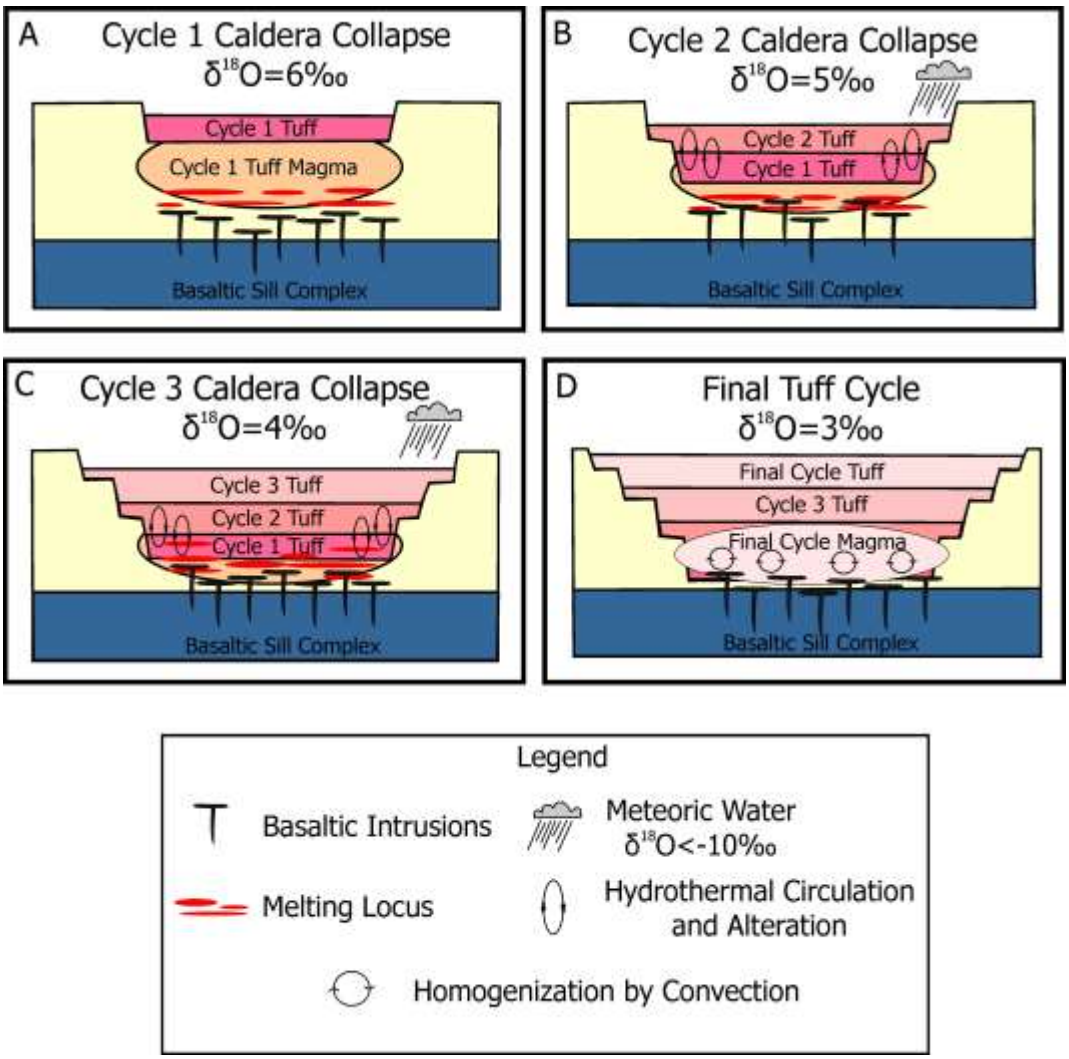
A
Cycle 1 Caldera Collapse
δ18O=6‰
Cycle 1 Tuff
Cycle 1 Tuff Magma
Basaltic Sill Complex
B
Cycle 2 Caldera Collapse
δ18O=5‰
Cycle 2 Tuff
Cycle 1 Tuff
Basaltic Sill Complex
C
Cycle 3 Caldera Collapse
δ18O=4‰
Cycle 3 Tuff
Cycle 2 Tuff
Cycle 1 Tuff
Basaltic Sill Complex
D
Final Tuff Cycle
δ18O=3‰
Final Cycle Tuff
Cycle 3 Tuff
Final Cycle Magma
Basaltic Sill Complex
Legend
Basaltic Intrusions
Meteoric Water
δ18O<-10‰
Melting Locus
Hydrothermal Circulation
and Alteration
Homogenization by Convection

Figure 1.3: Caldera Collapse Model

This figure after Watts et al. (2011) shows the steps of the caldera collapse model. (A) The initial normal magma of Cycle 1 is produced by partial melting of the normal $\delta^{18}O$ Snake River Plain crust by an underlying basaltic sill complex. Cycle 1 caldera collapse occurs and intracaldera fill of Cycle 1 tuff accumulates. (B) Cycle 2 magma is produced from evolved normal $\delta^{18}O$ Snake River Plain crust. Cycle 2 caldera collapse occurs and the Cycle 2 tuff intracaldera fill overlaps the Cycle 1 tuff. A nested caldera complex is then formed. Meteoric water is able to penetrate the surface by caldera fractures and hydrothermal circulation begins altering the intracaldera fill. (C) Cycle 3 magma is produced by further evolved normal $\delta^{18}O$ Snake River Plain crust. The Cycle 3 tuff produced by the caldera collapse is lower in $\delta^{18}O$ due to the contribution of hydrothermally altered intracaldera fill. With the addition of the Cycle 3 tuff, the intracaldera fill units from each caldera collapse are drawn down to the heat source which (D) leads to the Cycle 4 magma being produced by a homogenized low-$\delta^{18}O$ magma body. The Cycle 4 tuff is significantly depleted relative to the normal $\delta^{18}O$ tuffs produced originally.

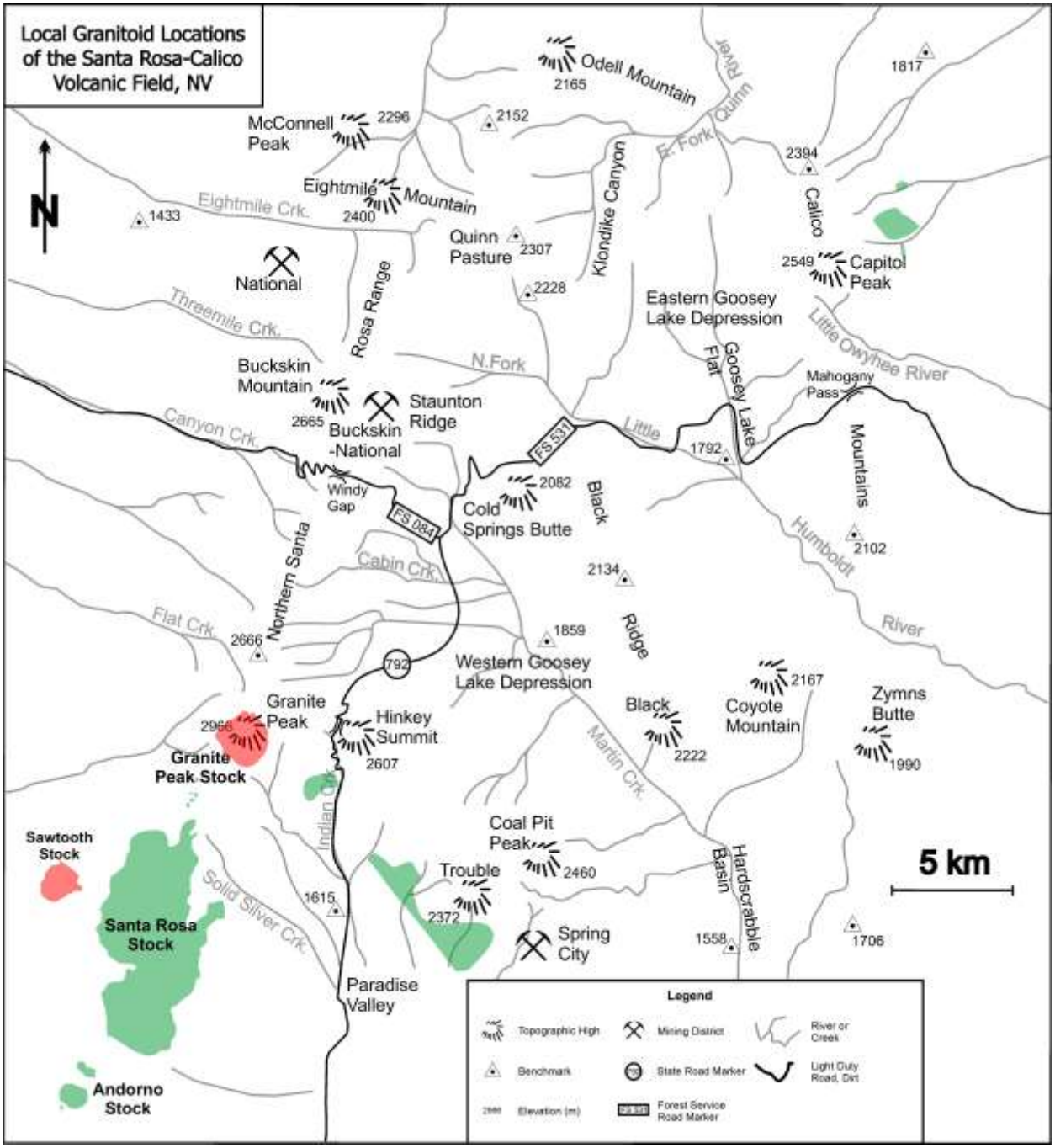

Figure 1.4: Locations of SC Granitoids

This map after Brueseke and Hart (2008) shows the locations of the Cretaceous granitoids that predate the Santa Rosa-Calico volcanic field. Green fields represent the Santa Rosa-Andorno group and red fields represent the Granite Peak-Sawtooth group. Granitoid distribution taken from Compton (1960), Struck (1993), and Brueseke and Hart (2008).

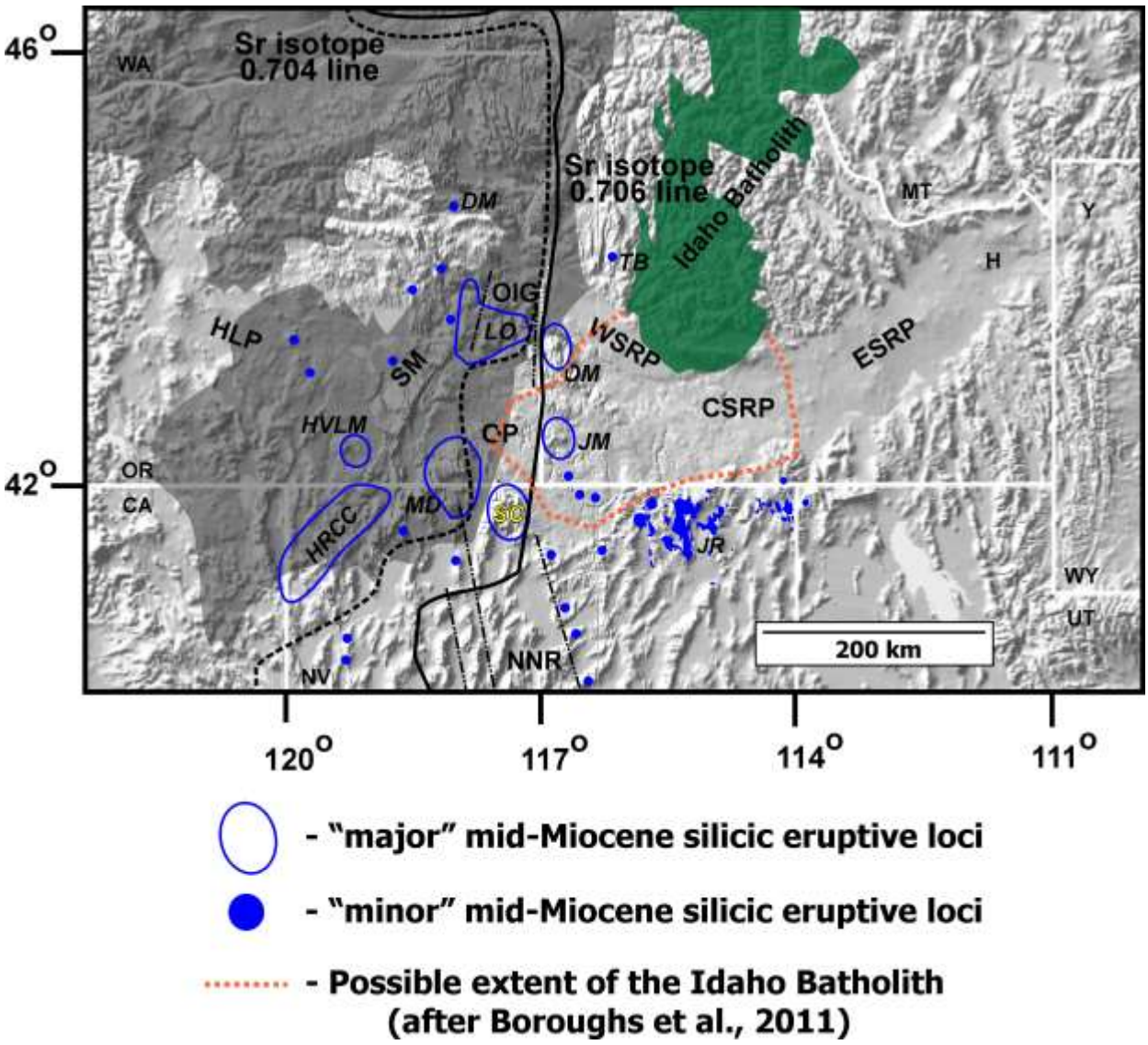

Figure 1.5: Idaho Batholith

Regional map after Brueseke and Hart (2008) showing the location of the Idaho Batholith and possible extension under the Snake River Plain (orange dashed line). Idaho Batholith position is from Chase et al. (1978).

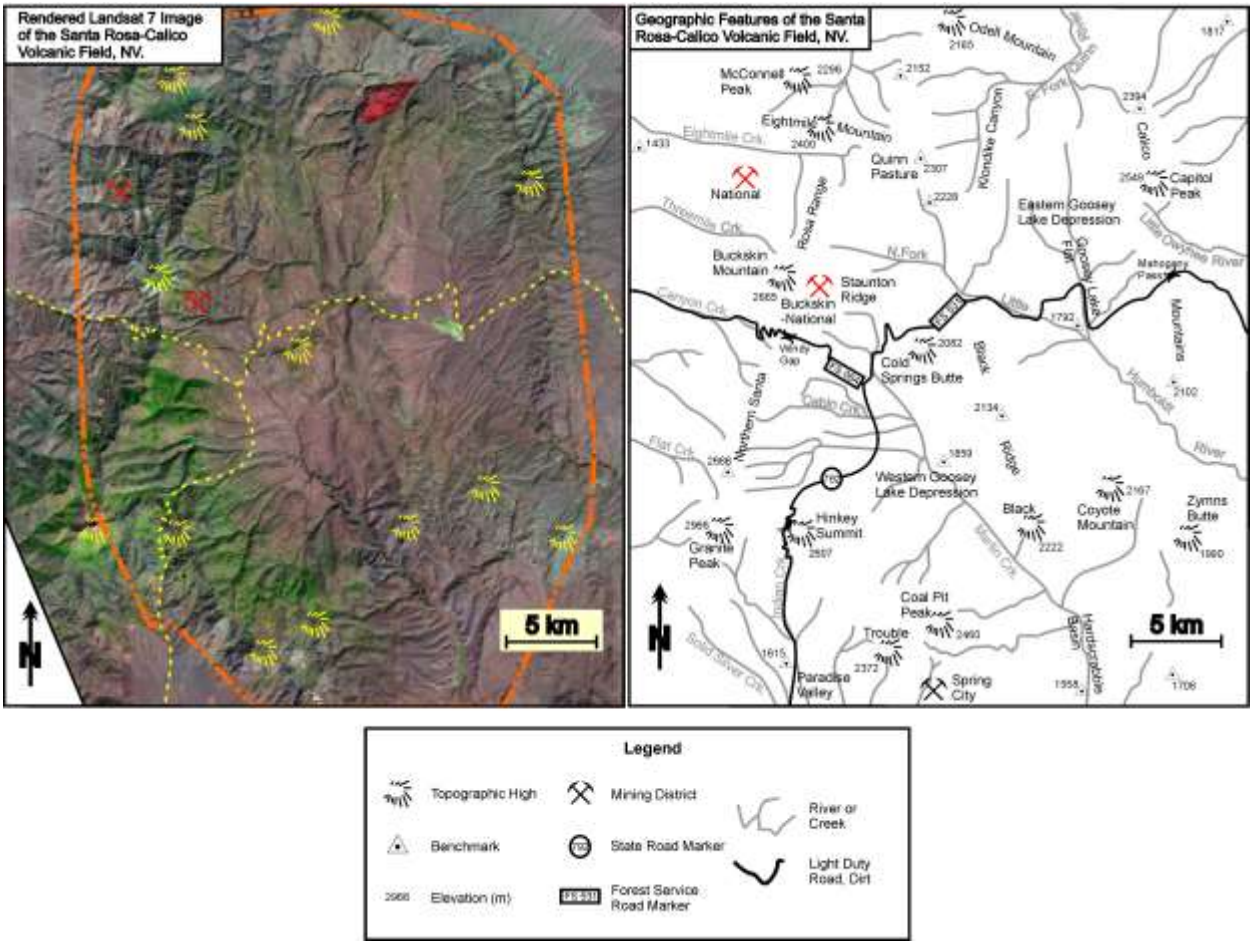

Figure 1.6: Satellite and Physical Landmark Maps of the Santa Rosa-Calico Volcanic Field A rendered Landsat 7 image where band 7 is red, band 4 is green, and band 3 is blue. The orange dashed line represents the approximate boundary of the SC and the dashed yellow lines represent major roads. Yellow circular symbols represent topographic highs that correspond to the black ones on the map. The physical landmark map shows the location of high points, rivers and streams, mining districts, and other geographic features. Maps after Brueseke and Hart (2008).

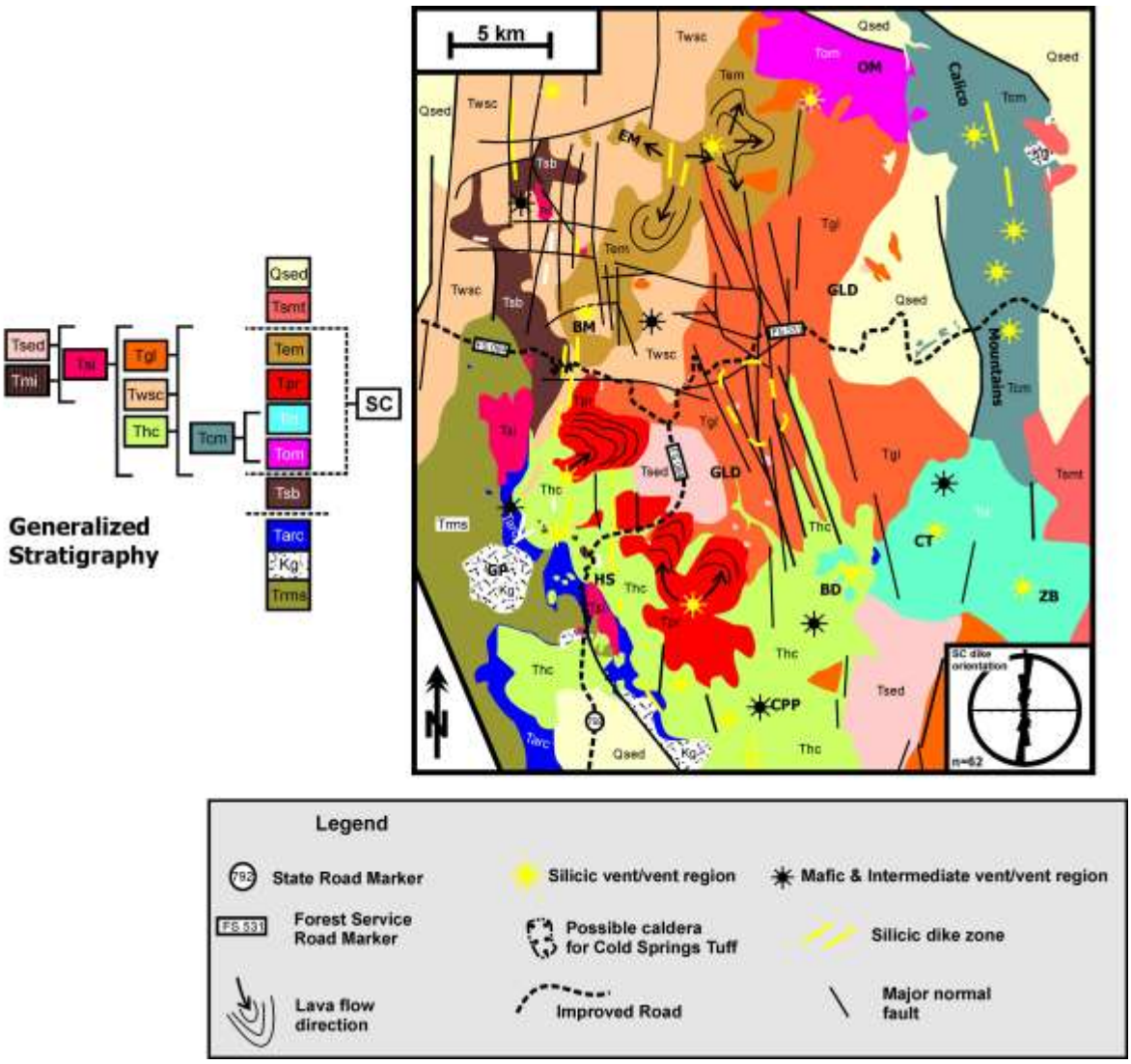

Figure 1.7: Generalized Geologic Map of the SC

A generalized geologic map of the SC (after Brueseke and Hart, 2008) showing lava flow directions indicated by the arrows and flow bands, silicic vent locations, the Cold Springs tuff caldera in yellow dashed lines, silicic dikes in yellow, and major normal faults in black. Tgl unit represents the map unit of the Cold Springs tuff (Tcst).

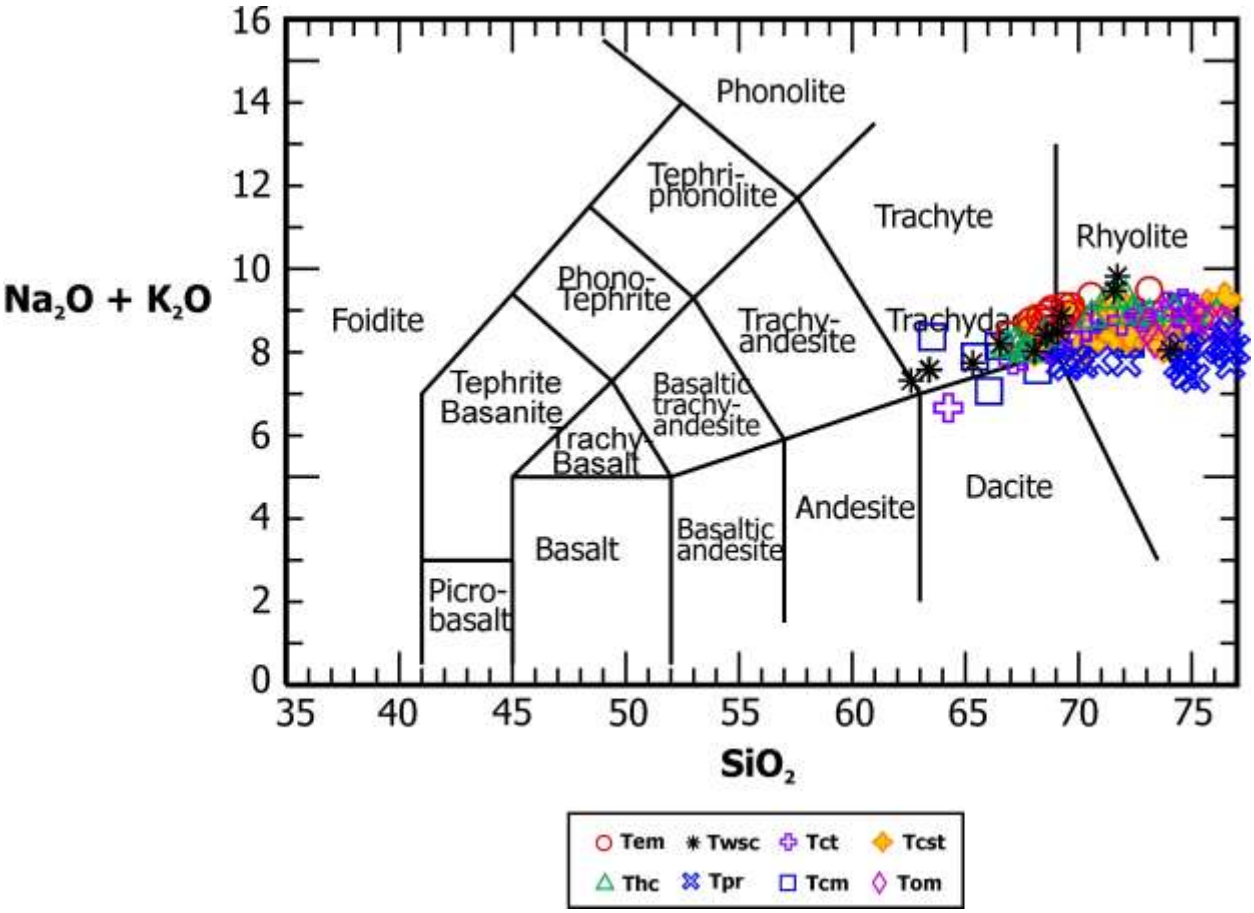

Figure 1.8: Total Alkali diagram

A total Alkali diagram showing the compositional range of SC silicic units (after Le Bas et al, 1986). All concentrations are in Wt. %.

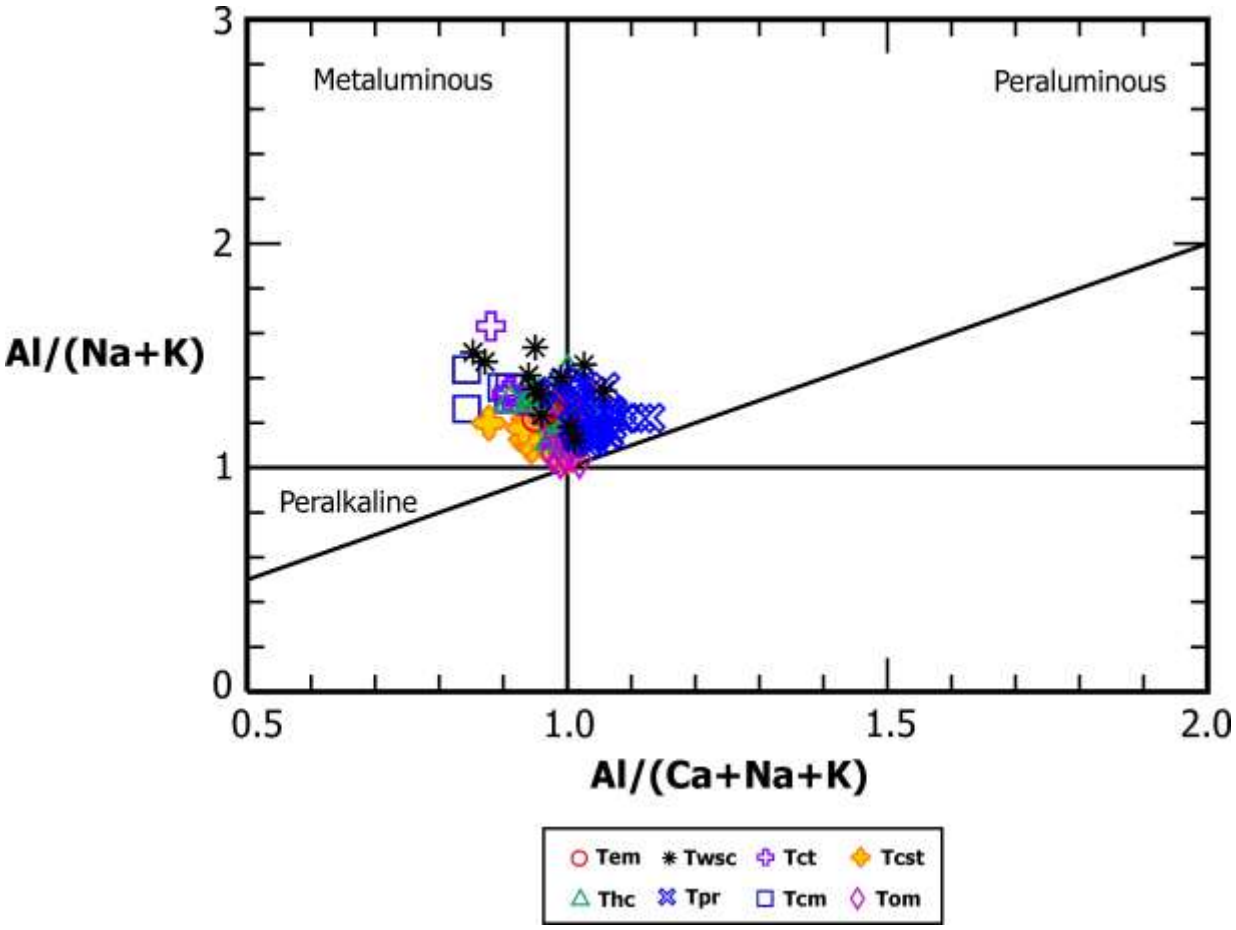

Figure 1.9: Alumina Saturation Diagram

Plot of the aluminum saturation index of SC silicics showing that the silicics plot in the metaluminous and peraluminous fields. Values are molecular proportion.

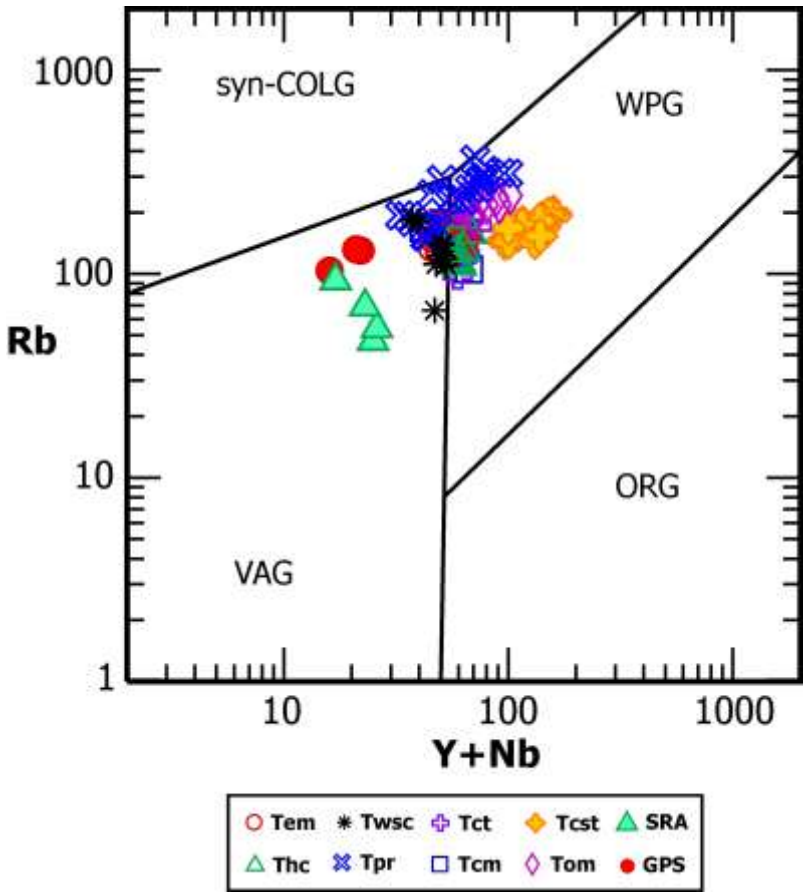

Figure 1.10: Granite Classification Diagram

Pearce (1984) silicic classification of SC silicics. Variations within units can be seen while the Cold Springs tuff (Tcst) plots completely in the within-plate granite field. Both SC granitoid stocks plot in the volcanic-arc granites. Concentrations are in ppm.

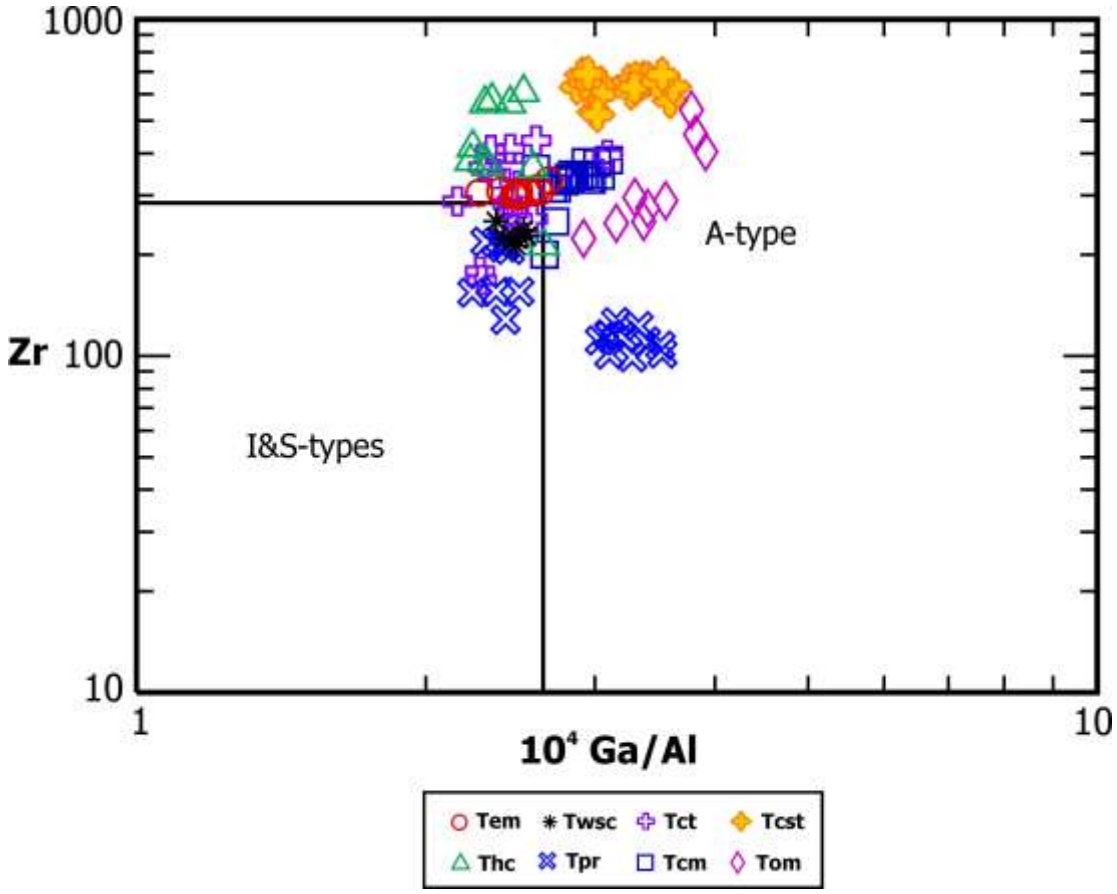

Figure 1.11: Granite Type Classification Diagram

Whalen et al. (1987) granite type classification diagram. Again variations exist within units except for the Cold Springs tuff (Tcst) and Odell Mountain (Tom) units which are located in the A-type field. The western margin lava flows (Twsc) plot within the I and S-type granite field and the remaining units show both A, I, and S-type characteristics. Concentrations are in ppm.

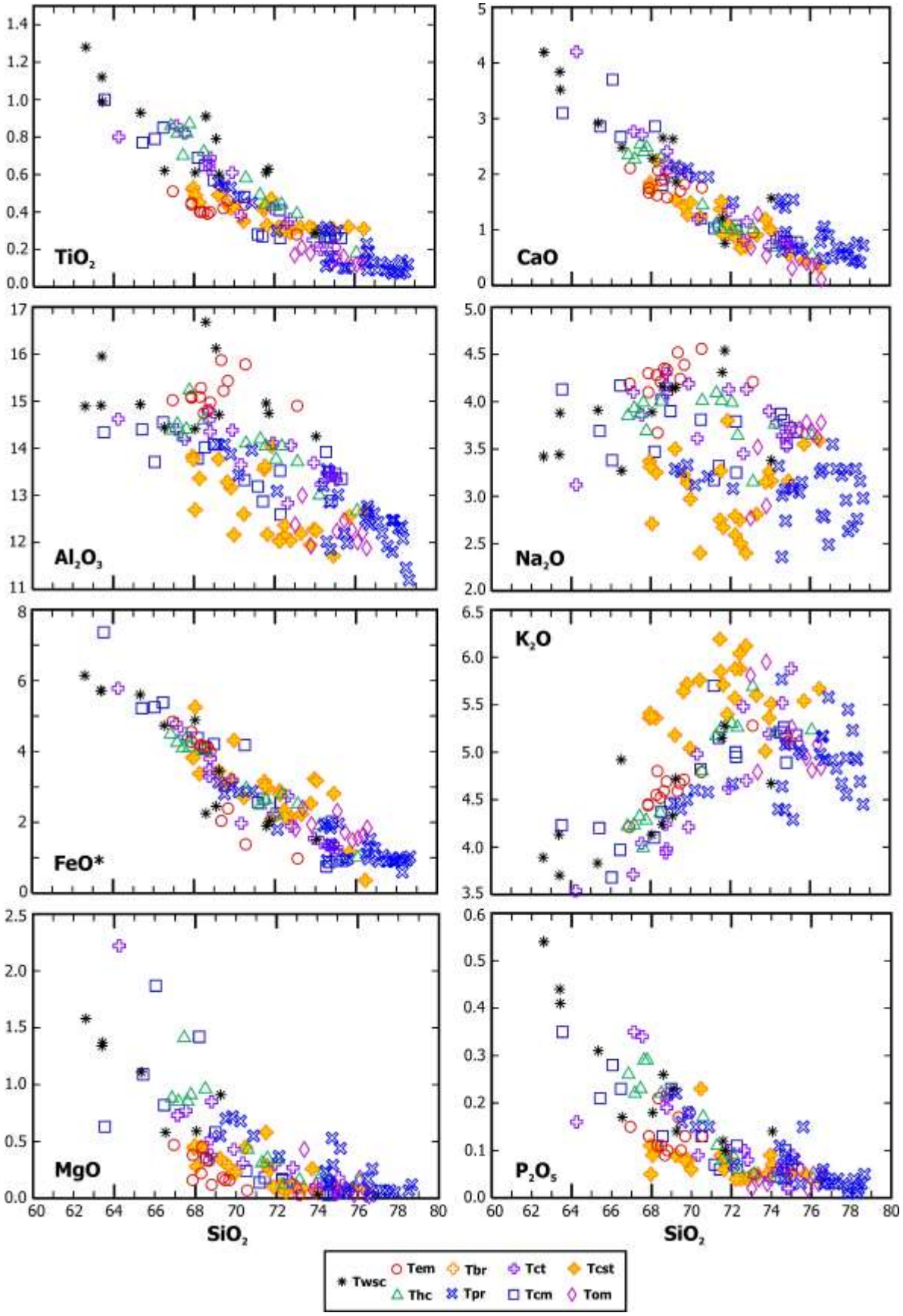
TiO2
CaO
Al2O3
Na2O
FeO*
K2O
MgO
P2O5
SiO2
SiO2
Twsc
Tem
Tbr
Tct
Tcst
Thc
Tpr
Tcm
Tom

Figure 1.12: Harker Diagrams

Previous page – Harker diagrams of major element concentrations (wt. %) for SC silicic units (Brueseke and Hart, 2008).

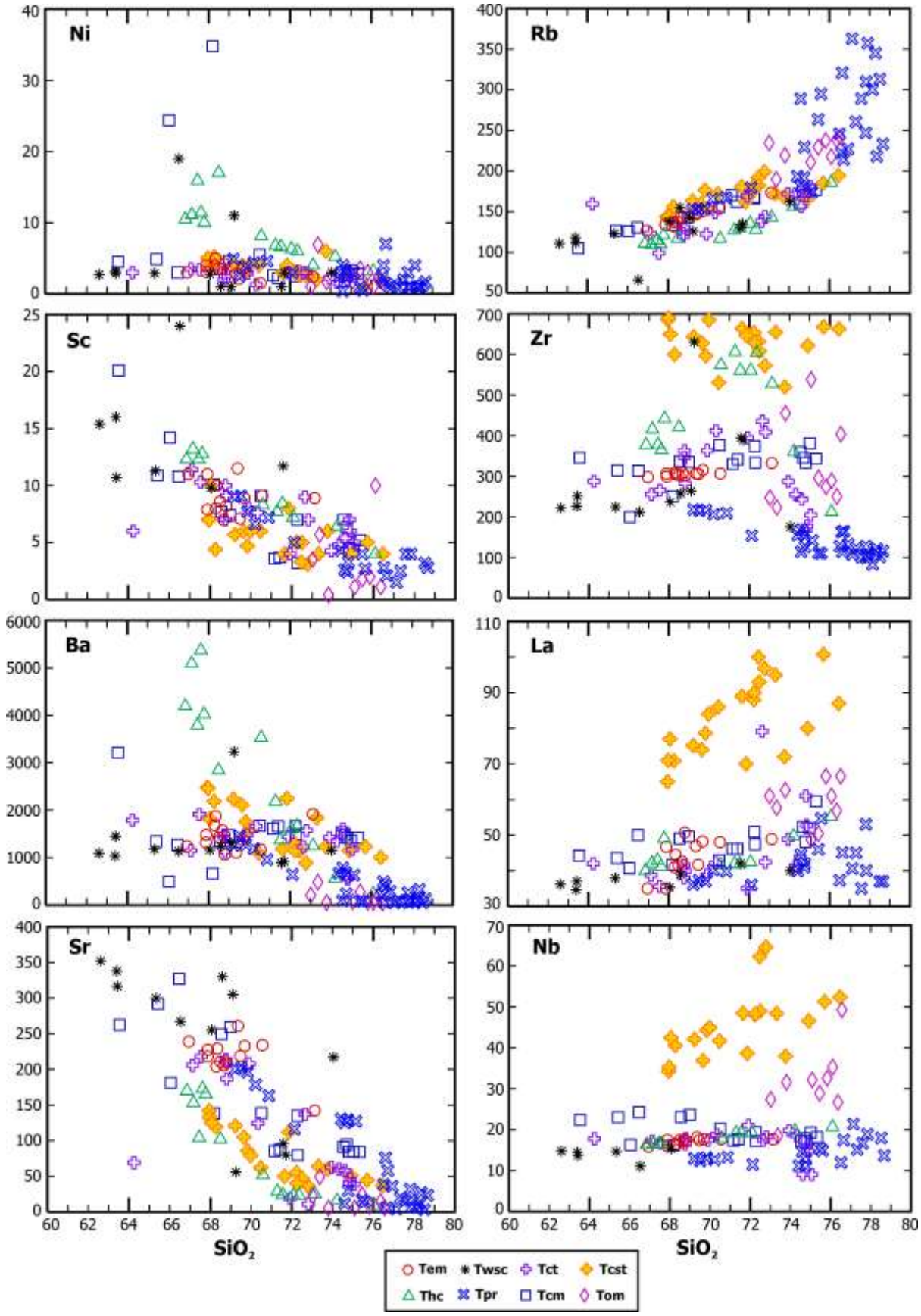
Ni
Rb
Sc
Zr
Ba
La
Sr
Nb
SiO2
SiO2
Tem
Twsc
Tct
Tcst
Thc
Tpr
Tcm
Tom

Figure 1.13: Trace Element Diagrams

Previous page – Select trace element concentrations (ppm) plotted against SiO_2 (wt. %) for SC silicic units (Brueseke and Hart, 2008).

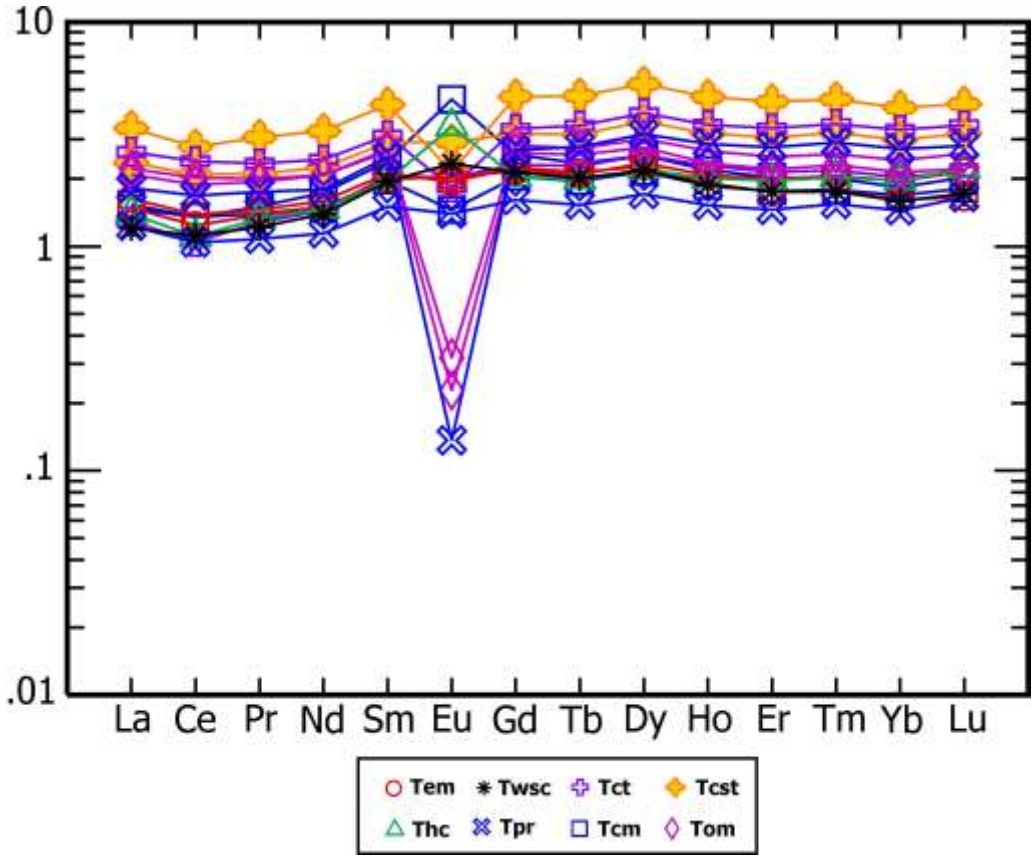

Figure 1.14: Upper Continental Crust Normalized Rare Earth Element Diagram Rare earth element spider diagram of silicic units of the SC normalized to upper continental crust after Taylor and McLennan (1985)

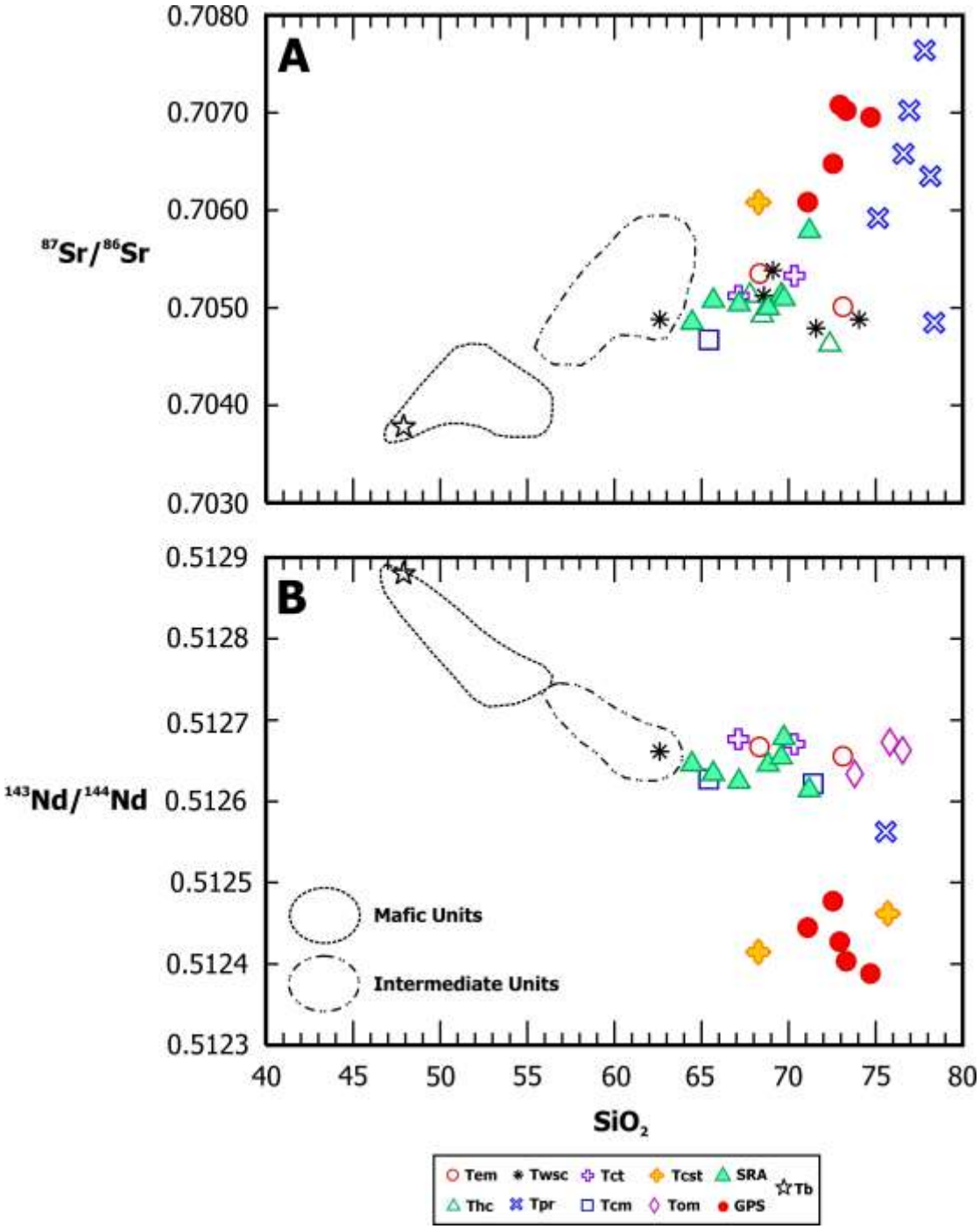

Figure 1.15: Sr and Nd of SC Silicic Units against Wt. % SiO_2

$^{87}Sr/^{86}Sr_i$ and $^{143}Nd/^{144}Nd_i$ of SC silicic units plotted with the fields of mafic and intermediate SC units. Initial Sr and Nd isotope concentrations of the two SC granitoid groups are also plotted. SC granitoid data age corrected to 16.5 Ma (data from Stuck, 1993; Brueseke and Hart, 2008)

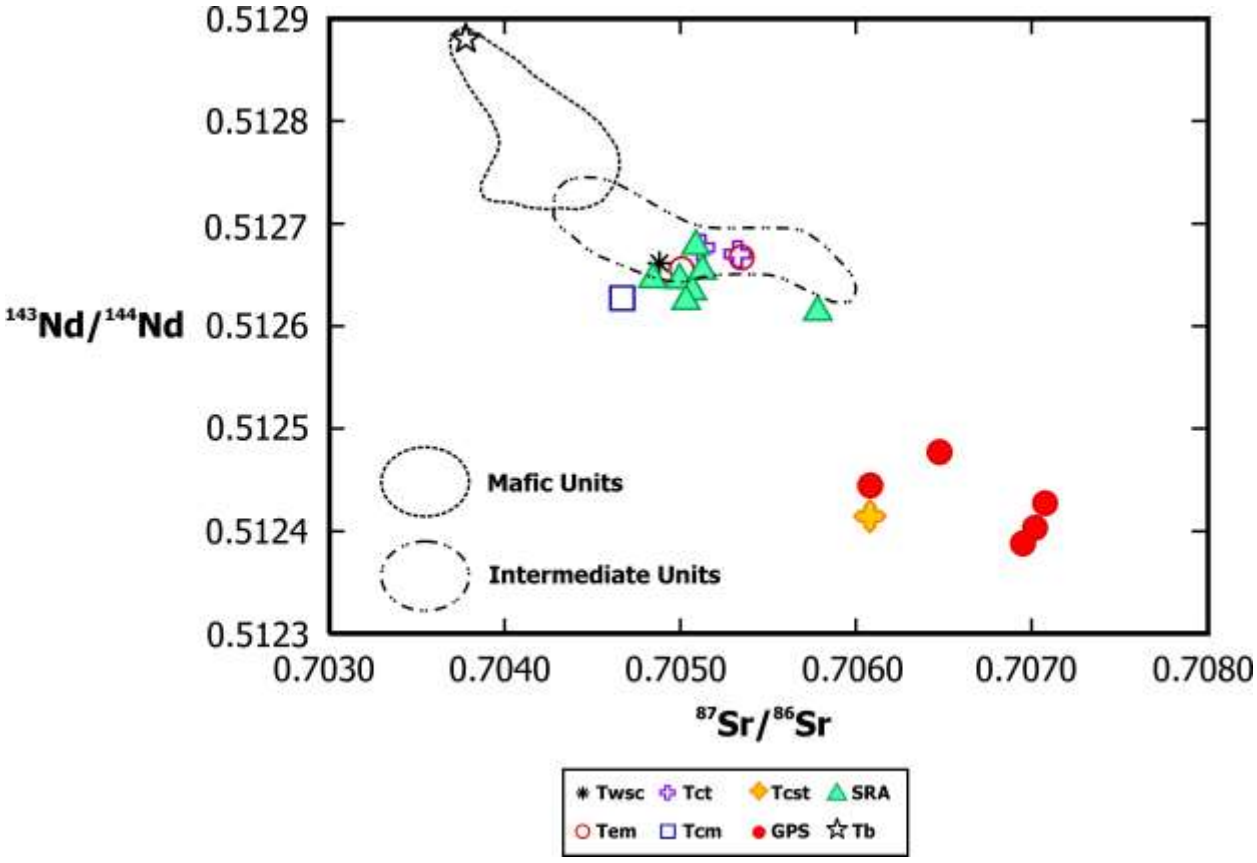

Figure 1.16: SC Silicic Sr and Nd Diagram

A plot showing $^{87}Sr/^{86}Sr_i$ versus $^{143}Nd/^{144}Nd_i$ for SC silicic units against fields representing the mafic and intermediate SC units. Initial Sr vs. Nd concentrations of the two SC granitoid groups are plotted also. SC granitoid data age corrected to 16.5 Ma (data from Stuck, 1993; Brueseke and Hart, 2008).

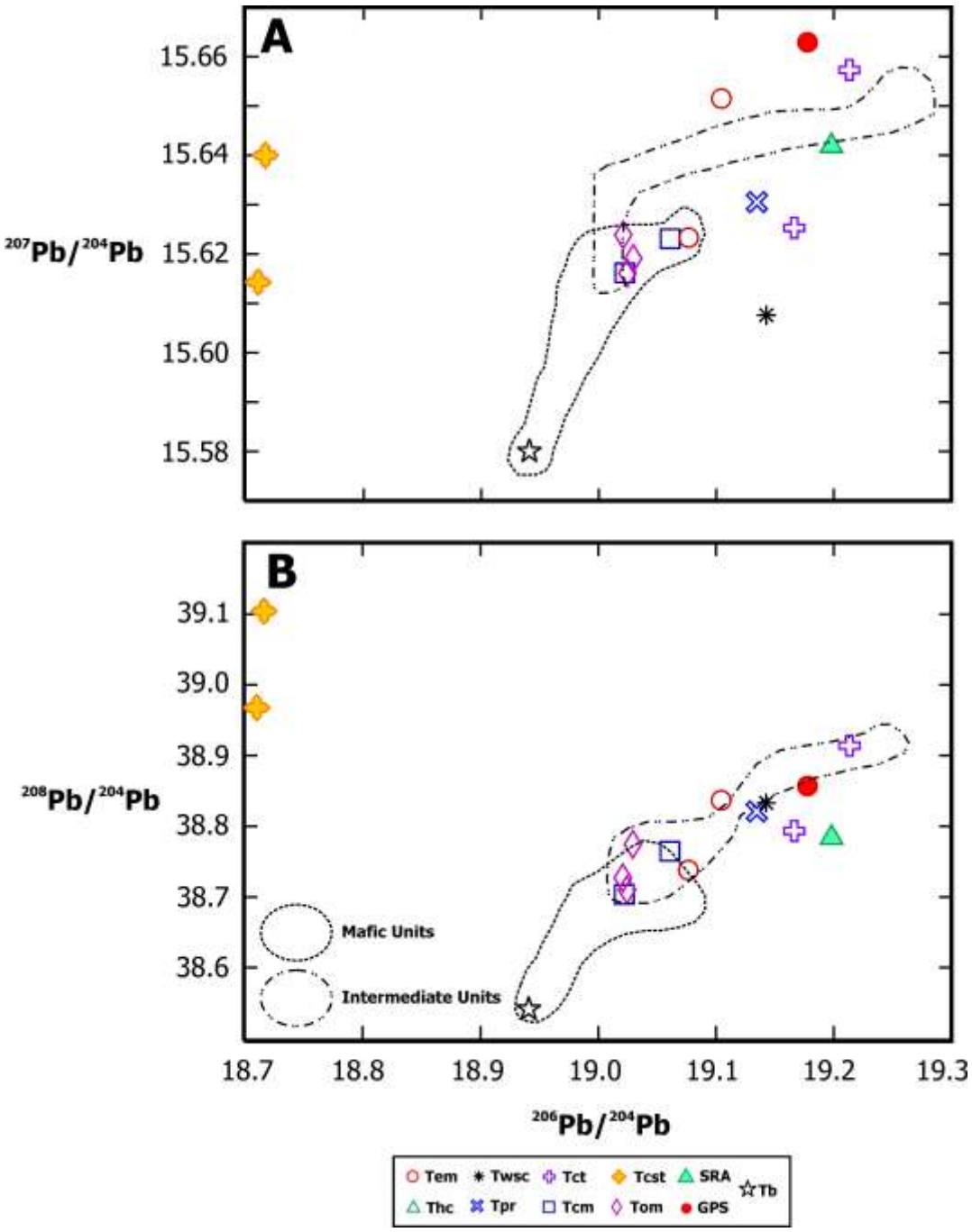

Figure 1.17: Pb Isotope Diagrams

Pb isotope concentrations (from Brueseke and Hart, 2008) of SC silicic units against fields of SC mafic and intermediate units. (A) $^{207}Pb/^{204}Pb$ vs. $^{206}Pb/^{204}Pb$. (B) $^{208}Pb/^{204}Pb$ vs. $^{206}Pb/^{204}Pb$. Pb isotope concentrations of the two SC granitoid groups are plotted. SC granitoid data from Brown et al. (2011).

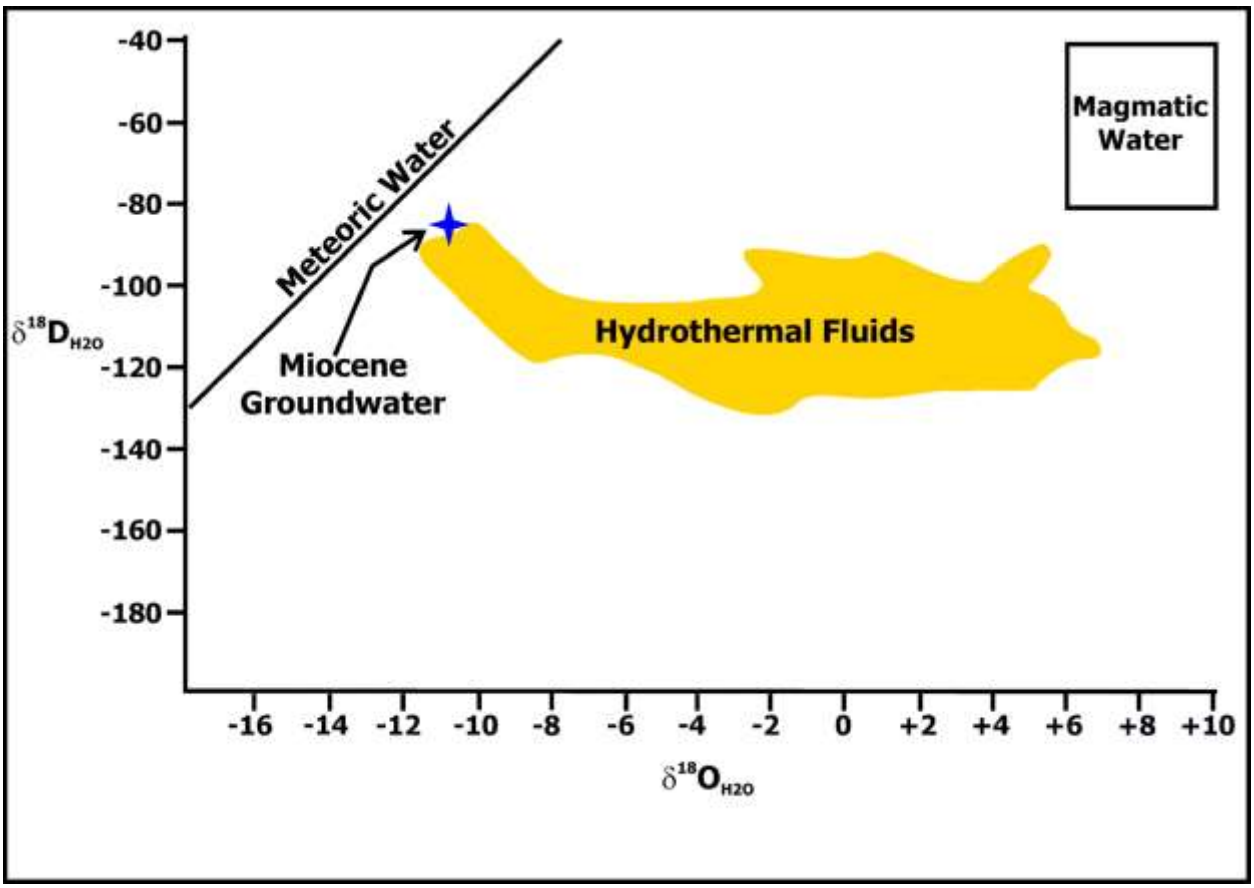

Figure 1.18: $\delta^{18}O_{H20}$ Buckskin Mountain Hydrothermal Fluid Diagram

This figure shows the range of $\delta^{18}O$ values for Miocene groundwater, Buckskin hydrothermal fluids, and coeval magmatic water from Vikre (1987). The enrichment of $\delta^{18}O$ values in the hydrothermal fluids is due to fluid/wall rock interaction.

Chapter 2 - Methods

Sample Selection

Twenty SC silicic samples were obtained from storage at Miami University (OH). These samples were originally studied by Brueseke (2006) and Brueseke and Hart (2008). The twenty initial sample set was chosen by evaluating physical, geochemical and isotope (Sr-Nd-Pb) data as well as location and sample unit data from a master list of multiple samples over the entire SC study area compiled by Brueseke and Hart (2008). Samples were selected from a subset that have already determined major/trace element bulk chemistry and Sr-Nd-Pb isotope values, as well as being representative of the diversity of silicic units across the study area. The ultimate goal was to have fifteen samples analyzed for oxygen isotope analysis. Emphasis was placed on analyzing multiple samples of Cold Springs tuff (Tcst), since this unit was geochemically and isotopically different from all of the other silicic units found in the SC, as well as the only caldera-sourced unit. The selection of the final fifteen samples depended on the amount of feldspar and/or quartz crystals present in the crushed and sieved sample that could be hand-picked. At least 20 mg of each feldspar and quartz crystals per rock sample was obtained. The five samples that were not selected as part of the final sample set were not chosen because of: a sparse amount of feldspar and/or quartz crystals present and/or the feldspars were too altered (yellow discoloration). The feldspar crystals that were analyzed were milky white to transparent with cleavage planes distinctly present. There was one sample that had a few melt inclusions in the feldspar (MB02-63B; Tcst). Quartz crystals that were analyzed were all smoky quartz and were transparent, with many showing concoidal fracture. One of the quartz samples did have small melt inclusions (MB00-18; Tpr). Cold Springs tuff samples do not have quartz, so only feldspar are reported. The finalized sample set included eight of the stratigraphically constrained Cold Springs tuff (Tcst) (e.g. multiple cooling units to document whether $\delta^{18}O$ values of the CST change through time, ala the caldera-based model of Bindeman et al, 2001) and the remaining samples consist of other SC silicic units to fully constrain other volumetrically dominant local silicic magmatic systems (Table 2.1): three samples of the porphyritic rhyolite (Tpr), one sample from Calico Mountain (Tcm), one sample from Coyote Mountain-Zymns Butte (Tct), and two samples from Odell Mountain area units (Tom) (Table 2.1). Detailed sample descriptions and pictures of analyzed crystals are in Appendix A.

Oxygen Isotope Analysis

Samples were prepared for oxygen isotope analysis at Kansas State University. The twenty samples were crushed with a RockLabs hydraulic press. Weathered pieces were removed during this process so that the freshest sample remained, based on visual inspection and handpicking with tweezers. The crushed samples were sieved to concentrate crystals that were between 0.25 and 2 mm in size (Figure 2.1B). Using a binocular microscope, quartz and feldspar, were handpicked from the crushed sample split (Figure 2.1C). Only the freshest quartz and feldspar grains were chosen; weathered pieces of rock were removed during crushing so that the remaining sample would be as fresh and unaltered as possible. When hand picking, the whitest and most transparent (if possible) crystals of feldspar were chosen using a background of light blue paper which made the altered, yellowed crystals stand out more and made choosing the whitest crystals much easier (Figure 2.1). Quartz grains were chosen that were the least included by other minerals and were as clear as possible (Figure 2.2). Approximately 20 mg of feldspar and quartz (when present), was collected (Figure 2.1D and Table 2.2). Quartz is not found in the Cold Springs tuff unit so only feldspars were analyzed from those samples. All samples were then sent to Washington State University's GeoAnalytical Lab for analysis by Dr. Peter Larson, using laser fluorination as outlined by Sharp (1990). Oxygen isotope compositions were measured using a Finnigan Delta S Isotope Ratio Mass Spectrometer (IRMS) operating an ISODAT NT software operating system. The samples were run using the UWG-2 garnet standard and the data was then normalized to this standard ($\delta^{18} = 5.8‰$) with an error of +/- 0.15‰ (Valley et al., 1995; Takeuchi and Larson, 2005).

Table 2.1: Representative Unit Geochemistry

Major element (wt. %), select trace and rare earth element (ppm) concentrations and radiogenic isotope ratios for the samples analyzed (Brueseke and Hart, 2008).

Sample	MB01-62	MB02-55	MB02-63B	MB03-24	MB03-26A	MB03-26F	MB03-32	MB01-36A	MB01-76	MB03-45	MB00-33	MB03-10B	MB00-18	MB02-13	MB02-19
Rock Unit	Tcst	Tcst	Tcst	Tcst	Tcst	Tcst	Tcst	Tcst	Tcm	Tct	Tom	Tom	Tpr	Tpr	Tpr
SiO_2 (wt. %)	69.22	68.27	72.47	76.46	75.70	71.64	67.94	70.47	75.32	74.87	76.56	75.82	69.83	74.58	75.59
TiO_2 (wt. %)	0.49	0.45	0.32	0.31	0.32	0.33	0.52	0.35	0.26	0.13	0.16	0.11	0.53	0.11	0.10
Al_2O_3 (wt. %)	13.77	13.36	12.15	12.67	12.55	12.17	13.83	12.60	13.35	13.43	11.88	12.26	13.87	12.02	11.98
Fe_2O_3 (wt. %)	2.00	1.94	1.42	0.23	0.72	1.72	2.19	1.55	0.56	0.82	1.13	0.91	1.70	0.55	0.59
FeO (wt. %)	1.64	1.62	1.06	0.16	0.51	1.40	1.86	1.30	0.40	0.62	0.82	0.67	1.47	0.43	0.44
MnO (wt. %)	0.06	0.07	0.05	0.01	0.01	0.06	0.07	0.06	0.01	0.05	0.02	0.02	0.06	0.02	0.01
MgO (wt.%)	0.35	0.45	0.06	0.06	0.08	0.25	0.44	0.45	0.05	0.05	0.02	0.03	0.72	0.12	0.10
CaO (wt. %)	1.54	2.24	0.82	0.33	0.46	0.91	1.85	1.23	0.78	0.75	0.11	0.41	2.10	0.61	0.67
Na_2O (wt. %)	3.50	3.25	2.75	3.59	3.55	2.67	3.37	2.40	3.68	3.64	3.78	3.78	3.33	2.36	3.15
K_2O (wt. %)	5.18	5.36	6.04	5.67	5.54	5.71	5.36	5.76	5.18	5.10	4.84	4.94	4.50	5.77	4.98
P_2O_5 (wt. %)	0.09	0.10	0.04	0.04	0.05	0.06	0.11	0.23	0.06	0.02	0.05	0.02	0.18	0.04	0.15
Ni (ppm)	4.2	5.2	2.7	2.0	1.0	3.0	5.0	4.0	2.8	3.0	1.6	3.0	3.9	0.4	0.5
Cr (ppm)	2.20	5.00	<1	<1	<1	<1	2.00	1.00	<1	<1	---	1.00	2.90	---	2.40
Sc (ppm)	5.7	4.4	3.3	4.0	5.0	4.0	7.0	6.0	5.2	6.0	---	2.0	7.7	2.6	2.7
Ba (ppm)	2233	2188	1148	1005	1235	1185	2480	1095	1419	585	49	65	1278	95	83
Rb (ppm)	163	156	192	194	185	181	143	172	177	170	241	237	154	289	295
Sr (ppm)	121	119	44	37	45	50	142	62	84	46	6	8	196	12	14
Zr (ppm)	644	600	632	663	668	664	685	531	343	178	404	274	217	114	110
Nb (ppm)	42.1	40.6	62.3	52.4	51.3	48.5	34.3	41.7	18.2	14.8	49.3	32.6	13.2	14.7	14.9
Zn (ppm)	93	87	117	129	97	116	101	84	49	53	100	93	63	54	55
Pb (ppm)	24.2	24.4	27.6	27.0	29.9	29.0	23.0	29.0	26.1	25.1	21.0	47.0	23.7	29.4	31.0
Cs (ppm)	---	3.41	---	---	2.83	---	---	---	---	3.86	6.28	6.95	4.34	---	13.70
Hf (ppm)	---	16.6	---	---	18.4	---	---	---	---	6.0	12.9	10.2	6.3	---	4.7
La (ppm)	75.1	70.9	100.0	87.0	100.7	89.0	65.0	86.0	59.5	52.7	66.5	66.5	37.0	44.5	54.6
Ce (ppm)	116.1	133.7	149.5	170.0	178.0	191.0	134.0	182.0	86.9	82.6	137.0	129.4	66.5	84.0	108.0
Nd (ppm)	---	58.5	---	---	85.1	---	---	---	---	41.7	56.1	54.0	29.7	---	46.6
Sm (ppm)	---	13.1	---	---	19.3	---	---	---	---	8.4	12.0	11.9	6.8	---	11.3
Eu (ppm)	---	2.6	---	---	1.9	---	---	---	---	1.0	0.3	0.2	1.2	---	0.1
Yb (ppm)	---	6.6	---	---	9.1	---	---	---	---	3.2	4.9	4.7	3.2	---	6.0
Lu (ppm)	---	1.0	---	---	1.4	---	---	---	---	0.5	0.8	0.7	0.5	---	0.9
$^{87}Sr/^{86}Sr_i$	---	0.70608	---	---	---	---	---	---	---	---	---	---	---	---	---
$^{143}Nd/^{144}Nd_i$	---	0.51241	---	---	0.51246	---	---	---	---	---	0.51266	0.51267	---	---	0.51256
epsilon Nd	---	-3.93348	---	---	-3.01355	---	---	---	---	---	0.93793	1.13368	---	---	-1.02575
$^{206}Pb/^{204}Pb$	---	18.71631	---	---	18.71010	---	---	---	---	---	19.02950	19.02098	---	---	19.13465
$^{207}Pb/^{204}Pb$	---	15.64001	---	---	15.61430	---	---	---	---	---	15.61910	15.62387	---	---	15.63052
$^{208}Pb/^{204}Pb$	---	39.10421	---	---	38.96760	---	---	---	---	---	38.77420	38.72691	---	---	38.82090

Table 2.2: Amount of Sample Used

A table of the weight (mg) of crystals picked for each sample.

Sample	Unit	Quartz Amount	Feldspar Amount
MB01-62	Tcst	N/A	21.5 mg
MB02-55	Tcst	N/A	21.6 mg
MB02-63B	Tcst	N/A	22.5 mg
MB03-24	Tcst	N/A	21.1 mg
MB03-26A	Tcst	N/A	22.2 mg
MB03-26F	Tcst	N/A	20.7 mg
MB03-32	Tcst	N/A	21.5 mg
MB03-36A	Tcst	N/A	20.6 mg
MB01-76	Tcm	20.9 mg	20.5 mg
MB03-45	Tct	21.2 mg	20.1 mg
MB00-33	Tom	20.6 mg	21.0 mg
MB03-10B	Tom	20.7 mg	20.9 mg
MB00-18	Tpr	20.2 mg	21.0 mg
MB02-13	Tpr	20.8 mg	20.9 mg
MB02-19	Tpr	20.3 mg	21.1 mg

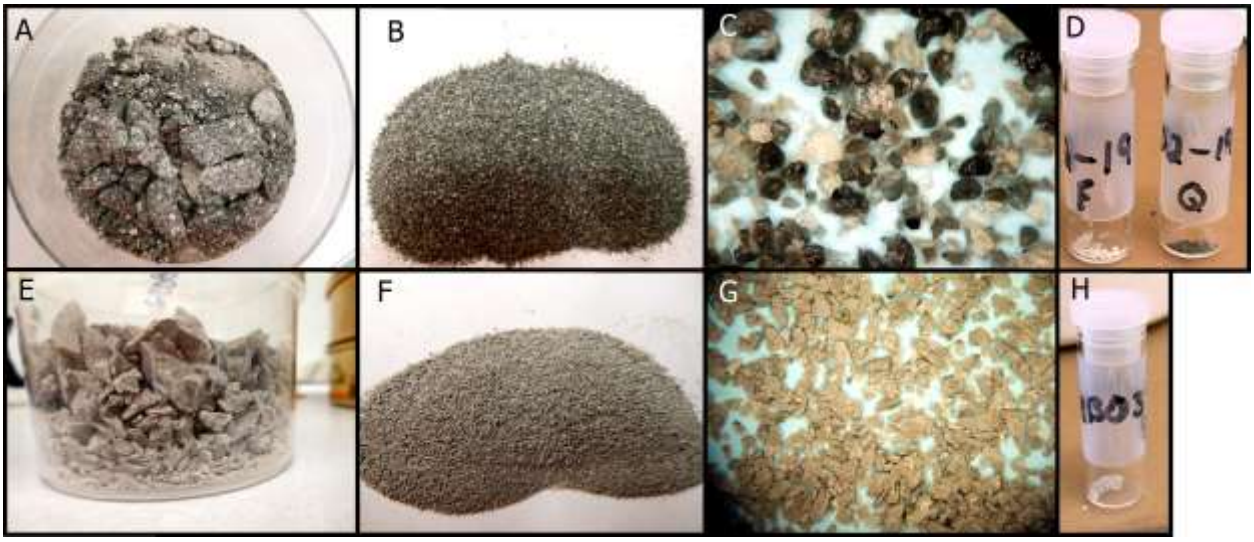

Figure 2.1: Sample Preparation Pictures

A series of photos showing the steps of sample preparation. A-D show sample MB02-19 (Tpr) and E-H show sample MB03-26A (Tcst) (A) Non-Cold Springs tuff sample after crushing, (B) sample after sieving, (C) view of crystals during picking, and (D) final picked quartz and feldspar. (E) Cold Springs tuff sample after crushing, (F) sample after sieving, (G) view of the sample during picking, and (H) final picked feldspar.

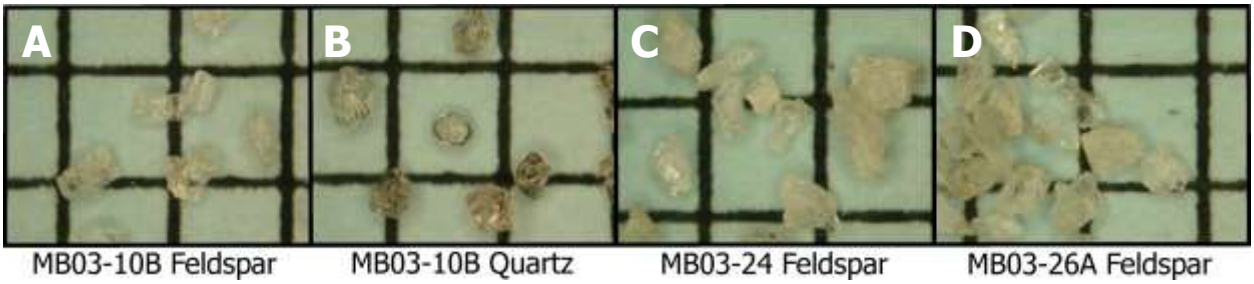

Figure 2.2: Representative Photos of Quartz and Feldspar Crystals

Photos representing non-Cold Springs tuff quartz and feldspar (A and B) and two photos representing what the Cold Springs tuff feldspars look like (C and D).

Chapter 3 - Oxygen Isotope Results

Fifteen silicic samples from the Santa Rosa - Calico volcanic field were analyzed for their $\delta^{18}O$ compositions. Eight of these samples were from the Cold Springs tuff (Tcst) and the remaining samples were from the remaining silicic units in the field area (porphyritic rhyolite (Tpr), Calico Mountain (Tcm), Coyote Mountain-Zymns Butte (Tct), and Odell Mountain (Tom)). All oxygen isotope values are reported relative to VSMOW.

The results of the analysis show two groupings of values; the Cold Springs tuff samples have $\delta^{18}O_{feldspar}$ values ranging from 2.36 to 4.05‰. The remaining silicic samples all had $\delta^{18}O_{feldspar}$ values ranging from 7.19 to 9.77‰ (Table 3.1 and Fig. 3.1). All reported ratios have a two sigma error of 0.15‰. Two samples, MB00-18 and MB02-19 have discrepancies with their $\delta^{18}O_{quartz}$ values and did not behave like quartz during laser analysis (e.g. they resembled the feldspars; starred samples in Table 3.1). When looking at the quartz crystals from these samples, the crystals do not resemble the other quartz from the other samples. They are more opaque and the MB00-18 quartz is darker. It is possible (but not likely) that in the case of MB02-19, these are altered feldspars, and in MB00-18 these are pieces of the matrix. Because of these discrepancies, the quartz values will not be used in further discussions. For the non-Cold Springs tuff silicic samples, $\delta^{18}O_{quatz}$ values range from 8.49 to 9.73‰ which fall within the range (6 to 10‰) for unaltered rhyolite (Taylor, 1968).

According to Taylor (1968) and Boroughs et al. (2005), whole rock samples that have $\delta^{18}O_{feldspar} < \delta^{18}O_{quartz}$ and $\Delta_{quartz - feldspar}$ less than 2‰ can be inferred to contain minerals that are in isotopic equilibrium with the melt and have not undergone any alteration since cooling. Since the Cold Springs tuff does not contain quartz, $\Delta_{quartz - feldspar}$ values do not exist, but for the remainder of the samples, the $\Delta_{quartz - feldspar}$ values fall below 2‰, with a range of 0.83 to 1.83‰ (Figure 3.2). Feldspars from these samples are in isotopic equilibrium before they were erupted, thus their $\delta^{18}O$ values can be used as a proxy for the magmatic $\delta^{18}O$ composition (Taylor, 1968 and Boroughs et al., 2005). Since SC silicics with quartz and feldspar show isotopic equilibrium with the melt, it is inferred that the Cold Springs tuff feldspars also represent magmatic values (Taylor, 1979; Boroughs et al., 2005).

Table 3.1: Oxygen Isotope Results

A table showing the $\delta^{18}O$ values (‰) for each of the samples along with ages. The Cold Springs tuff samples do not contain quartz so no $\delta^{18}O_{quartz}$ values are reported. The $\Delta_{quartz\text{-}feldspar}$ values for the four non-Cold Springs tuff samples to show equilibrium are reported. All values are within the 0-2 ‰ (0.15 error) equilibrium range.

Sample	Unit	Age (Ma)	$\delta^{18}O_{quartz}$	$\delta^{18}O_{feldspar}$	$\Delta_{quartz - feldspar}$
MB01-62	Tcst	--------	--------	3.54	-------
MB02-55	Tcst	15.46	--------	3.15	-------
MB02-63B	Tcst	--------	-------	3.09	-------
MB03-24	Tcst	--------	-------	2.78	-------
MB03-26A	Tcst	--------	-------	3.68	-------
MB03-26F	Tcst	15.75	-------	4.05	-------
MB03-32	Tcst	--------	-------	2.36	-------
MB03-36A	Tcst	15.40	-------	3.56	-------
MB01-76	Tcm	16.47	-------	7.39	-------
MB03-45	Tct	16.44	9.14	7.85	1.29
MB00-33	Tom	--------	9.44	7.61	1.83
MB03-10B	Tom	16.43	8.49	7.54	0.95
MB02-13	Tpr	--------	9.73	9.77	-0.04
MB00-18	Tpr	16.23	8.51*	7.19	-------
MB02-19	Tpr	16.18	8.51*	9.00	-------

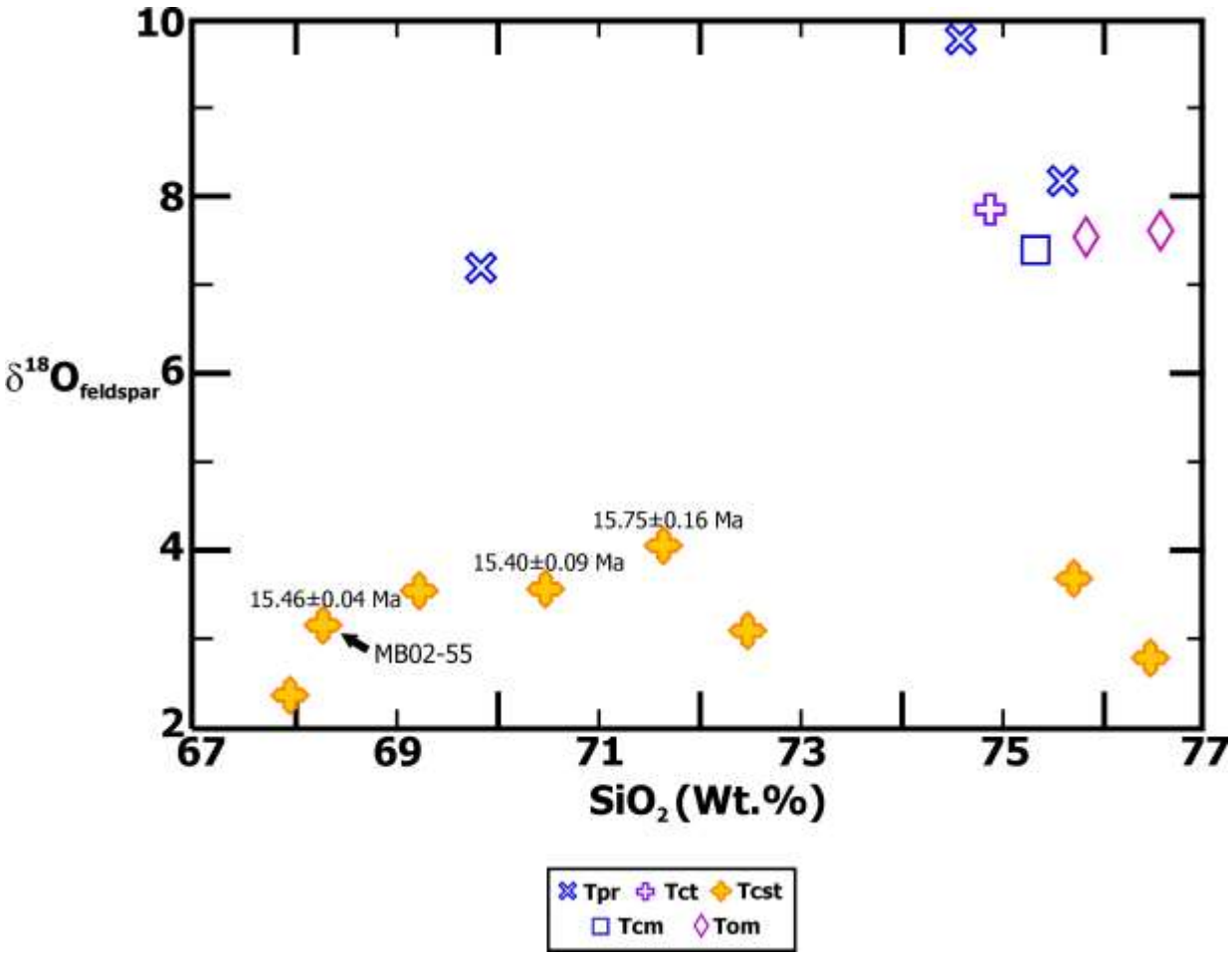

Figure 3.1: Oxygen Isotope Result Diagram

Plot showing the $\delta^{18}O_{feldspar}$ values vs. wt. % SiO_2 for the samples analyzed. Ages for the Cold Springs tuff samples have been included to show that there is not a decrease in $\delta^{18}O$ over time (errors = 2 sigma). Sample MB02-55 which is used in the models for this study is defined. Ages from Brueseke and Hart (2008).

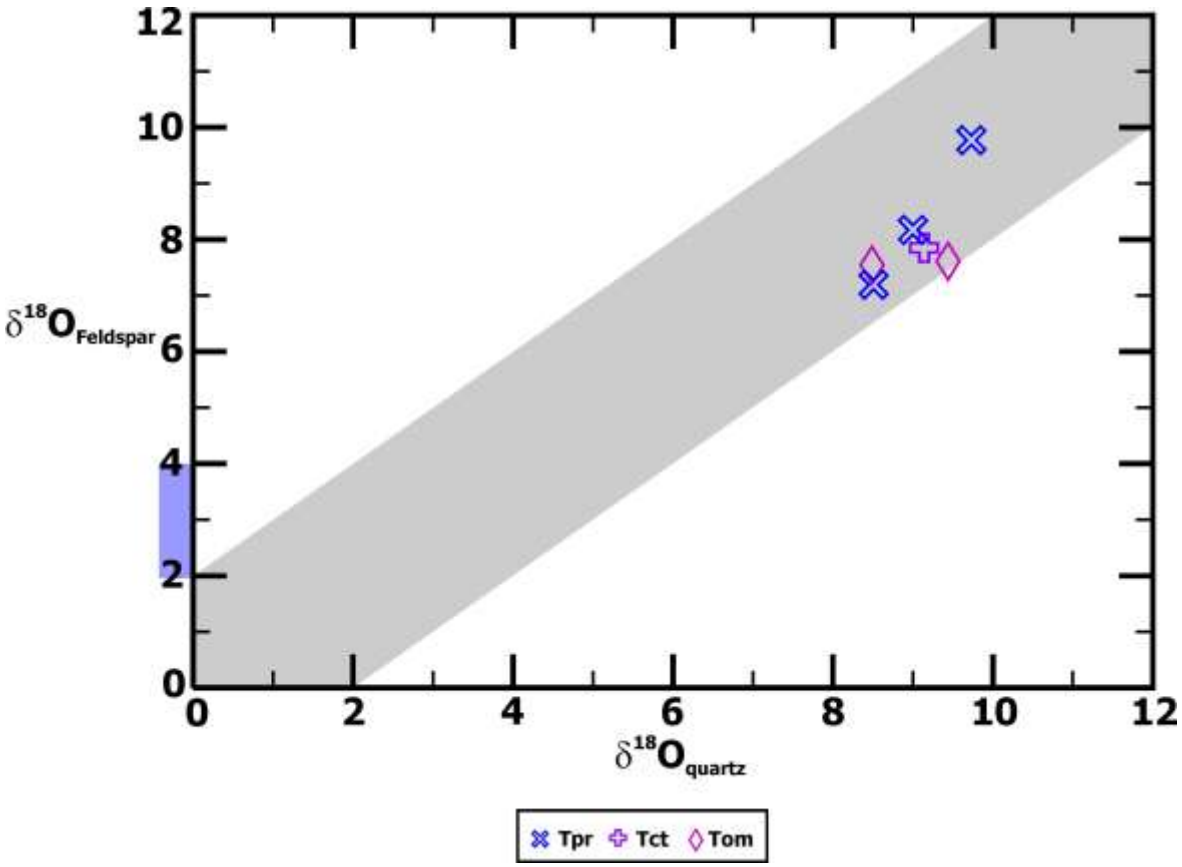

Figure 3.2: Equilibrium Oxygen Isotope Diagram

A plot of $\delta^{18}O_{quartz}$ vs. $\delta^{18}O_{feldspar}$. Samples that fall within the shaded region are in isotopic equilibrium. The purple bar along the $\delta^{18}O_{feldspar}$ axis show the range of $\delta^{18}O$ of the Cold Springs tuff. All $\delta^{18}O$ values are all relative to VSMOW.

Chapter 4 - Interpretation and Significance of $\delta^{18}O$ Compositions for Santa Rosa-Calico Volcanic Field Silicic Units

The samples that have $\delta^{18}O$ values which fall within the normal range of silicic magmas (6 to 10‰) coupled with bulk chemistry and radiogenic isotope data show that the normal samples are consistent with an unaltered upper crustal granitoid source. This is consistent with the previous conclusion of Brueseke and Hart (2008), whereas the CST samples that have low $\delta^{18}O$ compositions indicate that their source was previously altered crust (Boroughs et al., 2005, Brueseke and Hart, 2008, Watts et al., 2011). Radiometric ages of the three Cold Springs tuff samples show that there is not a progressive lowering of $\delta^{18}O$ values over time that would indicate cannibalism of intracaldera fill as modeled by Bindeman and Valley (2001) and Watts et al. (2011). This leaves the prior alteration model by Boroughs et al. (2005) as a possible model to explain the low-$\delta^{18}O$ values in the Cold Springs tuff.

Petrologic Model to Determine the Source and Oxygen Isotope Depletion of the Cold Springs Tuff

It is apparent that the bulk geochemical and radiogenic isotope compositions of the Cold Springs tuff differentiate it from other SC silicic units; this is consistent with its lower $\delta^{18}O$ compositions. Brueseke and Hart (2008) performed simple batch melting trace element models to address the petrogenesis of SC silicic magmas, including the Cold Springs tuff. Using 18% melting and 47% melting, it was found that melting of the Cretaceous granitoids can produce magmas that are geochemically similar to the SC silicic units. Some variations of the percent melting could be a reason for some of the differences seen between the calculated magmas and the measured values for these units. Also, there could be influences of fractional crystallization and mixing/assimilation with mafic and intermediate SC units to cause the variations seen (Brueseke and Hart, 2008). This modeling suggests that the Cold Springs tuff magmas could have formed via melting of only Cretaceous Granite Peak-Sawtooth group granitoids, which is also somewhat consistent with $^{87}Sr/^{86}Sr$, and $^{143}Nd/^{144}Nd$ isotope compositions that essentially overlap between the granitoids and Cold Springs tuff. In regards to oxygen isotope compositions, it is important to decipher why the Cold Springs tuff is has low $\delta^{18}O$ compositions, while the other analyzed silicic units do not. Based on $^{87}Sr/^{86}Sr$ and $^{143}Nd/^{144}Nd$ isotope

compositions, the other normal $\delta^{18}O$ silicic magmas were more than likely products of the melting of the Santa Rosa-Andorno Cretaceous granitoids (Struck, 1993, Brueseke and Hart, 2008). These units are not depleted in ^{18}O because they predate local hydrothermal activity and were not caldera sourced. This also means that their crustal source was not hydrothermally altered or influenced by fluids to lower the $\delta^{18}O$.

$\delta^{18}O$ depleted fluids associated with the active Buckskin-National hydrothermal system that existed adjacent to the Goosey Lake depression, which was an active extensional basin and topographic low, prior to and during Tcst volcanism, likely played a role in altering the source rocks of the Cold Springs tuff. To test this hypothesis, simple two component mixing models were created to confirm the possible crustal source of the Cold Springs tuff by refining the earlier modelling of Brueseke and Hart (2008); and determine whether hydrothermally altered Cretaceous granitoid/basalt mix could produce the low $\delta^{18}O$ Cold Spring tuff compositions. The mixing equation, $R_{mix} = [R_A C_A + R_B C_B (1-F_A)]/[C_A F_A + C_B (1-F_A)]$, (after Watts et al., 2010) where R is the isotope ratio of the element, F is the mass fraction value, and C is the concentration of the element, was used for the modeling. A represents the crustal component of the Granite Peak-Sawtooth granitoid (sample CH-7). B represents the mafic component of a locally erupted basalt (MB01-12). A table of the C and R values used is located in Appendix B along with the geochemical data for the endmembers used in the models.

This equation was applied using two different end members (silicic and mafic), to initially determine whether the $^{87}Sr/^{86}Sr$ and $^{143}Nd/^{144}Nd$ isotope ratios of the CST could be approximated, given that the modeling of Brueseke and Hart (2008) did not fully consider stable or radiogenic isotope characteristics in their modelling. Since the Cold Springs tuff unit is similar geochemically and isotopically to the Snake River Plain rhyolites (e.g. high Nb, etc.) silicic and mafic endmembers were chosen based on work by Christiansen and McCurry (2008) that suggest that Snake River Plain rhyolites were generated not just by solely melting upper curst, but contain a mantle component as well (Christiansen and McCurry, 2008; Callicoat, 2010). Numerous trials were performed using Granite Peak-Sawtooth granitoid samples with known Sr and Nd isotope values paired with locally erupted basalts and andesites with known Sr and Nd isotope values. Two mixing endmember samples were finally selected as representing the best fit to the Tcst data; CH-7 (Granite Peak-Sawtooth granite group) as the felsic endmember and MB01-12 (locally erupted 16.7 Ma basalt) as the mafic endmember. The two endmembers

were chosen based on the mixing curve approximating the location of the Cold Springs tuff sample in $^{87}Sr/^{86}Sr$ and $^{143}Nd/^{144}Nd$ as best as possible. This model was only applied toward one Cold Springs tuff sample (MB02-55) because this sample is the only reported by Brueseke and Hart (2008) that has both Sr and Nd isotope data. Also, MB01-12 is representative of the most geochemically and isotopically primitive mafic unit (Tb); all more evolved rocks, including the locally erupted Steens basalt (Tba) and the intermediate units, were poor fits as mafic endmembers. When performing the mixing calculations for $^{87}Sr/^{86}Sr$, ~70% of the felsic (e.g granitoid upper crustal component) best fits the $^{87}Sr/^{86}Sr_i$ Cold Springs tuff value. This is different from the $^{143}Nd/^{144}Nd$ mixing calculations that yield a felsic component of ~94%. The mixing curve is shown in Figure 4.1, from which the Cold Springs tuff sample lies along the curve at a value of ~75% felsic component. This range of 70 to 94% for the felsic endmember is higher than the calculated crustal components (≤40%) of McCurry and Rodgers (2009) for Snake River Plain rhyolites. However, Nash et al. (2006), found that mantle contribution at the craton boundary in distal fall deposits of Yellowstone hotspot sourced silicic eruptions is between 20-40% and as low as 5%. The 6 to 30% range of the mafic component calculated in this study fall within this range and is consistent with the transitional location of the SC, relative to the craton boundary. McCurry and Rodgers (2009) speculate that the mantle input is higher east of the craton boundary due to the presence of Archean crust. To help verify these modeling results, the NCI (Neodymium Crustal Index) was also used to determine the amount of upper crustal (e.g. silicic granitoid) input. Using the equation $NCI = (\varepsilon_{Nd\ (rock)} - \varepsilon_{Nd\ (mantle\ component)}) / (\varepsilon_{Nd\ (crustal\ component)} - \varepsilon_{Nd\ (mantle\ component)})$ after DePaolo et al. (1992), the NCI was determined to be 0.90 (Appendix B contain the ε_{Nd} values used in the equation). This means that the source is composed of 90% upper crust (e.g. granitoid). This number is comparable to the 94% granitoid that was calculated from the $^{143}Nd/^{144}Nd$ mixing calculations, but higher than the 70% granitoid component found from the $^{87}Sr/^{86}Sr$ mixing calculations; both are consistent in that the results require a substantial (e.g. 70 to 94% %) upper crustal granitoid component in the Cold Springs tuff magma. The difference seen between Sr and Nd isotope calculations may result from either Rb or Sr mobility, affecting the Sr isotope compositions of local magmas, post-emplacement. Brueseke (2006) reported post-eruptive modification of $^{87}Sr/^{86}Sr$ ratios from some SC silicic units due to this issue, as a result, calculated Nd mixing values are likely a more accurate reflection of the percentage of mixing components.

Modeling the $\delta^{18}O$ composition of the Cold Springs tuff was performed in a similar manner as discussed above, however because local Cretaceous and Cenozoic rocks aside from the new data generated in this study, lack $\delta^{18}O$ compositional data, the mafic endmember value was estimated from appropriate literature values. Two different model calculations were performed with a 5‰ and 6‰ value for the MB01-12 basalt, based on work by Bindeman et al. (2007) and Watts et al. (2010) that put the range of SRP basalts between 5 to 6‰, as well as prior work on global basalts that show similar values (Faure and Mensing, 2005). $\delta^{18}O$ values for the Granite Peak-Sawtooth felsic endmember were also varied from between -2‰ to 4‰, which are similar to those reported from the Idaho Batholith in the Owyhee Mountains, ID (Criss and Taylor, 1983; Boroughs et al., 2005). Oxygen isotope values were varied in the Granite Peak-Sawtooth samples to see whether the Cold Springs tuff sample would either fall on the curve or as close to the curve a possible since this would indicate the approximate $\delta^{18}O$ value of the Granite Peak-Sawtooth endmember. Originally, normal crustal values (9‰) were used to calculate the models but the Cold Spring tuff sample was far off the curve and in reevaluating the $\delta^{18}O$ value used, it was determined that in order to produce the low-$\delta^{18}O$ values seen in the Cold Springs tuff, the upper crustal endmember needed to be low in $\delta^{18}O$ due to hydrothermal alteration. Values of -2 to 4‰ were chosen as good $\delta^{18}O$ values from previous studies done on the Idaho Batholith where granitoid $\delta^{18}O$ values were lower than -4‰ and had an average of 2.3‰ (Criss and Taylor, 1983; Boroughs et al., 2005). These values are in the range of permissible fluid values, as calculated by Vikre (1987) for hydrothermal fluids at Buckskin Mountain. Figures 4.2 and 4.3 depict all of the model results. Figure 4.2A is a plot of $\delta^{18}O$ versus $^{87}Sr/^{86}Sr$ and 4.2B is a plot of $\delta^{18}O$ versus $^{143}Nd/^{144}Nd$ with 6‰ for the oxygen mafic component. Each small tick represents 10% increments of mixing and based on where the Cold Springs sample falls in Sr isotope space, there is almost a 50% silicic to mafic component. When looking at the $^{143}Nd/^{144}Nd$ mixing diagram, ~70% silicic to ~30% mafic input is present. In regards to Figure 4.3 with 5‰ being used for the mafic component, the results are similar to the 6‰ models and verify that the mafic component $\delta^{18}O$ composition is most likely within the 5 to 6‰ range.

In regards to oxygen isotope values, when varying the $\delta^{18}O$ values for the Granite Peak-Sawtooth sample, the Cold Springs tuff sample falls almost on the 2‰ model curve for $^{87}Sr/^{86}Sr$ and between the 2 to 4‰ curves. The range of $\delta^{18}O$ values of Cold Springs tuff samples are

represented by the purple bar along the x-axis of the diagrams and also fall within that 2 to 4 per mill envelope. Although the Sr and Nd isotope compositions have only been determined for a limited number of Cold Springs tuff samples, it can be inferred based on the relationships depicted in Figures 4.2 and 4.3 that the samples would fall within the 2 to 4‰ range of the altered Granite Peak-Sawtooth sample. This range of $\delta^{18}O$ values coincide with values found in the Idaho Batholith. Eocene meteoric water had a $\delta^{18}O$ of approximately -16‰ and altered granitoids have values of as low as -8‰ (Criss and Taylor, 1983). In the local Buckskin Mountain hydrothermal system, Miocene meteoric water $\delta^{18}O$ was calculated at -10.7‰ and hydrothermal fluids with a range of -12 to 6‰ present preceding the Cold Springs tuff eruption. There is also the prescience of Eightmile Mountain rhyolites adjacent to the Bell vein with $\delta^{18}O$ values of between 4.7 to 2‰ which are comparable to what is seen in the Cold Springs tuff (Vikre, 1987). However, we do not see $\delta^{18}O$ values as low as -8‰ as seen by Criss and Taylor (1983) but the average of all the whole rock $\delta^{18}O$ values they analyzed in the Idaho Batholith is 2.3‰ which is very similar to the lowest values found in the Cold Springs (Criss and Taylor, 1983; Boroughs et al., 2005). -2‰ and 0‰ curves in the models (Figures 4.2 and 4.3) would produce Cold Springs tuff values of <2‰ and since we do not see values of less than that in the analyzed Cold Spring samples, it is not probable that the source had values under 2‰. Testing $\delta^{18}O$ values of >4‰ do not make sense since again $\delta^{18}O$ values in the Cold Springs tuff are not higher than ~4‰ and a upper crustal source having greater than 4‰ $\delta^{18}O$ composition would not produce melts lower than 4‰.

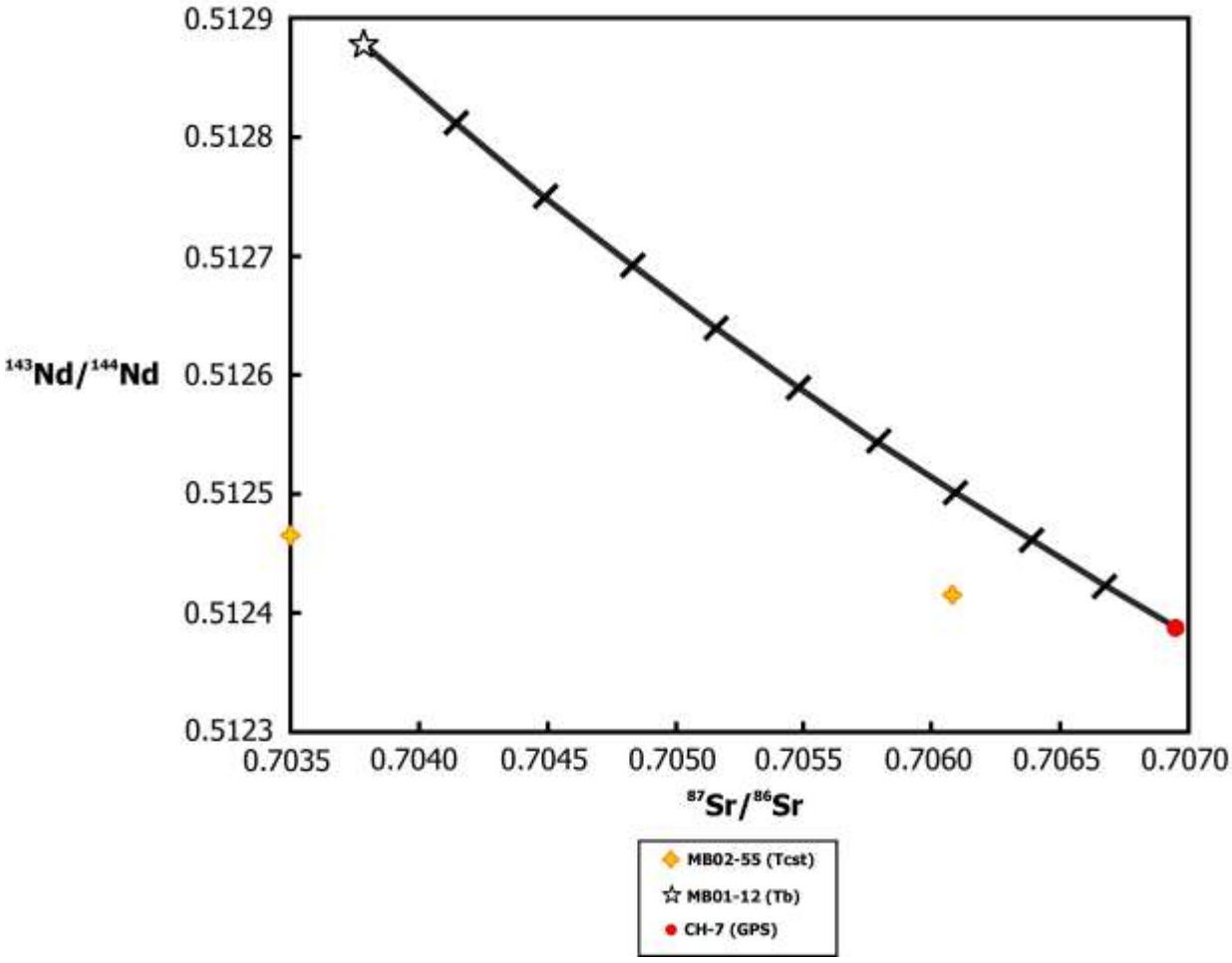

Figure 4.1: $^{87}Sr/^{86}Sr$ vs. $^{143}Nd/^{144}Nd$ Mixing Modeling Curve

A plot showing the modeling curve for initial $^{87}Sr/^{86}Sr$ vs. $^{143}Nd/^{144}Nd$. The red dot represents the upper crustal endmember and the star represents the mafic endmember. The Cold Springs tuff samples are represented by the yellow crosses. $^{87}Sr/^{86}Sr$ is not known for one of the Cold Springs tuff samples. Each line on the curve represents 10% mixing. 16.5 Ma age corrected Granite Peak-Sawtooth sample (data from Stuck, 1993; Brueseke and Hart, 2008).

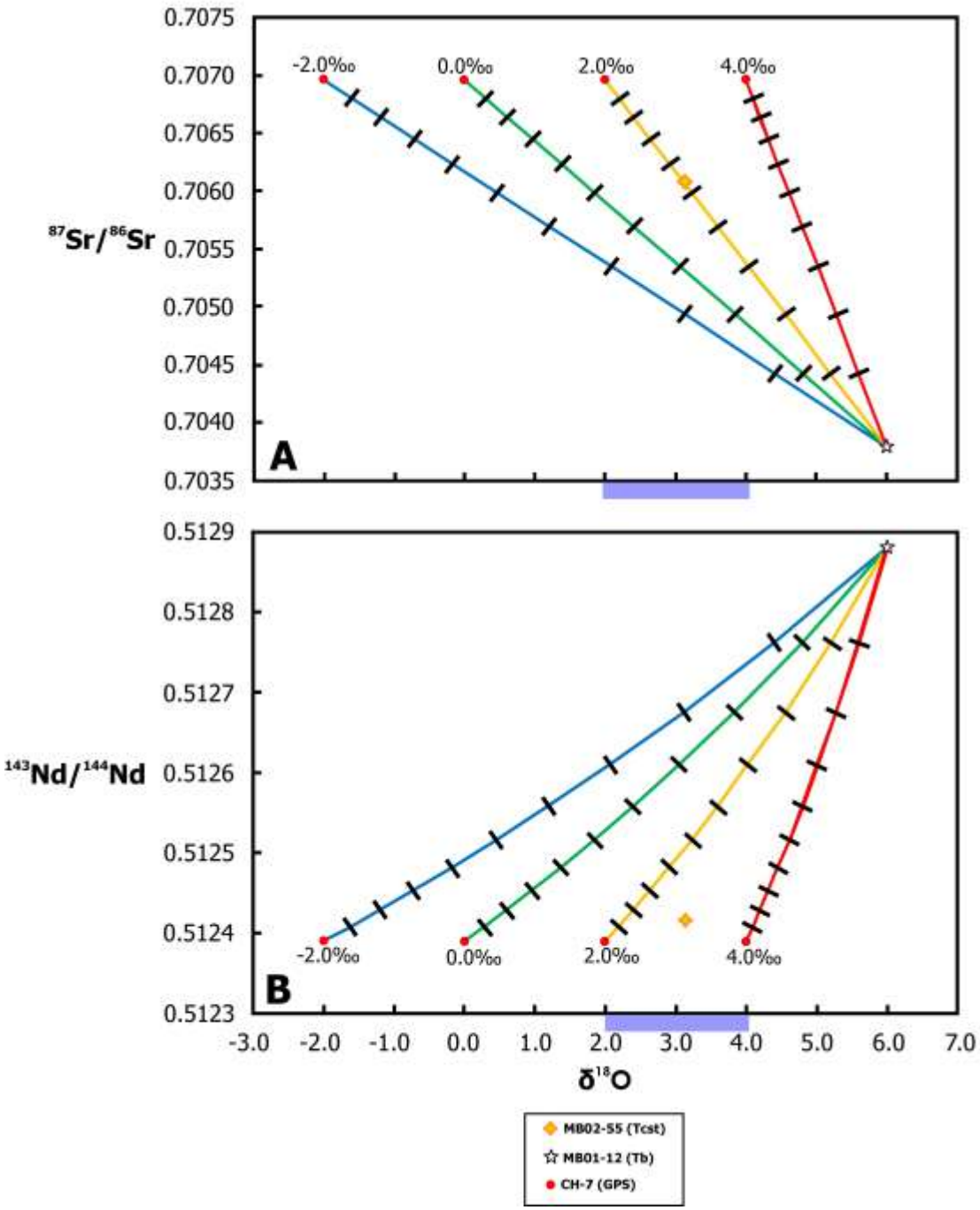

Figure 4.2: 6 ‰ Mafic $^{87}Sr/^{86}Sr$ and $^{143}Nd/^{144}Nd$ vs. $\delta^{18}O$ Mixing Modeling Curves
Plots showing the mixing modeling curves with the mafic endmember $\delta^{18}O$ value at 6 ‰. (A) $^{87}Sr/^{86}Sr$ vs. $\delta^{18}O$ and (B) $^{143}Nd/^{144}Nd$. Each curve represents the indicated crustal endmember $\delta^{18}O$ value with each line on the curve representing 10% mixing. The crustal endmember is represented by the red dots and the star is the mafic endmember. The purple bar indicates the range of Cold Springs tuff $\delta^{18}O$ values.

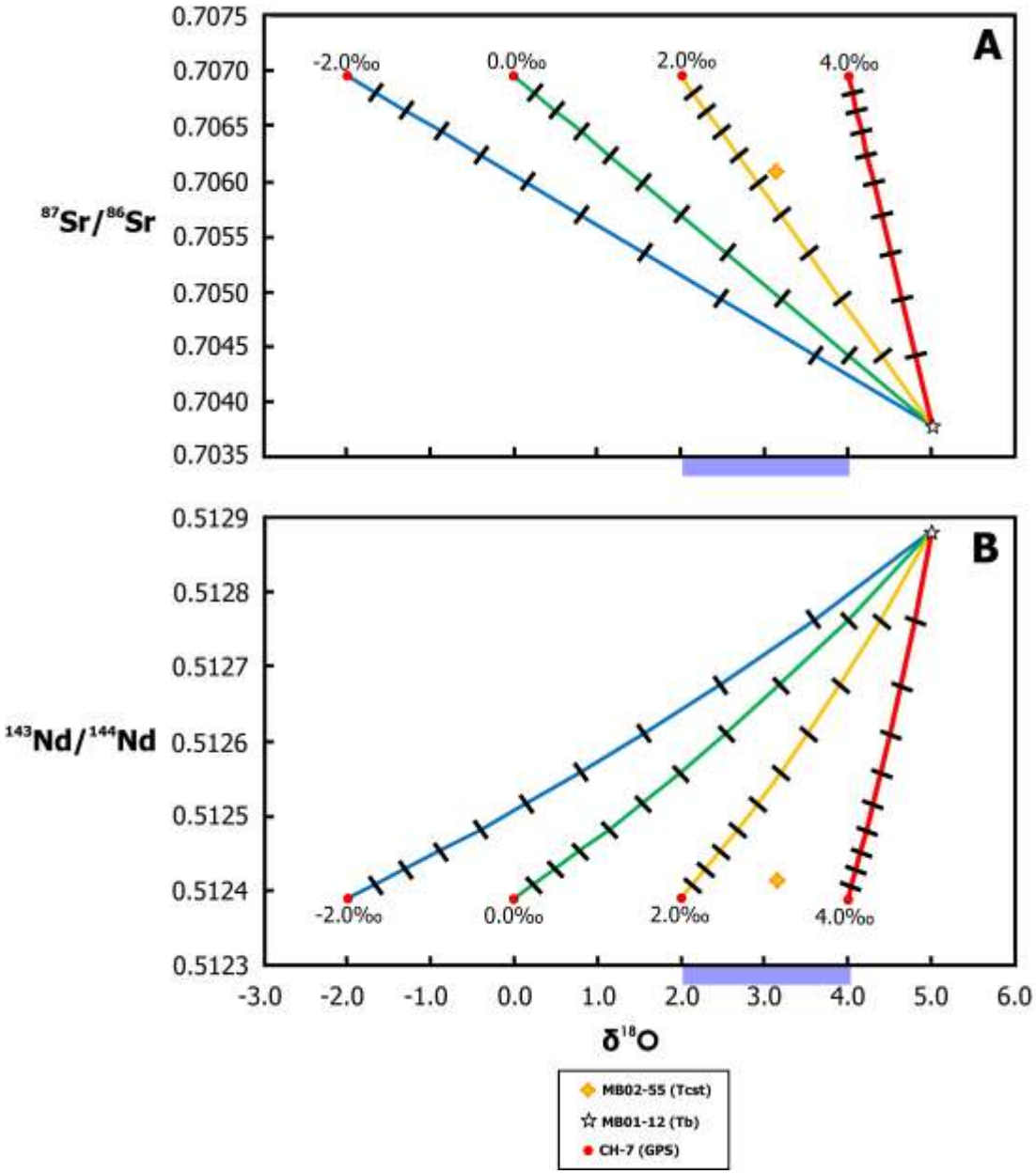

Figure 4.3: 5 ‰ Mafic $^{87}Sr/^{86}Sr$ and $^{143}Nd/^{144}Nd$ vs. $\delta^{18}O$ Mixing Modeling Curves

Plots showing the mixing modeling curves with the mafic endmember $\delta^{18}O$ value at 5 ‰. (A) $^{87}Sr/^{86}Sr$ vs. $\delta^{18}O$ and (B) $^{143}Nd/^{144}Nd$. Each curve represents the indicated crustal endmember $\delta^{18}O$ value with each line on the curve representing 10% mixing. The crustal endmember is represented by the red dots and the star is the mafic endmember. The purple bar indicates the range of Cold Springs tuff $\delta^{18}O$ values.

Chapter 5 - Discussion

The Cold Springs tuff is geochemically, isotopically, and temporally different from all other SC silicic units and is also the only unit to have been erupted from a small caldera (Brueseke and Hart, 2008). Based on these differences and the fact that after determining Cold Springs tuff $\delta^{18}O$ compositions and finding only low-$\delta^{18}O$ values, it is relevant to ask why is this unit the only unit in the SC characterized by low $\delta^{18}O$ compositions?

Simple two-component isotope mixing models suggest that in order to produce low-$\delta^{18}O$ Cold Springs tuff compositions, the upper crustal endmember (Granite Peak-Sawtooth group granitoid) had to have oxygen isotope values between 2 to 4‰. According to Criss and Taylor (1983) and Boroughs et al. (2005), it is possible to have $\delta^{18}O$ values as low as ~2‰ for hydrothermally altered granitoid. To produce these low-$\delta^{18}O$ values, there needs to be interaction between the rock and meteoric water/hydrothermal fluids in which temperature controls the amount of alteration and depletion of ^{18}O (e.g. the greater the temperature, the greater the alteration of the host rock; Criss and Taylor 1983; Bindeman and Valley, 2000; Boroughs et al., 2005; Watts et al., 2011). In this context, the local mid-Miocene hydrothermal system (e.g. Buckskin-National) is important. Vikre (1987) showed that alteration of volcanic rocks occurred at Buckskin Mountain to produce $\delta^{18}O$ values of 4.7 to 2.1‰ and that the hydrothermal fluids traveled deep below the surface. Leeman et al. (2009) show that it is possible for fluids to be transported as deep as 10 to 15 km to produce a viable amount of source magma. $\delta^{18}O$ values for Buckskin-area hydrothermal fluids were found between -12 to 6‰ and Miocene meteoric water was calculated to be -10.7‰ (Vikre, 2007). Also, there are numerous faults that cut across Buckskin Mountain and the Goosey Lake depression directly to the east. The Goosey Lake depression was a basin that formed via syn-magmatic extension that initiated at least 16.2 Ma, based on contact relationships between porphyritic rhyolite lavas that flowed east into the basin that overlie fluvial-lacustrine sedimentary strata (Brueseke, 2006; Brueseke and Hart, 2008). It is likely that these fluids, which are strongly depleted in $\delta^{18}O$, traveled along lithosphere-scale faults (e.g. 5 to 10+ km) down below the Goosey Lake depression and altered the primary upper-crustal source (e.g. Granite Peak-Sawtooth granitoid) of the Cold Springs tuff, depleting the granitoid $\delta^{18}O$ values to between 2 to 4‰. Figure 5.1 illustrates the potential shallow crustal hydrothermal circulation and surface flow of the fluids. In summary, the source of the Cold

Springs tuff is primarily Cretaceous Granite Peak-Sawtooth group granitoid upper crust, that was affected by partial melting initiated by upwelling mid-Miocene basalt (e.g. MB01-12). The Sr and Nd isotope modeling and NCI calculations performed in this study also indicate that the Cold Springs tuff source was not solely silicic upper-crust crust or melts of that crust (e.g. GPS granitoid); it had to have been a hybridized source of Cretaceous granitoid with a minor mafic component (e.g. 6% basalt, based on the Nd isotope mixing results and NCI calculations), which agress with the prior work of Nash et al. (2006). Furthermore, the O isotope results and modeling indicate that this hybridized source had to have been affected by the hydrothermal fluids prior to Cold Springs tuff magmatism; these fluids were likely sourced from the nearby Buckskin-National district (e.g. mineralization centered around Buckskin Mountain).

Relationship to the low-$\delta^{18}O$ production models

Prior work by Brueseke and Hart (2008) and the modeling performed in this study indicate that the source of the Cold Springs tuff was hybridized (e.g. by mafic input) Cretaceous granitoid, similar to CSRP rhyolites (Nash et al, 2006; Leeman et al, 2009). Furthermore, local geologic relationships and the Oxygen isotope compositions determined in this study shed light on which of the two competing models (e.g. "prior alteration" or "caldera cannibalization") for low Oxygen rhyolites best fits the SC. The "caldera cannibalization" model of Bindeman and Valley (2001) attribute the lowering of $\delta^{18}O$ values through caldera collapse and eruption, followed by hydrothermal alteration of the intra-caldera fill that over time and after successive eruptions and caldera collapses, lowers the fill-sourced magma $\delta^{18}O$ values. The "prior alteration" model of Boroughs et al. (2005) is best seen in the CSRP, where no normal rhyolite $\delta^{18}O$ values exist, and there is not a progressive lowing of the $\delta^{18}O$ values through time, suggesting that the magma source region must have been affected by a previous hydrothermal event. A recent study of the Picabo volcanic field (10.4 - 6.6 Ma), another Yellowstone-Snake River Plain caldera complex located east of the Twin Falls eruptive center (Figure 5.2), was found characterized by a lowering of $\delta^{18}O$ values over time, like Heise and Yellowstone. However, unlike Yellowstone and Heise, an early appearance of abundant low-$\delta^{18}O$ rhyolites are attributed to prior hydrothermal alteration of the crustal magma source due to fluids migrating along faults that formed via Basin and Range extension (Drew et al., 2013). These results are similar to the results obtained in this study. In the case of Picabo, the prior alteration

model (Boroughs et al. 2005) was the initial mechanism for generating a low-$\delta^{18}O$ source and over the successive caldera collapses, the $\delta^{18}O$ values were lowered in the manner proposed by Bindeman and Valley (2001), indicating that both models can exist together in the same magmatic system.

The cannibalization model of Bindeman and Valley (2001) does not work for the production of the Cold Springs tuff because there is not a successive lowering of $\delta^{18}O$ over time. Also, in both the Yellowstone and Heise volcanic fields (Watts et al., 2011), the amount of time to create significantly lower $\delta^{18}O$ magmas was over 0.5 Ma while the Cold Springs tuff caldera was only active for 0.3 Ma (Bindeman and Valley, 2001; Brueseke and Hart, 2008; Watts et al., 2011). These discrepancies suggest that the primary mechanism for the low $\delta^{18}O$ compositions that characterize the Cold Springs tuff was prior hydrothermal alteration of the Cold Springs tuff source; this follows the "prior alteration" model of Boroughs et al. (2005). Furthermore, it is significant that hydrothermal activity associated with the Buckskin-National district ceased when Cold Springs magmatism initiated and caused a lowering of the water table by subsidence that apparently shut off the hydrothermal system (Vikre, 1987; 2007; Brueseke and Hart, 2008; Brueseke, 2011). Prior to Cold Springs tuff volcanism, hydrothermal fluids from Buckskin Mountain traveled along faults into the Goosey Lake depression, altering Granite-Peak-Sawtooth granitoid upper crust. This crustal source was then partially melted by upwelling basalt, to form the least evolved Cold Springs tuff magma, which then underwent fractional crystallization in the upper crust prior to eruption (Knight et al., 2004; Brueseke and Hart, 2008).

Regional to Global Comparisons

Low-$\delta^{18}O$ rhyolites are found in other areas of the United States and the world, including Iceland, South Africa, and Missouri, USA. In Iceland, the Krafla central volcano is located on the North Iceland Rift Zone and associated with the Krafla geothermal field, which has been drilled for geothermal energy sources (Zierenberg, 2013). The Krafla geothermal field lies in a collapse caldera that formed about 110 ka (Zierenberg, 2013). There are multiple fissure swarms that cut through the field which are part of the North Iceland Rift and most the caldera is filled with basaltic lavas, however rhyolites have erupted periodically (Zierenberg, 2013). Recent drilling in the Krafla field encountered a rhyolite melt (Zierenberg, 2013). Vesiculated glass that cooled from this melt was analyzed for $\delta^{18}O$ and was found to be depleted in oxygen ($\delta^{18}O$ =

3.2‰; Zierenberg, 2013). Zierenberg et al. (2013) determined that the rhyolite became low in $\delta^{18}O$ due to the incorporation of prior hydrothermally altered wall rock into the original melt by the results of their data and of data from previous studies, supporting the prior alteration model by Boroughs et al. (2005; 2012).

In the Bushveld Complex in South Africa, granites were found to have an average magmatic $\delta^{18}O_{zircon}$ value of around 6.6 ‰ (Fourie and Harris, 2011). Zircon was used as a more reliable mineral because of its resistance to alteration. This magmatic value of 6.6 ‰ is on the lower spectrum of average granite $\delta^{18}O$ values (6 to 10.3 ‰) (Taylor, 1968; Fourie and Harris, 2011). These granites are not from true low-$\delta^{18}O$ magmas but there is some interaction of water into the system (Fourie and Harris, 2011). Unlike the Boroughs et al. (2005) model, there was not an input of a foreign low-$\delta^{18}O$ contaminant like the Idaho Batholith influencing the melts of the Snake River Plain. It was determined that the probable cause of the lower $\delta^{18}O$ was due to fluids interacting with the roof rock under high temperature conditions causing alteration and a lowering of the $\delta^{18}O$ values (Fourie and Harris, 2011). These altered roof rocks were then assimilated into the magma body that formed the granites of the Bushveld Complex (Fourie and Harris, 2011). So even though the process is slightly different than the Boroughs et al. (2005) model, the prior alteration of the assimilated rocks is still similar and that is possible that the processes that make up the model can vary.

Another example of low oxygen rhyolites and associated alteration affecting silicic magmas is found in the St. Francois Mountains in Missouri, USA. There are two large Mesoproterozoic (~1470 Ma) calderas (the Bulter Hill and Taum Sauk) in this region. Associated with the calderas are rhyolite lavas and tuffs, dacites, and granitic plutons (e.g. ring intrusions, resurgent domes, and likely "mother plutons") (King et al., 2008). King et al (2008) identified two major hydrothermal events, the first at 1.48 Ga, that affected the older Taum Sauk caldera and the second event at 1.33 Ga, the affected the younger Butler Hill caldera. The first event caused the formation of Fe-oxide deposits in the region and the second event was a high temperature hydrothermal event associated with fluorite mineralization that occurred about 100 Ma after the intrusion of the Stono Mountain Granite (King et al., 2008). Taum Sauk zircon and quartz from Profit Mountain Formation rhyolite tuffs, Johnson Shut-Ins ash-flow tuffs, Cope Hollow water laid tuff, Munger granite, Graniteville granite, and Pilot Knob felsite were measured for $\delta^{18}O$ compositions, as well Butler Hill quartz and zircon from the Stouts Creek

rhyolite, Lake Killarney Formation tuff, Grassy Mountain Ignimbrite, Knob Lick quarry granite and rhyolite, Silvermine granite, and Hawn State Park granite (King et al., 2008). King et al. (2008) document that all of the $\delta^{18}O$ values show normal levels and no major alteration. In the Taum Sauk caldera there was a low temperature alteration event (King et al., 2008). Most of the rhyolite and nearby intrusions associated with the Taum Sauk caldera show $\delta^{18}O$ values ~ equal to 8‰, though units found in Johnson Shut-Ins all show enrichment in $\delta^{18}O$ (up to 16‰, the highest in the region). King et al, 2008 attribute the high $\delta^{18}O$ values to low temperature hydrothermal activity (<300°C) that enriched the rocks in $\delta^{18}O$, unlike high temperature hydrothermal activity (>500°C) that depletes $\delta^{18}O$. These altered rocks could have been remelted after caldera collapse and would have raised the overall $\delta^{18}O$ to around 10‰ which would match the granite intrusions analyzed in the area (King et al., 2008). In the Butler Hill caldera, evidence for local high temperature hydrothermal activity is observed in one ring intrusion. $\delta^{18}O$ values for the main rhyolite unit (Grassy Mountain ignimbrite) are ~8‰, which is consistent through the region. The one ring intrusion (Stono Mountain granite) has values of 8.2 to 4.2‰. These lower values are thought to have formed by incorporation of hydrothermally altered crust into the larger Butler Hill magma body during cooling, which lowered the $\delta^{18}O$ of the magma that sourced the subsequent intrusions (King et al., 2008). The process of lowering the $\delta^{18}O$ of these St. Francois Mountains area magmas is the same as observed in the Snake River Plain.

In summary, studies show that both models can be applied to various regions around the world and are not just applicable in the northern Great Basin and Pacific Northwest, USA. However, it seems that the prior alteration model by Boroughs et al. (2005; 2012) is the more common method of producing low-$\delta^{18}O$ magmas and can be applied to caldera and non-caldera systems. The model by Bindeman and Valley, 2001 is only applicable to large scale caldera systems. This conclusion is consistent with the results of this study. The Cold Spring tuff source was hydrothermally altered before eruption and even though the unit was erupted from a caldera, there was only one unit erupted and no evidence that there was a lowering of the $\delta^{18}O$ values over time. In South Africa, the Bushveld Complex did see hydrothermal alteration but the water influence was not as much as is seen in the Idaho Batholith, and Iceland. The same could be said for the St. Francois Mountains where there was more low temperature hydrothermal activity, which in fact, raised the $\delta^{18}O$ values. The one high temperature alteration event was minor and

caused a range of $\delta^{18}O$ values from 8.2 to 4.2 ‰. In the Iceland study, hydrothermal fluids played a strong role in altering the source rocks which caused lower $\delta^{18}O$ values of 3.2‰, which is what is seen in the Cold Springs tuff (Zierenberg, 2013). Out of the three areas analyzed, Iceland seems to be the best comparison to the processes that altered the Cold Springs tuff source.

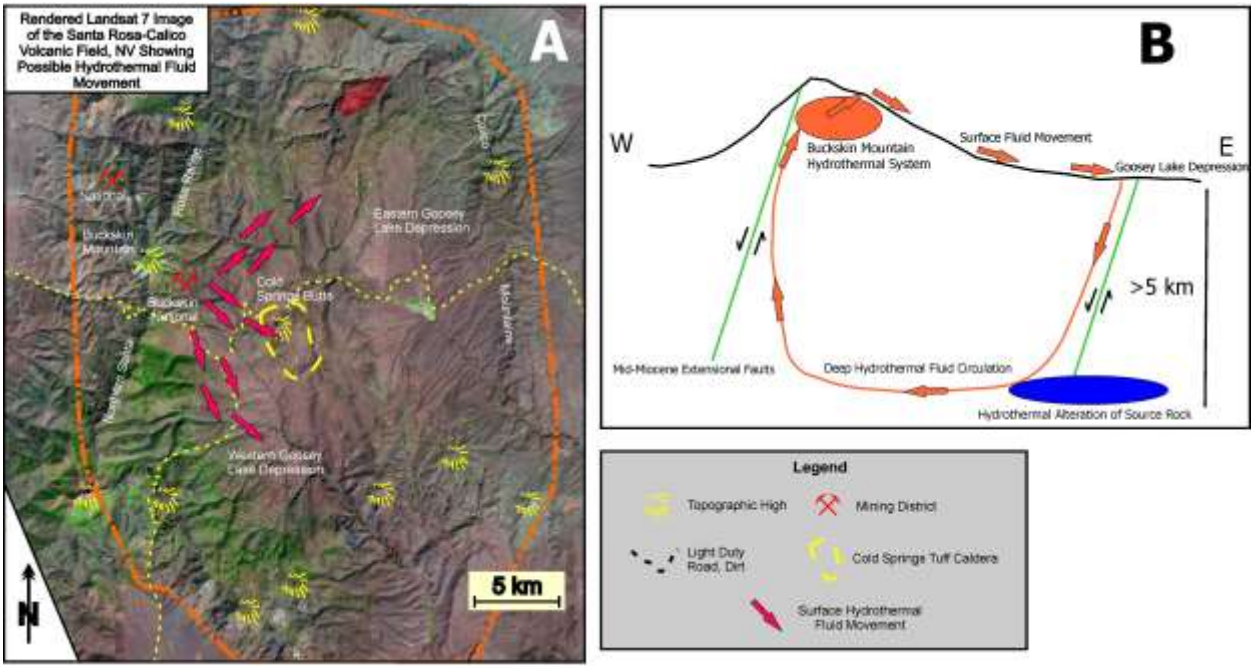

Figure 5.1: Local Hydrothermal Fluid Movement

(A) A Rendered Landsat 7 image of the SC showing the location of Buckskin National mining district with topographic highs and other geographic features. The orange dashed line represents the extent of the SC and the dashed yellow lines represent major roads. Pink arrows indicate probable surface fluid movement from Buckskin Mountain (from Brueseke and Hart, 2008). (B) Possible deep hydrothermal fluid movement diagram of fluids from Buckskin Mountain. Surface fluids traveled down into the Goosey Lake Depression and traveled along extensional faults deep underground altering the preexisting Cold Springs tuff source rock. These fluids then continued underground to other extensional faults under Buckskin Mountain and up to the surface again.

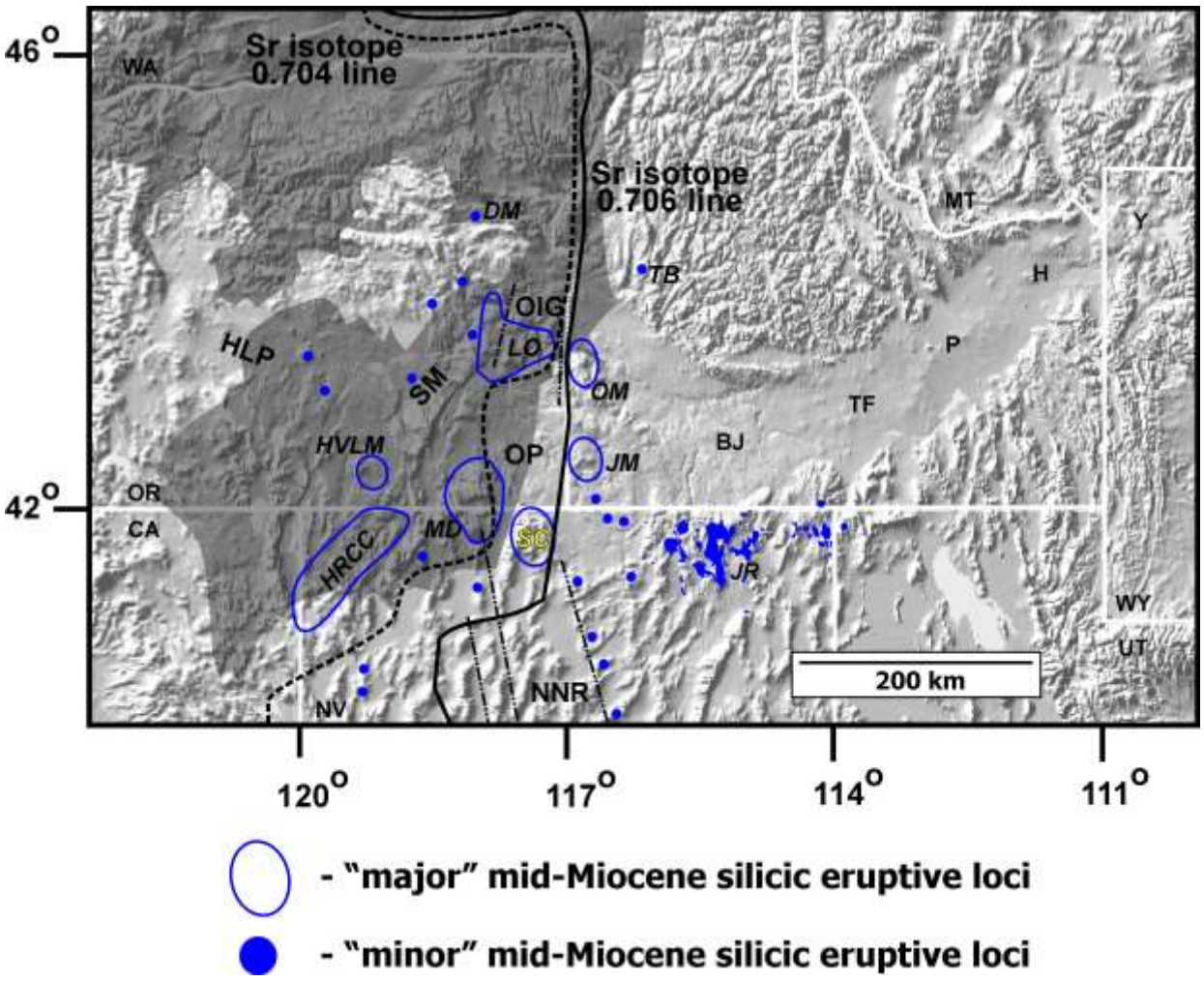
46°
42°
120°
117°
114°
111°
WA
OR
CA
NV
Sr isotope
0.704 line
Sr isotope
0.706 line
DM
TB
OIG
LO
HLP
SM
OM
HVLM
OP
JM
MD
SC
HRCC
JR
NNR
MT
Y
H
P
TF
BJ
WY
UT
200 km
- "major" mid-Miocene silicic eruptive loci
- "minor" mid-Miocene silicic eruptive loci

Figure 5.2: Picabo Location Map

Map of the northwestern United States depicting selected Cenozoic tectonomagmatic features (after Brueseke and Hart, 2008). Gray shading depicts the region where mid-Miocene Columbia River (WA-OR-ID) and Steens (OR-NV-ID-CA) flood basalt lavas crop out. Extensional features (e.g. the northern Nevada rift [NNR], the Oregon-Idaho graben [OIG], and others) are depicted as dashed black lines. The SC is labeled in yellow. The location of large mid-Miocene volcanic fields are depicted: MD, McDermitt; LO, Lake Owhyee; HRCC, High Rock Caldera Complex; SC, Santa Rosa-Calico volcanic field; JR, Jarbidge Rhyolite domes and flows; JM, Juniper Mountain volcanic center; OM, Owyhee mountains and Silver City district centers; DM, Dooley Mountain; TB, Timber Butte; HVLM, Hawks Valley-Lone Mountain complex. Blue dots are other coeval silicic eruptive loci. Y, Yellowstone volcanic field; H, Heise volcanic field; P, Picabo volcanic field; TF, Twin Falls eruptive center; BJ, Bruneau-Jarbidge volcanic field; HLP, Oregon high lava plains; OP, Owyhee Plateau; WSRP, western Snake River plain; CSRP, central Snake River plain; ESRP, eastern Snake River plain. The initial $^{87}Sr/^{86}Sr$ 0.706 and 0.704 isopleths are depicted as dotted and dashed black lines. These are commonly interpreted to define the western edge of the Precambrian North American craton (the 0.706 isopleth), and a zone of transitional lithosphere (after Armstrong et al., 1977; Kistler and Peterman, 1978; Leeman et al., 1992; Crafford and Grauch, 2002).

Chapter 6 - Summary

Cenozoic low-$\delta^{18}O$ rhyolites are found throughout the Snake River Plain and in Yellowstone volcanic field, USA. Two competing models exist that focus on the origin of these low-$\delta^{18}O$ rhyolites. One model first proposed by Bindeman and Valley (2000) at Yellowstone suggests that low-$\delta^{18}O$ rhyolites formed due to caldera collapse and remelting of hydrothermally altered intra-caldera fill; each successive eruption-collapse-remelting cycle progressively lowered $\delta^{18}O$ values of the erupted magma over time. The second model, proposed by Boroughs et al. (2005), suggests that low-$\delta^{18}O$ rhyolites in the CSRP formed via melting of Idaho Batholith upper crust, that was hydrothermally altered prior to the silicic melting event(s).

The SC is a good location to test both of these competing models because it was petrogenically and geochemically well constrained by Brueseke and Hart (2008) and its location is adjacent to the work of Boroughs et al. (2005). Furthermore, there is a small caldera present and accompanying explosive silicic eruptive deposits exist. Volcanism in the SC began at 16.7 Ma and lasted till about 14 Ma. The youngest erupted silicic unit, the Cold Springs tuff, is geochemically and isotopically different than all other silicic units the SC and was the only unit that erupted from a caldera (Brueseke and Hart, 2008). Along with mid-Miocene volcanism, there was an active hydrothermal system at Buckskin Mountain, within the volcanic field, that now hosts Au-Ag mineral deposits that formed prior to and ended around the time of the eruption of the Cold Springs tuff at ~15.6 Ma (Vikre, 2007; Brueseke and Hart, 2008; Brueseke, 2011).

Sr and Nd isotope data show a relationship between the Cold Springs tuff and the Granite Peak-Sawtooth granitoids, one of two groups of Cretaceous granitoid upper crust that underlies the Cenozoic volcanic package in the SC (Brueseke and Hart, 2008). $\delta^{18}O$ analysis of SC silicic units yield normal compositions ($\delta^{18}O$ >6‰) for all major silicic units of the SC except the younger Cold Springs tuff, which has $\delta^{18}O$ compositions between 2.36 to 4.05‰. Petrologic modeling indicates that the melting of the Granite Peak-Sawtooth group granitoid, coupled with a mantle component (e.g. $^{144}Nd/^{143}Nd$ modeling suggests ~6% mid-Miocene basalt) is the most likely source of Cold Springs tuff magmas. To produce the low-$\delta^{18}O$ values observed the Cold Springs tuff, the granitoid had to be hydrothermally altered, which likely occurred by interaction with hydrothermal fluids sourced from the hydrothermal system centered on Buckskin Mountain. The process of forming the low-$\delta^{18}O$ rhyolites in the SC follows the prior hydrothermal

alteration model of Boroughs et al. (2005). Mid-Miocene mineralization affected a wide region of the northern Great Basin and area adjacent to and including parts of the CSRP and Owyhee Plateau studied by Boroughs et al. (2005; 2012). Thus, this work suggests that mid-Miocene hydrothermal alteration of regional crust, where the fluids followed lithosphere-scale faults related to syn-magmatic extension, is also a viable mechanism to generate altered upper crust that could later melt and form low-$\delta^{18}O$ rhyolites.

Chapter 7 - Suggested Future Work

To better constrain the origin of the Cold Springs tuff, more Pb isotope data is needed on the local granitoids to see if the differences of Pb isotopes in the Cold Springs tuff can be correlated with the Granite Peak-Sawtooth. Obtaining oxygen isotope data would also help better constrain the models in this study and provide insight as to whether or not the Granite Peak-Sawtooth granitoids were hydrothermally altered. This data is currently being obtained at Miami University and will should provide a more detailed understanding of the local granitoids and more conclusive relationships between the granitoids and SC silicic units.

Another way to better constrain the origin of the Cold Springs tuff is to obtain $\delta^{18}O$ values on zircons in the Cold Springs tuff since they are very resistant to alteration and would give better insight in to the source magmatic $\delta^{18}O$ values. Then the oxygen isotopes obtained could then be compared to the oxygen isotopes of quartz and feldspar already obtained.

References

Almeev, R.R., Bolte, T., Nash, B.P., Holtz, F., Erdmann, M., and Cathey, H.E., 2012, High-temperature, low H_2O silicic magmas of the Yellowstone hotspot: an experimental study of rhyolite from the Bruneau-Jarbidge eruptive center, Central Snake River Plain, USA: Journal of Petrology, v. 53, p. 1837-1866.

Armstrong, R.L., Taubneck, W.H., and Hales, P.O., 1977, composition, Oregon, Washington, and Idaho Rb-Sr and K-Ar geochronometry of Mesozoic granitic rocks and their Sr isotopic: Geological Society of America Bulletin, v. 88, p. 397-411.

Bindeman, I.N, and Valley, J.W, 2000, Formation of low-$\delta^{18}O$ rhyolites after caldera collapse at Yellowstone, Wyoming, USA: Geology, v. 28, p. 719-722.

Bindeman, I.N., and Valley, J.W., 2001, Low-$\delta^{18}O$ rhyolites from Yellowstone: Magmatic evolution based on analyses of zircons and individual phenocrysts: Journal of Petrology, v. 42, p. 1491-1517.

Bonnichsen, B., Leeman, W.P., Honjo, N., McIntosh, W.C., and Godchaux, M.M., 2008, Miocene silicic volcanism in southwestern Idaho; geochronology, geochemistry, and evolution of the central Snake River Plain: Bulletin of Volcanology, v. 70, p. 315-342.

Boroughs, S., Wolff, J., Bonnichsen, B., Godchaux, M., Larson, P., 2005, Large-volume, low-$\delta^{18}O$ rhyolites of the central Snake River Plain, Idaho, USA: Geology, v. 33, p. 821-824.

Boroughs, S., Wolff, J.A., Ellis, B.S., Bonnichsen, B., Larson, P.B., 2012, Evaluation of models for the origin of Miocene low-$\delta^{18}O$ rhyolites of the Yellowstone/Columbia River Large Igneous Province: Earth and Planetary Science Letters, v. 313-314, p. 45-55.

Brown, K.L, 2011, Geochemical heterogeneities along a paleo-continental margin: An example from late Cretaceous intrusions, Santa Rosa Range, Northwestern Nevada: Geological Society of America Abstracts with Programs, v. 43, p. 90

Brueseke, M.E., 2006, Mid-Miocene magmatic system development in the northwestern United States [Dissertation]: Miami University, p. 440.

Brueseke, M.E., Heizler, M.T., Hart, W.K., and Mertzman, S.A., 2007, Distribution and geochronology of Oregon Plateau (U.S.A.) flood basalt volcanism; the Steens Basalt revisited: Journal of Volcanology and Geothermal Research, v. 161, p. 187-214.

Brueseke, M.E., and Hart, W.K., 2008, Geology and petrology of the mid-Miocene Santa Rosa-Calico volcanic field, northern Nevada, Nevada Bureau of Mines and Geology, Bulletin 113, p. 83.

Brueseke, M.E., and Hart, W.K., 2009, Geology and geochemistry of early Miocene intermediate composition volcanism in northern Nevada and its relationship to regional tectonomagmatic processes: Geologocical Society of America Abstracts with Programs, v. 41, p. 337-338.

Brueseke, M.E., and Hart, W.K., 2009, Intermediate composition magma production in an intracontinental setting: Unusual andesites and dacites of the Mid-Miocene Santa Rosa-Calico volcanic field, Northern Nevada: Journal of Volcanology and Geothermal Research, v. 188, p. 197-213.

Brueseke, M.E., 2011, Magmatism and mineralization in the northern Great Basin: Mid-Miocene volcanism related to the inception of the Yellowstone hotspot and its relationship to regional bonanza ore deposits: in R. Steininger, and W. Pennell, eds., Great Basin Evolution and Metallogeny, Geological Society of Nevada 2010 Symposium Proceedings, p. 247-255.

Brueseke, M.E., Callicoat, J.S., Hames, W., Larson, P.B., in review, Mid-Miocene rhyolite volcanism in northeastern Nevada: the Jarbidge Rhyolite and its relationship to the Cenozoic evolution of the northern Great Basin (U.S.A.), The Geological Society of America Bulletin.

Callicoat, J., 2010, Significance of Mid-Miocene Volcanism in Northeast Nevada: Petrographic, Chemical, Isotopic, and Temporal Importance of the Jarbidge Rhyolite [Master Thesis]: Kansas State University, p.116.

Camp, V.E., Ross, M.E., and Hanson, W.E., 2003, Genesis of flood basalts and Basin and Range volcanic rocks from Steens Mountain to the Malheur River gorge, Oregon: Geological Society of America Bulletin, v. 115, p. 105-128.

Camp, V.E., and Ross, M.E., 2004, Mantle dynamics and genesis of mafic magmatism in the intermontane Pacific Northwest: Journal of Geophysical Research, v. 109, p. B08204.

Cathey, H.E., and Nash, B.P., 2009, Pyroxene thermometry of rhyolite lavas of the Bruneau–Jarbidge eruptive center, Central Snake River Plain: Journal of Volcanology and Geothermal Research, v. 188, p. 173-185.

Chase, R.B., Bickford, M.E., and Tripp, S. E., 1978, Rb-Sr and U-Pb isotopic studies of the northeastern Idaho batholith and border zone: Geological Society of America Bulletin, v. 89, p. 1325-1334.

Christiansen, E.H., and McCurry, M., 2008, Contrasting origins of Cenozoic silicic volcanic rocks form the western Cordillera of the United States: Bulletin of Volcanology, v. 70, p. 251-267.

Church, S.E., 1985, Genetic interpretation of lead-isotopic data from the Columbia River Basalt Group, Oregon, Washington, and Idaho: Geological Society of America Bulletin, v. 96, p. 676-690.

Coble, M.A., and Mahood, G.A., 2012, Initial impingement of the Yellowstone plume located by widespread silicic volcanism contemporaneous with Columbia River flood basalts: Geology, v. 40, p. 655-658.

Colgan, J.P., and Henry, C.D., 2009, Rapid middle Miocene collapse of the Mesozoic orogenic plateau in north-central Nevada: International Geology Review, v. 51, p. 920-961.

Colgan, J.P., 2013, Reappraisal of the relationship between the northern Nevada rift and Miocene extension in the northern Basin and Range Province: Geology, v. 41, p. 211-214.

Compton, R.R., 1960, Contact metamorphism in Santa Rosa Range, Nevada: Geological Society of America Bulletin, v. 71, no. 9, p. 1383-1416.

Coney, P.J., and Reynolds, S.J., 1977, Cordilleran Benioff zones: Nature, v. 270, p.403-406.

Crafford, E.E.J., and Grauch, V.J.S., 2002, Geologic and geophysical evidence for the influence of deep crustal structures on Paleozoic tectonics and the alignment of world-class gold deposits, north-central Nevada, USA: Ore Geology Reviews, v. 21, p. 157–184.

Criss, R.E., and Taylor, H.P., 1983, An $^{18}O/^{16}O$ and D/H study of Tertiary hydrothermal systems in the southern half of the Idaho batholith: Geological Society of America Bulletin, v. 94, p. 640-663.

DePaolo, D.J., Perry, F.V., Baldridge, W.S., 1992, Crustal versus mantle sources of granitic magmas: A two-parameter model based on Nd isotope studies: Transactions of the Royal Society of Edinburgh: Earth Sciences, v. 83, p. 439-446.

Drew, D., Bindeman, I., Watts, K., Schmitt, A.K, Fu, B., McCurry, M., 2013, O and Hf isotopic evidence in zircons for crustal recycling in caldera complexes and rifts, Picabo volcanic field, Yellowstone hotspot track: Mineralogical Magazine, v. 77, p. 1008.

Ellis, B.S., and Wolff, J.A., 2012, Complex storage of rhyolite in the Central Snake River Plain: Journal of Volcanology and Geothermal Research, v. 211-212, p. 1-11.

Ekren, E.B., McIntyre, D.H., and Bennett, E.H., 1984, High-temperature, large-volume, lava like ash-flow tuffs without calderas in southwestern Idaho: Geological Survey Professional Paper 1272, p. 1-73.

Farmer, G.L., and DePaolo, D.J., 1983, Origin of Mesozoic and Tertiary granite in the western United States and implications for pre-Mesozoic crustal structure 1. Nd and Sr isotopic studies in the geocline of the northern Great Basin: Journal of Geophysical Research, v. 88, p. 3379-3401.

Faure, G., and Mensing, T.M., 2005, Isotopes; Principles and applications: John Wiley & Sons: Hoboken, NJ, United States, p. 897.

Frost, B.R., Barnes, C.G., Collins, W.J., Arculus, R.J., Ellis, D.J., and Frost, C.D., 2001, A geochemical classification for granitic rocks: Journal of Petrology, v. 42, p. 2033-2048.

Frost, C.D., and Frost, B.R., 2011, On ferroan (A-type) granitoids: Their composition variability and modes of origin: Journal of Petrology, v. 52, p. 39-53.

Ford, M.T., Grunder, A.L., Duncan, R.A., 2013, Bimodal volcanism of the high lava plains and northwestern Basin and Range of Oregon: The distribution and tectonic implications of age-progressive rhyolites: Geochemistry, Geophysics, Geosystems, DOI: 10.1002/ggge.20175.

Fourie, D.S., and Harris, C., 2011, O-isotope study of the Bushveld Complex granites and granophyres: constraints on source composition, and assimilation: Journal of Petrology, v.52, no. 11, p. 2221-2242.

Gaschnig, R.M., Vervoort, J.D., Lewis, R.S., and McClelland, 2010, Migrating magmatism in the northern US Cordillera: in situ U–Pb geochronology of the Idaho batholith: Contributions in Mineral Petrology, v. 159, p. 863-883.

Gaschnig, R.M., Vervoort, J.D., Lewis, R.S., and Tikoff, B., 2011, Isotopic evolution of the Idaho Batholith and Challis intrusive province, northern US Cordillera: Journal of Petrology, v. 52, no. 12, p. 2397-2429.

Hanson, R.E., Girty, G.H., Harwood, D.S., and Schweickert, R.A., 2000, Paleozoic subduction complex and Paleozoic-Mesozoic island-arc volcano-plutonic assemblages in the northern Sierra terrane: Geological Society of America Field Guide 2, p. 255-278.

Hasten, Z.L., 2012, Mid-Miocene magmatism in the Owyhee Mountains, ID: Origin and petrogenesis of volcanic rocks in the Silver City District [Master Thesis]: Kansas State University, p. 222.

Henry, C.D., McGrew, A.J., Colgan, J.P., Snoke, A.W., and Brueseke, M.E., 2011, Timing, distribution, amount, and style of Cenozoic extension in the northern Great Basin: Geological Society of America Field Guide 21, p. 27-66.

Jordan, B.T., Grunder, A.L., Duncan, R.A., and Deino, A.L., 2004, Geochronology of age progressive volcanism of the Oregon High Lava Plains: Implications for the plume interpretation of Yellowstone: Journal of Geophysical Research, v. 109, p. B10202.

King, E.M., Valley, J.W., Stockli, D.F., and Wright, J.E., 2004, Oxygen isotope trends of granitic magmatism in the Great Basin: Location of the Precambrian craton boundary as reflected in zircons: GSA Bulletin, v. 116, p. 451-462

King, E.M., Trzaskus, A.P., and Valley, J.W., 2008, Oxygen isotope evidence for magmatic variability and multiple alteration events in the Proterozoic St. Francois Mountains, Missouri: Precambrian Research, v. 165, p. 49-60.

Kistler, R.W., and Peterson, Z.E., 1973, Variations in Sr, Rb, K, Na, and Initial Sr87/Sr86 in Mesozoic Granitic Rocks and Intruded Wall Rocks in Central California: Geological Society of America Bulletin, v. 84, p. 3489-3512.

Kistler, R.W., and Peterson, Z.E., 1978, Reconstrction of crustal blocks of California on the basis of initial strontium isotopic compositions of Mesozoic granitic rocks: Geological Survey Professional Paper 1071, p. 1-17.

Kolb, J., Whiting, E., Brueseke, M.E., and Hasten, Z.E.L., 2011, Petrographic and geochemical characterization of granitoid and metamorphic basement rocks, Owyhee Mountains, ID: Abstracts with Programs - Geological Society of America, v. 43, p. 66.

Le Bas, M.J., Le Maitre, R.W., Streckeisen, A., and Zanettin, B.A., 1986, Chemical classification of volcanic rocks based on the total alkali-silica diagram: Journal of Petrology, v. 27, p. 745-750.

Leeman, W.P., Oldow, J.S., and Hart, W.K., 1992, Lithosphere-scale thrusting in the western U.S. Cordillera as constrained by Sr and Nd isotopic transitions in Neogene volcanic rocks: Geology v. 20, p. 63–66.

Leeman, W.P., Huang, S., and Tonarini, S., 2002, Comparative thermal models for subduction zones; evaluation of slab contributions to volcanic arc magmas: Geochimica et Cosmochimica Acta, v. 66, p. 444.

Leeman, W. P., Annen, C., and Dufek, J., 2008, Snake River Plain-Yellowstone silicic volcanism: Implications for magmatic genesis and magma fluxes: Dynamics of Crustal Magma Transfer, Storage and Differentiation, Geological Society of London, Special Publications, v. 304, p. 235-259.

Leeman, W.P., Schutt, D.L., Hughes, S.S., 2009, Thermal structure beneath the Snake River Plain: Implications for the Yellowstone hotspot: Journal of Volcanology and Geothermal Research, v. 188, p. 57-67.

Lipman, P.W., Prostka, H.J., and Christiansen, R. L., 1971, Evolving subduction zones in the western United States, as interpreted from igneous rocks: Science, v. 174, p. 821-825.

Manley, C.R., and McIntosh, W.C., 2002, The Juniper Mountain volcanic center, Owyhee County, southwestern Idaho; age relations and physical volcanology: Tectonic and magmatic evolution of the Snake River Plain volcanic province, v. 30, p. 205-227.

McCurry, M., and Rodgers, D.W., 2009, Mass transfer along the Yellowstone hotspot track I: Petrologic constraints on the volume of mantle-derived magma: Journal of Volcanology and Geothermal Research, v. 188, p. 86-98.

Nash, B.P., Perkins, M.E., Christensen, J.N., Lee, D., and Halliday, A.N., 2006, The Yellowstone hotspot in space and time: Nd and Hf isotopes in silicic magmas: Earth and Planetary Science Letters, v. 247, p. 143-156.

Norman, M.D., and Leeman, W.P., 1989, Geochemical evolution of Cenozoic-Cretaceous magmatism and its relation to tectonic setting, southwestern Idaho, U.S.A.: Earth and Planetary Science Letters, v. 94, p. 78-96.

Norman, M.D., and Mertzman, S.A., 1991, Petrogenesis of Challis Volcanics from central and southwestern Idaho; trace element and Pb isotopic evidence: Journal of Geophysical Research, v. 96, p. 13,279–13,293.

Pearce, J.A., Harris, N.B.W., and Tindle, A.G., 1984, Trace element discrimination diagrams for the tectonic interpretation of granitic rocks: Journal of Petrology, v. 25, p. 956-983.

Pierce, K.L., and Morgan, L.A., 1992, The track of the Yellowstone hotspot: Volcanism, faulting, and uplift: Regional geology of eastern Idaho and western Wyoming: v. 179, p. 1-53.

Ragland, P.C., 1989, Basic Analytical Petrology: Oxford University Press Inc., New York, New York, United States, p. 369.

Saunders, J.A., Unger, D.L., Kamenov, G.D., Fayek, M., Hames, W.E., and Utterback, W.C., 2008, Genesis of middle Miocene Yellowstone Hot Spot-related bonanza epithermal Au-Ag deposits, northern Great Basin, USA: Mineralium Deposita, v. 43, p. 715-734.

Sharp, Z.D., 1990, A laser-based microanalytical method for the in situ determination of oxygen isotope ratios of silicates and oxides: Geochimica et Cosmochimica Acta, v. 54, p. 1353-1357.

Shand, S.J., 1943, Eruptive rocks, their genesis, composition, classification, and their relation to ore deposits, with a chapter on meteorites (revised second edition), Thomas Murby & Co.: London, United Kingdom, p. 444.

Stuck, R.J., 1993, Petroligy and geochemistry of a late Cretaceous granitoid suite, Santa Rosa Mountain range, Humboldt County, Nevada [Master Thesis] Miami University, p. 179.

Takeuchi, A., and Larson, P.B., 2005, Oxygen isotope evidence for the late Cenozoic development of an orographic rain shadow in eastern Washington, USA: Geology, v. 33, p. 313-316.

Taylor, H.P., Jr., 1968, The oxygen isotope geochemistry of igneous rocks: Contributions to Mineralogy and Petrology, v. 19, p. 1-71.

Taylor, H.P., 1979, Oxygen and hydrogen isotope relationships in hydrothermal mineral deposits, in Barnes, H.L., ed., Geochemistry ofhydrothermal ore deposits (second edition): NewYork, John Wiley, p. 236-277.

Taylor, S.R., and McLennan, S.M., 1985, The continental crust; its composition and evolution; an examination of the geochemical record preserved in sedimentary rocks, Geoscience texts: United Kingdom, Blackwell Scientific Publ.: Oxford, United Kingdom, p. 312.

Valley, J.W., Kitchen, N., Kohn, M.J., Niendorf, C.R., and Spicuzza, M.J., 1995, UWG-2, a garnet standard for oxygen isotope ratios; strategies for high precision and accuracy with laser heating: Geochimica et Cosmochimica Acta, v.59, p. 5223-5231.

Vikre, P.G., 1985, Precious metal vein systems in the National District, Humboldt County, Nevada: Economic Geology, v. 80, p. 360-393.

Vikre, P.G., 1987, Paleohydrology of Buckskin Mountain, National District, Humboldt County, Nevada: Economic Geology, v. 82, p. 934-950.

Vikre, P.G., 2007, Sinter-vein correlations at Buckskin Mountain, National District, Humboldt County, Nevada: Economic Geology, v. 102, p. 193-224.

Watts, K.E., Leeman, W.P., Bindeman, I.N., and Larson, P.B., 2010, Supereruptions of the Snake River Plain: Two-stage derivation of low-$\delta^{18}O$ rhyolites from normal-$\delta^{18}O$ crust as constrained by Archean xenoliths: Geology, v. 38, p. 503-506.

Watts, K.E., Bindeman, I.N., and Schmitt, A.K., 2011, Large-volume rhyolite genesis in caldera complexes of the Snake River Plain: Insights from the Kilgore tuff of the Heise volcanic field, Idaho, with comparisons to Yellowstone and Bruneau-Jarbidge rhyolites: Journal of Petrology, v. 52, p. 857-890.

Whalen, J.B., Currie, K.L., and Chappell, B.W., 1987, A-type granites; geochemical characteristics, discrimination and petrogenesis: Contributions to Mineralogy and Petrology, v. 95, p. 407-419.

Wyld, S.J., 1992, Geology and geochronology of the Pine Forest Range, northwest Nevada: Stratigraphic, Structural, and magmatic history, and regional implications [Dissertation] Stanford University, p. 543.

Wyld, S.J., 2000, Triassic evolution of the arc and backarc of northwestern Nevada, and evidence for extensional tectonism: Geological Society of America Special Paper 347, p. 185-207.

Wyld, S.J., Rodgers, J.W., Copeland, P., 2003, Metamorphic Evolution of the Luning-Fencemaker Fold-Thrust Belt, Nevada: Illite Crystallinity, Metamorphic Petrology, and 40Ar/39Ar Geochronology: The Journal of Geology, v. 111, p. 17-38.

Zierenberg, R.A., Schiffman, P., Barfod, G.H., Lesher, C.E., Marks, N.E., Lowerstern, J.B., Mortensen, A.K., Pope, E.C., Bird, D.K., Reed, M.H., Friðleifsson, G.Ó, and Elders, W.A., Composition and origin of rhyolite melt intersected by drilling in the Krafla geothermal field, Iceland: Contributions in Mineral Petrology, v.165, p. 327-347.

Appendix A - Sample Descriptions and Pictures

The information and descriptions of the fifteen samples for this study are from Brueseke and Hart (2008). Crystal descriptions of the picked quartz (when possible) and feldspars are from this study. The UTM coordinates correspond to NAD 27 CONUS datum and are located in Zone 11. The samples are listed in alpha-numeric order.

Sample ID: MB00-18 Rock Unit: Tpr

Northing: 462074 Easting: 4613975

Description: Abundant feldspar and quartz grains (~2cm) with small amphibole laths and biotite phenocrysts (<1cm) in a gray glassy matrix. Hypocrystalline phanaritic matrix.
Picked Crystal Description: Feldspars are milky to transparent white with occasional small melt inclusions present. Cleavage faces very apparent. Quartz crystals are smoky gray in color and are rounded with melt inclusions. Some crystals show concoidal fracture.

Sample ID: MB00-33 Rock Unit: Tom

Northing: 469083 Easting: 4638444

Description: Spherulitic, hypocrystalline matrix that is blue/gray in color with abundant feldspars (1-3cm). Quartz phenocrysts also present (2mm) with oxidized mafic minerals.
Picked Crystal Description: Clear to white feldspar crystals with cleavage faces apparent. Quartz crystals are smoky gray and transparent with concoidal fracture. They are also rounded.

Sample ID: MB01-62 Rock Unit: Tcst

Northing: 469804 Easting: 4619910

Description: Rhyolite vitrophyre with abundant feldspar crystals (1-3mm). No quartz present.
Picked Crystal Description: Feldspars are milky white in color with cleavage faces present.

Sample ID: MB01-76 Rock Unit: Tcm

Northing: 475462 Easting: 4624446

Description: Purple/pink matrix with abundant feldspar and quartz (1-3mm). Some orange alteration present.

Picked Crystal Description: Feldspar crystals clear to milky white with cleavage faces present. Quartz crystals are rounded and transparent smoky gray with concoidal fracture.

Sample ID: MB02-13 Rock Unit: Tpr

Northing: 453475 Easting: 4616734

Description: Vitrophyric rhyolite with abundant feldspar (4mm) and some quartz (<2mm). Fined-grained amphibole and biotite also present.

Picked Crystal Description: Feldspars milky white in color with cleavage faces present. Quartz crystals are smoky gray with some concoidal fracture.

Sample ID: MB02-19 Rock Unit: Tpr

Northing; 456953 Easting: 4618371

Description: Vitrophyric rhyolite with abundant feldspar and some quartz and amphibole.

Picked Crystal Description: Feldspars are translucent white with some having a slight yellowish tint. Cleavage faces present. Quartz crystals are round and smoky gray and show some concoidal fracture.

Sample ID: MB02-55 Rock Unit: Tcst

Northing: 463995 Easting: 4621788

Description: Poorly welded ash flow with abundant feldspar crystals (2-3mm). No quartz present.

Picked Crystal Description: Feldspar crystals are translucent white with cleavage faces present.

Sample ID: MB02-63B Rock Unit: Tcst

Northing: 461855 Easting: 4622466

Description: Black Vitrophyric rhyolite with abundant feldspar phenocrysts (1-2mm). No quartz present.
Picked Crystal Description: Feldspars show some alteration with melt inclusions present and are more of a translucent gray. Cleavage faces present.

Sample ID: MB03-10B Rock Unit: Tom

Northing: 465783 Easting: 4636455

Description: Devitrified, spherulitic, hypocrystalline matrix with abundant feldspar and quartz phenocrysts (2-3mm).
Picked Crystal Description: Feldspars clear to translucent white with cleavage faces present. Quartz crystals are round and a clear smoky color with concoidal fracture.

Sample ID: MB03-24 Rock Unit: Tcst

Northing: 460195 Easting: 4626015

Description: Highly welded with a pink to gray matrix. Abundant feldspars (1-2mm) present.
Picked Crystal Description: Feldspars are milky white in color with cleavage faces present.

Sample ID: MB03-26A Rock Unit: Tcst

Northing: 462850 Easting: 4627544

Description: Highly welded white matrix with 1-3mm feldspars. Upper outcrop sample.
Picked Crystal Description: Milky to translucent white feldspars with cleavage faces present.

Sample ID: MB03-26F Rock Unit: Tcst

Northing: 462850 Easting: 4627544

Description: Non-welded lower outcrop sample. Abundant feldspars (2-3mm) present.
Picked Crystal Description: Feldspars are milky white in color with cleavage faces present.

Sample ID: MB03-32 Rock Unit: Tcst

Northing: 466789 Easting: 4629521

Description: Welded clast-rich lapilli tuff with abundant feldspars (1-3mm).
Picked Crystal Description: Milky white feldspars with some yellowish tint in some crystals. Cleavage faces present.

Sample ID: MB03-36A Rock Unit: Tcst

Northing: 470782 Easting: 4608204

Description: Laminated purple matrix with fiamme and abundant feldspars (1-2mm).
Picked Crystal Description: White transparent feldspars with cleavage faces present.

Sample ID: MB03-45 Rock Unit: Tct

Northing: 476386 Easting: 4612278

Description: Devitrified, hypocrystalline matrix with abundant 1-3mm feldspars and <1mm quartz phenocrysts.
Picked Crystal Description: Feldspars, clear to translucent white with cleavage faces present. Quartz crystals are rounded and a clear, smoky color with concoidal fracture.

Sample Pictures

The following pictures are of the picked feldspar and quartz crystals from each of the samples. The Cold Springs tuff samples do not contain quartz and so only pictures of the feldspar were taken. Grid spacing is 2 mm by 2 mm.

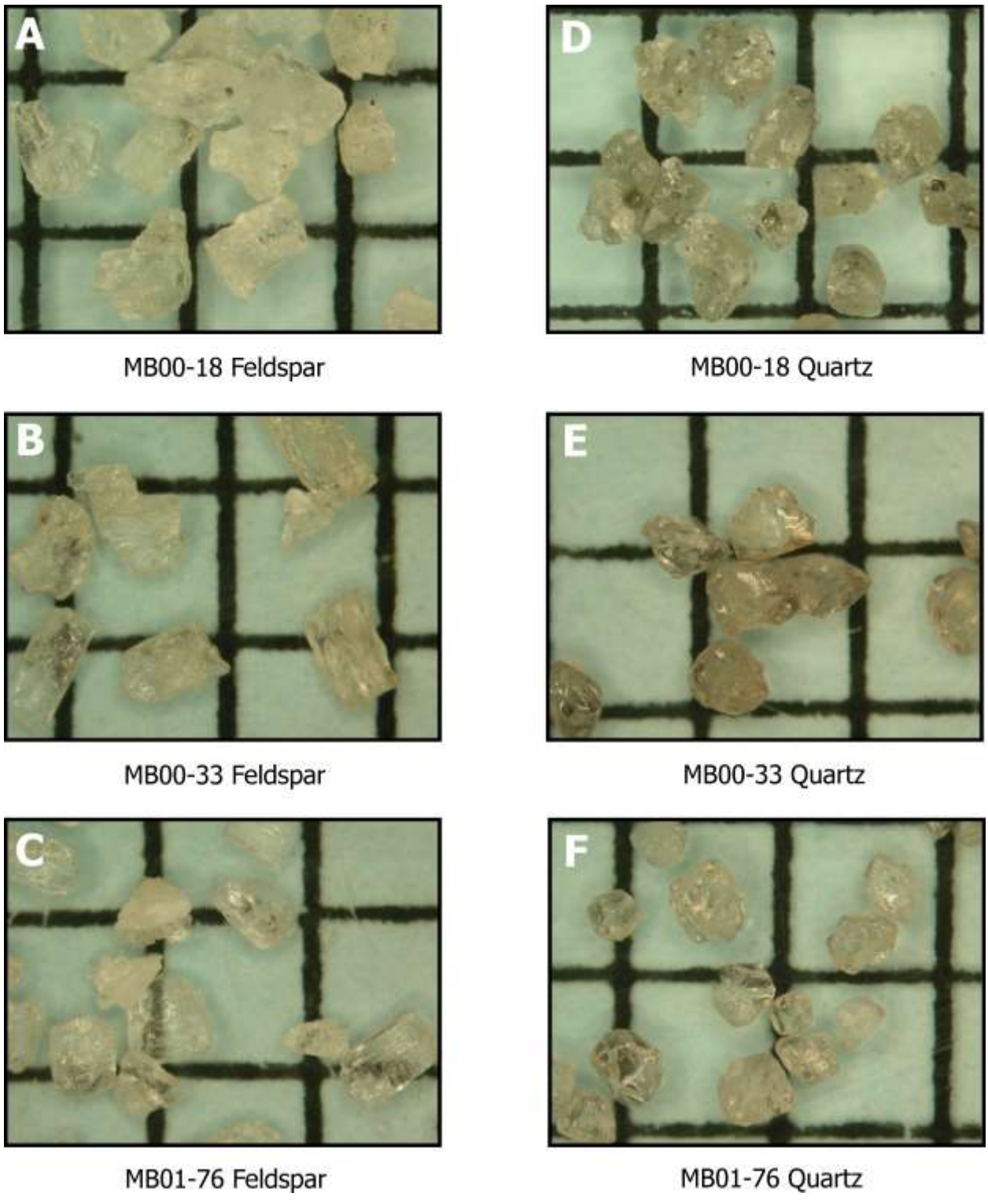

Figure A.1: Sample Pictures A through F

MB02-13 Feldspar

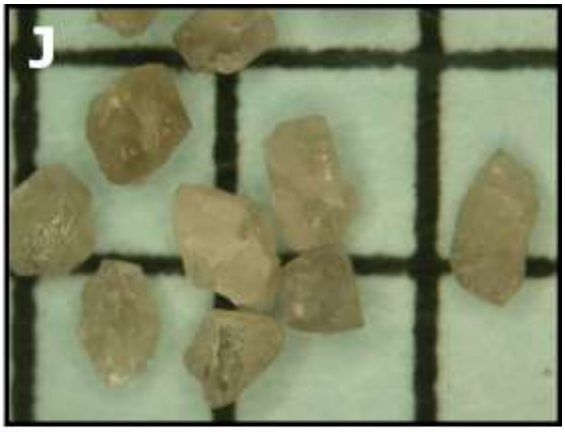

MB02-13 Quartz

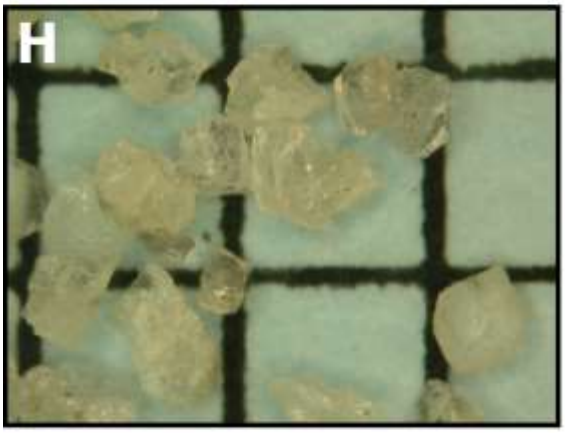

MB02-19 Feldspar

MB02-19 Quartz

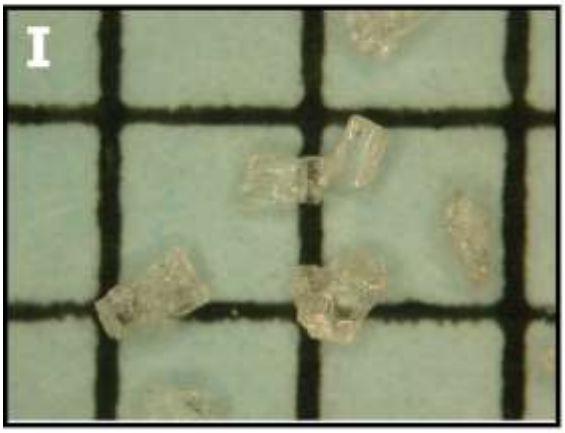

MB03-10B Feldspar

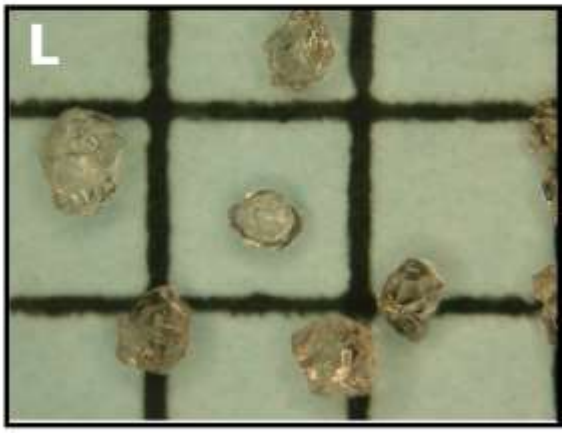

MB03-10B Quartz

Figure A.2: Sample Pictures G through L

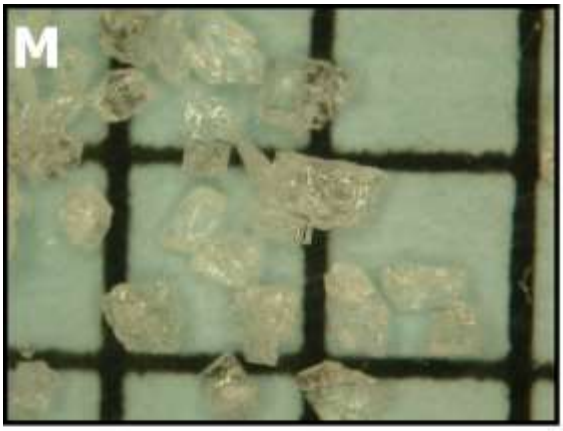

MB03-45 Feldspar

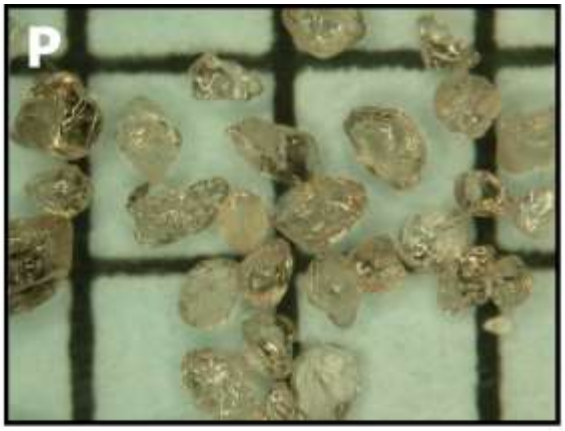

MB03-45 Quartz

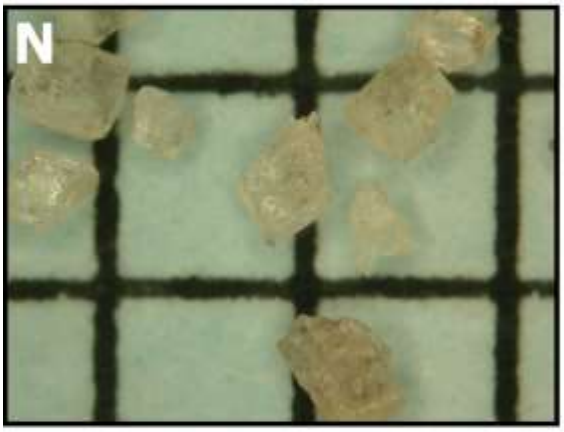

MB01-62 Feldspar

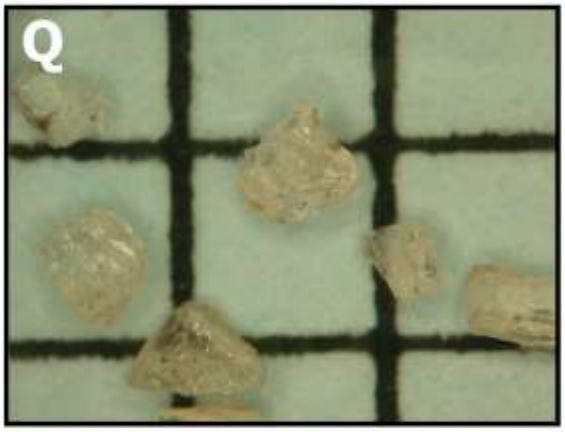

MB02-55 Feldspar

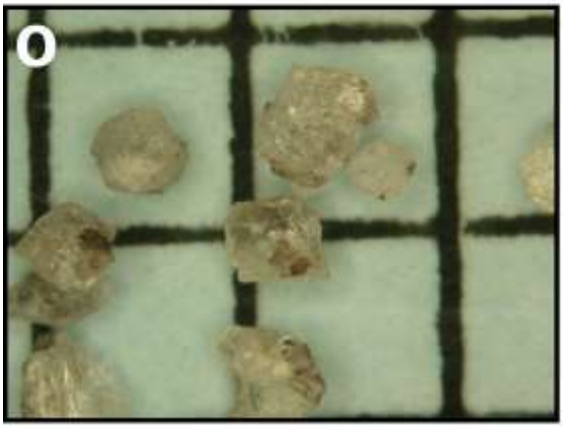

MB02-63B Feldspar

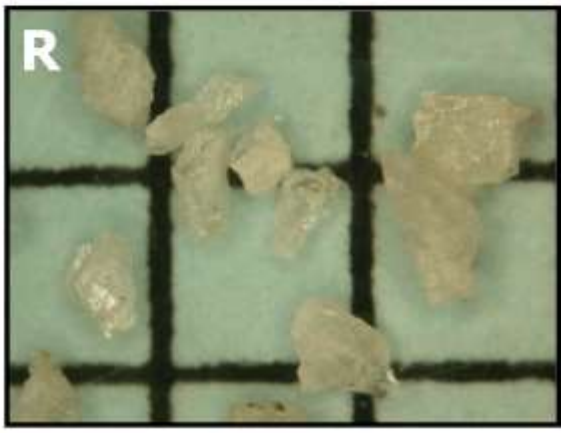

MB03-24 Feldspar

Figure A.3: Sample Pictures M through R

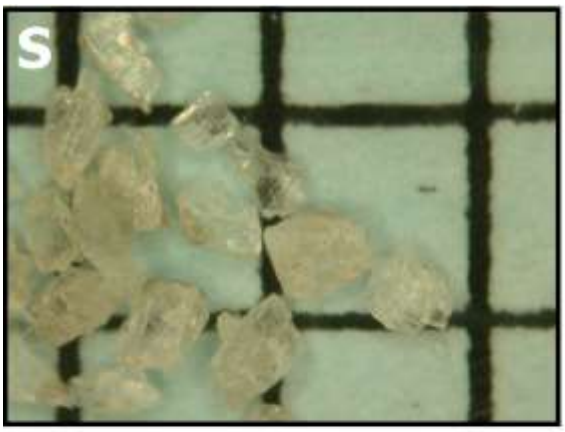

MB03-26A Feldspar

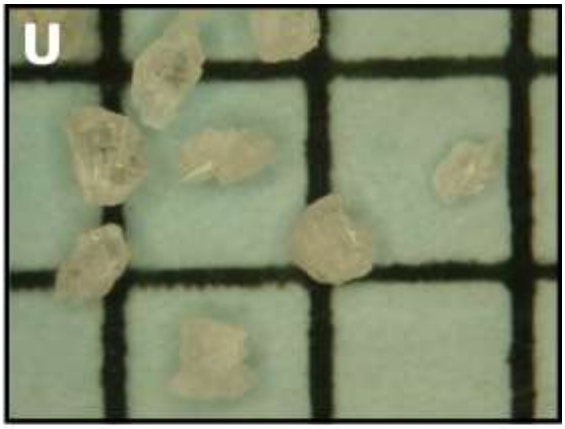

MB03-26F Feldspar

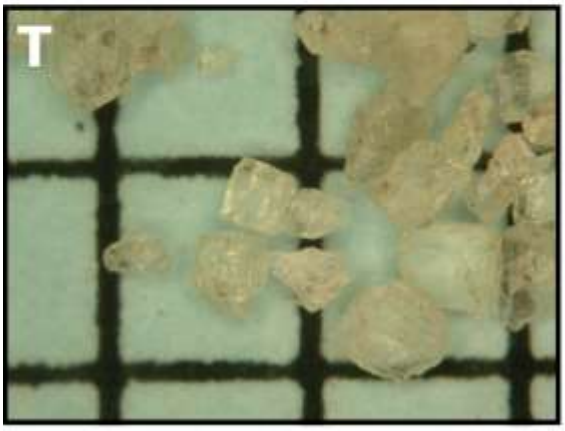

MB03-32 Feldspar

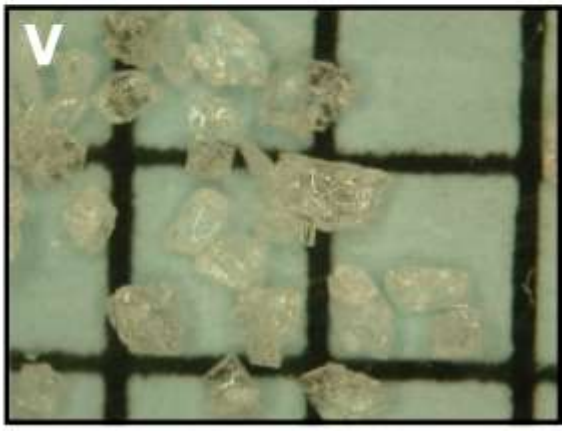

MB03-36A Feldspar

Figure A.4: Sample Pictures S through V

Appendix B - Model Endmembers and Mixing Model Components

Model endmember geochemistry and the representative Cold Springs tuff geochemistry can be found in the table below. NCI ε_{Nd} numbers can also be found within the table.

Table B.1: Model Endmember Geochemistry

Geochemistry table of the endmember and Cold Springs sample used in the model. Granite Peak-Sawtooth granitoids data age corrected to 16.5 Ma, all other data are initial isotope values.

Sample	Com. A Felsic CH-7	Com B Mafic MB01-12	Test Sample MB02-55
SiO_2 (wt. %)	74.71	47.59	68.27
TiO_2 (wt. %)	0.20	1.36	0.45
Al_2O_3 (wt. %)	14.97	16.62	13.36
Fe_2O_3 (wt. %)	0.57	3.77	1.94
FeO (wt. %)	0.48	7.39	1.62
MnO (wt. %)	0.02	0.18	0.07
MgO (wt.%)	0.13	8.64	0.45
CaO (wt. %)	1.54	9.88	2.24
Na_2O (wt. %)	3.87	2.63	3.25
K_2O (wt. %)	3.42	0.33	5.36
P_2O_5 (wt. %)	0.04	0.14	0.10
Ni (ppm)	2.0	149.8	5.2
Cr (ppm)	---	102.1	5.0
Sc (ppm)	---	26.4	4.4
Ba (ppm)	1457	166	2188
Rb (ppm)	117	4	156
Sr (ppm)	470	410	119
Zr (ppm)	100	73	600
Nb (ppm)	---	3.2	40.6
Zn (ppm)	---	82	87
Pb (ppm)	---	1.0	24.4
Cs (ppm)	---	0.30	3.41
Hf (ppm)	---	2.0	16.6
La (ppm)	23.0	6.3	70.9
Ce (ppm)	48.0	14.8	133.7
Nd (ppm)	16.0	11.2	58.5
Sm (ppm)	2.8	3.5	13.1
Eu (ppm)	0.6	1.3	2.6
Yb (ppm)	0.5	1.9	6.6
Lu (ppm)	0.1	0.3	1.0
$^{87}Sr/^{86}Sr$	0.70695	0.70378	0.70608
$^{143}Nd/^{144}Nd$	0.51239	0.51288	0.51241
epsilon Nd	-4.42	5.10	-3.93
$^{206}Pb/^{204}Pb$	---	18.941	18.716
$^{207}Pb/^{204}Pb$	---	15.580	15.640
$^{208}Pb/^{204}Pb$	---	38.541	39.104

Mixing Model Components

The following table shows the components used to calculate the mixing amounts used in the simple mixing equation after Watts et al. (2010). Oxygen concentration (ppm) of the crustal and mafic endmembers were calculated for each major element. The following equation: [(wt. % * atomic mass of element) / total mass of compound] was used to calculate the oxygen wt. % for each major element then those values were then added up and converted to ppm by multiplying by 10,000 (Ragland, 1989). Various values of $\delta^{18}O$ were used for the crustal endmember and mafic endmember to compare to Cold Springs tuff sample which can be seen in Table B.2. Isotope data for Granite Peak-Sawtooth granitoid (GPS) are age corrected to 16.5 Ma whereas isotope data for the mafic endmember (Tb) are initial values.

Table B.2: Mixing Model Components

	Sample	$\delta^{18}O$ (‰)	$^{87}Sr/^{86}Sr$	$^{143}Nd/^{144}Nd$	O (ppm)	Sr (ppm)	Nd (ppm)
Felsic (GPS)	CH-7	-2, 0, 2, 4	0.70695	0.51239	492,787	470	16
Mafic Tb	MB01-12	5, 6	0.70378	0.51288	435,842	410	11